



AD

Reports Control Symbol
OSD-1366

RESEARCH AND DEVELOPMENT TECHNICAL REPORT
ECOM-5459

RAINFALL EFFECTS ON SATELLITE COMMUNICATIONS IN THE K, X, AND C BANDS

By

Israel Cantor

Michael Hudlow

July 1972

Approved for public release; distribution unlimited.

ECOM

UNITED STATES ARMY ELECTRONICS COMMAND - FORT MONMOUTH, NEW JERSEY

NOTICES

Disclaimers

The findings in this report are not to be construed as an official Department of the Army position, unless so designated by other authorized documents.

The citation of trade names and names of manufacturers in this report is not to be construed as official Government endorsement or approval of commercial products or services referenced herein.

Disposition

Destroy this report when it is no longer needed. Do not return it to the originator.

Technical Report ECOM-5459

RAINFALL EFFECTS ON SATELLITE COMMUNICATIONS
IN THE K, X, AND C BANDS

By

Israel Cantor

Michael Hudlow

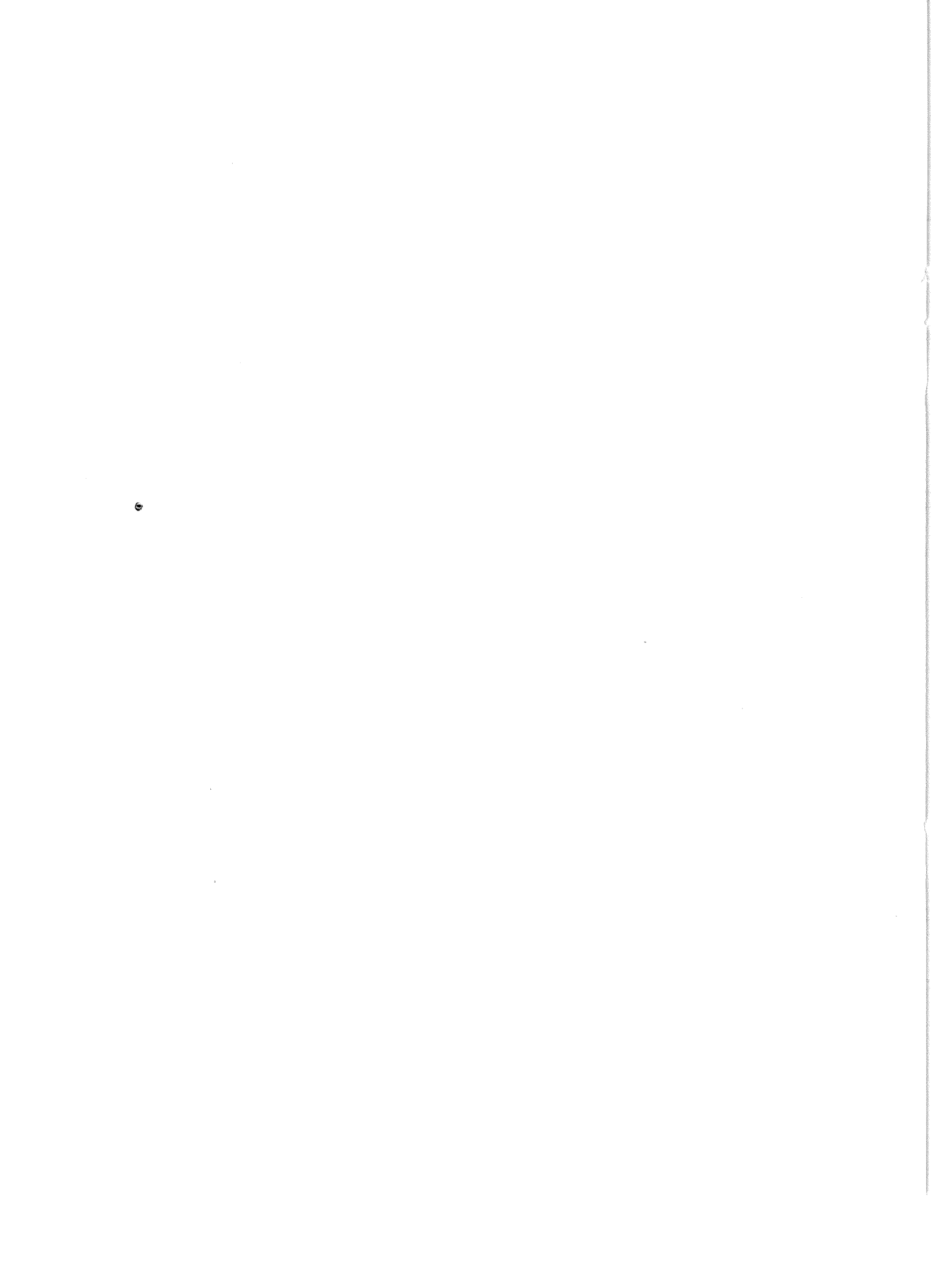
Atmospheric Sciences Laboratory
White Sands Missile Range, New Mexico

July 1972

DA Task No. IT06211A12605-54

Approved for public release; distribution unlimited.

U. S. Army Electronics Command
Fort Monmouth, New Jersey

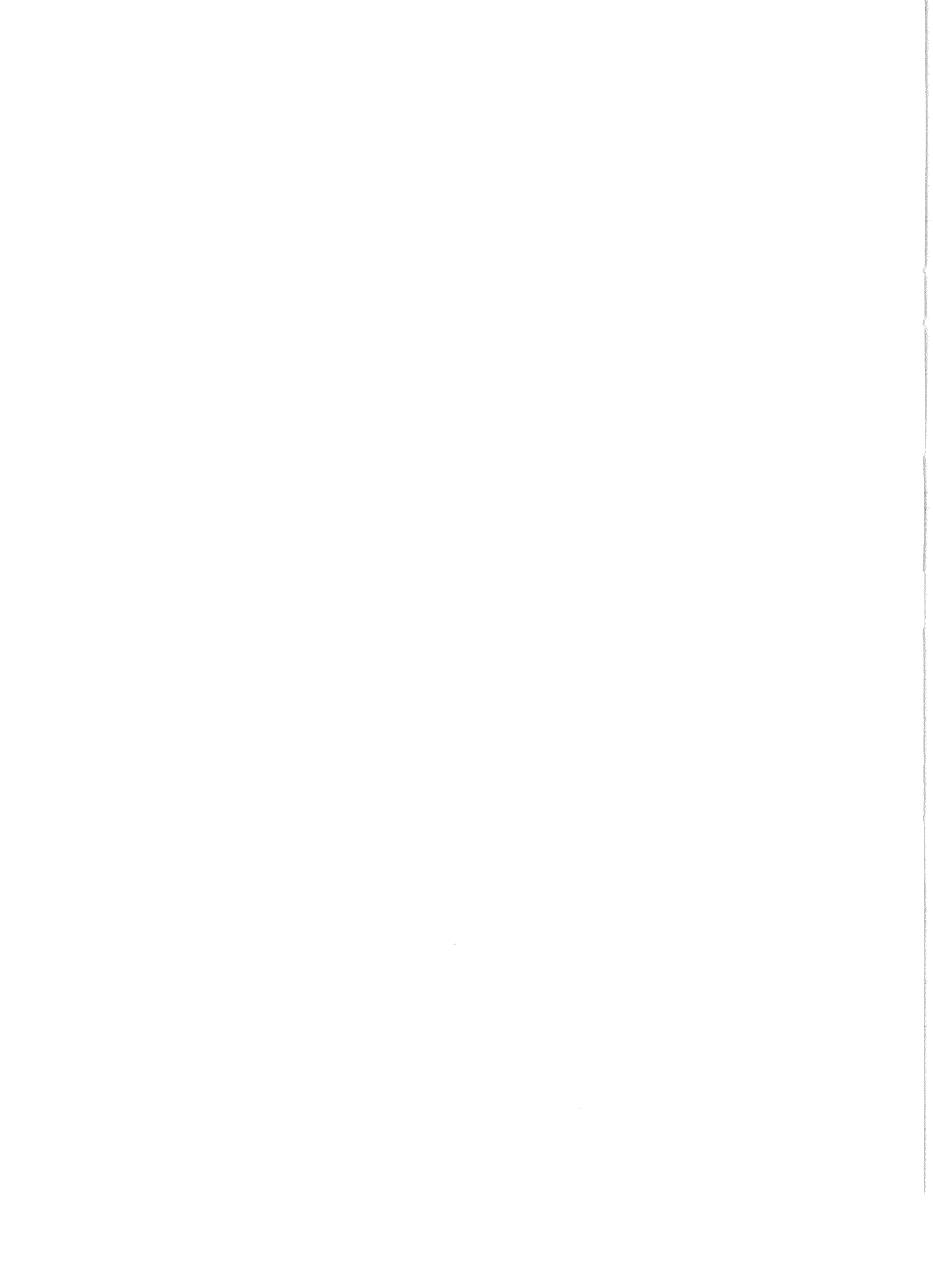


ABSTRACT

A survey-type investigation is made into the feasibility of short- and long-term predictions of attenuation and noise temperature fluctuations for satellite communications. The feasibility of using a weather radar, such as the AN/CPS-9, at 9.4 GHz (3.2 cm) for real-time predictions of the above parameters is explored. The suitability of weather radar for such applications is evaluated. Raindrop size data and Mie attenuation theory are used for the derivation of statistical curves that provide attenuation coefficients for various geographic areas and temperatures. Related results of other investigators are included. Some concepts are also presented of Mie vs Rayleigh scattering, absorption vs scattering, parameter and rain structure variability, path diversity, noise temperature, microwave radiometry, and dual-wavelength radar feasibility. Furthermore, information is added in regard to some of the general meteorological as well as the climatological aspects of precipitation, particularly thunderstorms.

CONTENTS

	Page
GLOSSARY OF SYMBOLS	vii
I. INTRODUCTION	1
II. THEORY AND PARAMETER VARIABILITY	2
A. Reflectivity, Rainfall Intensity, and Attenuation	2
B. Absorption vs Scattering, Temperature Effects, and Size Distribution	11
C. Parameter Variability	16
D. Path Diversity	20
III. DATA AND ANALYSES	27
IV. OTHER METHODS OF MEASURING ATTENUATION	42
A. Effective Noise Temperature and the Microwave Radiometer	42
B. Dual-Wavelength Radar	46
V. CONCLUSIONS AND RECOMMENDATIONS	51
VI. APPENDICES	
A. Radar Performance and Sensitivity to Noise Temperature	55
B. Comments on ETAC Report No. 4100	57
C. Meteorological and Climatological Features of Precipitation	59
D. Meteorological and Climatological Features of Thunderstorms	61
LITERATURE CITED	64



GLOSSARY OF SYMBOLS

\bar{P}_r	Average return power from a target at distance r
C	Radar equipment constant
K	Complex index of refraction defined as $K = \frac{m^2 - 1}{2}$
m	Complex index of refraction defined by $m = \frac{m^2 + 2}{n^2 - 1} + in'$
n	Real index of refraction
n'	Imaginary index of refraction
G(n)	Raindrop size spectrum parameter defined by $G(n) = D_0^{-3} \Sigma (ND^6) \div \Sigma (ND^3)$
Z_e	Target equivalent reflectivity factor as determined by the Mie theory
Z	Target reflectivity factor as determined by the Rayleigh theory
D_0	Median volume diameter
D	Raindrop diameter
\bar{v}	Mass weighted average fall speed of the size spectrum
v_0	Fall speed of the median volume raindrop
N	Concentration of drops per unit volume
R	Rain intensity
M	Total liquid water content
a	Rainfall parameter defined by Z or $Z_e = aR^b$
b	Rainfall parameter defined by Z or $Z_e = aR^b$
γ	Attenuation coefficient
c	Rainfall parameter defined by $\gamma = cR^d$
d	Rainfall parameter defined by $\gamma = cR^d$
e	Rainfall parameter defined by $\gamma = eZ_e^f$
f	Rainfall parameter defined by $\gamma = eZ_e^f$
A	Total path attenuation defined by $A = \int_{\text{path}} \gamma ds$
$\pi D/\lambda$	Size parameter where λ is the radar wavelength
Q_T	Attenuation cross section
$\Sigma\sigma$	Total backscattering cross section

Q_a	Absorption cross section
Q_s	Scattering cross section
$v(D)$	Terminal fall velocity for a drop of diameter D
$N(D)$	Number of drops of diameter D to $D+dD$
T_o	Standard temperature (taken as 290°K for electronic equipment)
B_n	Receiver bandwidth
F_n	Receiver noise figure
$(S_o/N_o)_{\min}$	Minimum ratio of the output signal-to-noise ratio for target detection
T_e	Effective noise temperature
$\alpha(s)$	Absorption coefficient as a function of distance s
$T(s)$	Water drop temperature as a function of distance s
P	Total precipitation defined by $P = \bar{\mu}t$ where $\bar{\mu}$ is the average rain intensity during time t
T	Total time during which the storm affects the communication path between the satellite and ground terminal
V	Mean scalar speed of the storm at 10,000'
e	Radar beam's elevation angle

1. INTRODUCTION

Atmospheric attenuation for satellite communications is most pronounced during rainfall wherein the raindrops somewhat scatter and strongly absorb the microwave radiation. For the wavelengths considered in this study, the absorption generally constitutes greater than 90% of the total attenuation. Its effect has seriously hampered adequate communications on frequent occasions. A joint communique between the Satellite Communication Agency (SATCOM) and the Atmospheric Sciences Laboratory (ASL), dated 1 April 1968, indicated the need for an investigation and predictability technique concerning serious or significant atmospheric effects on satellite communications. This report is, therefore, presented partially to meet this need by accomplishing two primary objectives, i.e., (1) formulation of attenuation vs rainfall intensity and reflectivity relationships for several wavelengths, temperatures, and geographic locations, and (2) feasibility investigation of the use of weather radar observations for real-time predictions of fluctuations of attenuation and noise temperature resulting from precipitation regions.

The objectives are to provide the US Army SATCOM with the type of specific guidelines required, namely, to effect a daily prediction capability of attenuation due to atmospheric conditions (approximately on a 24-hour basis) with a capability of updating predictions due to changing weather conditions, up to several hours before a suspected change. It was also the desire of SATCOM to establish the climatology of rainfall attenuation by location and season based on the best available models. Moreover, the following was also indicated: "the updating of ETAC Report No. 4100 [1] with the application of newly developed models, specific locations, and the addition of 16 GHz (between 1.8 and 1.9 cm) performance would appear to answer USASATCOMA requirements." It is to be noted that the ASL weather radar operates at 9.4 GHz (3.2 cm) while the SATCOM agency commonly utilizes 15 GHz (2 cm) and 7.5 GHz (4 cm) frequencies.

Attainment of the above objectives would enable satellite communication to proceed along directions and paths of lower or minimum attenuation after the radar ground station initially verifies areas of high or maximum attenuation associated with the presence of rainfall. Sufficient data for an adequate period of time in a given geographic area would also provide the statistics for formulating attenuation vs rainfall intensities and reflectivities for different wavelengths and temperatures.

A portion of this report is devoted to the feasibility of using the radiometer to supplement the radar for providing adequate real-time attenuation data. Such radiometer attenuation information could then support the radar attenuation data in providing the basis for shedding one or more channels (out of a possible total of 12, e.g., with modern multiple-channel equipment). Each channel shed will then provide approx-

imately an additional 3dB of signal strength which in effect will allow a 3dB additional loss in attenuation without degrading the signal-to-noise ratios for the remaining channels.

In addition, switched-path diversity operational advantages can be implemented to increase the reliability of adequate satellite-to-ground-terminal communications. Large spatial variations of rain intensity, which occur frequently, indicate the need to investigate the short-term average rain rate along more than one path. If, for example, the attenuation along one satellite-to-ground-terminal path should exceed that of another by at least 3dB, the communication system can be promptly switched to the more favorable path. This procedure, according to Hogg [2], can markedly improve the communication reliability aspects by decreasing the outage time up to a factor of about ten. He further indicates that a five-month study at McGill University, Montreal, Canada, reveals that good path diversity should be attainable in a space communication system with terminal spacings of 10 miles or more for the storm types encountered during that period and at that location. Heavy rains are often localized so that it becomes possible to optimize the distance between terminal receiving stations to ensure improved signal reception. However, the main difficulty presently is in identifying precipitation areas of various intensities at various altitudes and at different short-term intervals.

Real-time information regarding attenuation and noise temperature fluctuations, in addition to the above advantages, can permit the implementation of signal traffic control. This can be effected by the efficient routing and choosing of priority messages.

Due to the wide variations in rainfall attenuation properties, statistical analysis becomes necessary to determine the probabilities of varying degrees of attenuation for different time intervals in different geographic regions throughout the world. Such an analysis can ultimately lead to effective statistical models of varying rain intensity probabilities for different parts of the world which are applicable to military strategic planning for desirable terminal site locations. Operational planning could also be benefitted by such models, supplemented by daily variation probabilities during rainy seasons.

II. THEORY AND VARIABILITY OF PARAMETERS

A. Reflectivity, Rainfall Intensity, and Attenuation

1. Precipitation and Radar Equations

Rainfall parameter estimates or computations generally start with the basic radar equation for a nonattenuating radar beam filled with precipi-

tating particles:

$$\bar{P}_r = \frac{C|K|^2 Z_e}{r^2}$$

where \bar{P}_r is the average return power from a target at distance r , C is the radar hardware constant,

$$K = \left(\frac{m^2 - 1}{m^2 + 2} \right)$$

where m is the complex index of refraction of the precipitation particle defined in terms of the real and imaginary refractive index as $m = n - in'$ and $|K|^2$ is frequently chosen to be 0.93 for water in the centimeter wavelength range, Z_e^* is the target equivalent reflectivity factor denoted by the expression:

$$Z_e = 3.5 \times 10^3 \lambda^4 \Sigma \sigma_i$$

where $\Sigma \sigma_i$ is the summation of the backscatter cross sections of the raindrops in a unit volume as determined by the Mie scattering theory and λ is the wavelength. The units for Z_e are generally $\text{mm}^6 \text{m}^{-3}$ where λ is in millimeters, $\Sigma \sigma_i$ in mm^2 , and the unit volume taken as 1 cubic meter (m^3).

Rearrangement of the above equation shows that

$$Z_e = \frac{\bar{P}_r r^2}{C|K|^2}$$

\bar{P}_r and r can be measured with reasonable accuracy with a radar that is properly calibrated, and Z_e can therefore be evaluated. Z_e is thus dependent on that portion of the transmitted energy that is effectively backscattered into the antenna of the radar receiver. Furthermore, it can be shown from physical and mathematical considerations that the magnitude of Z_e is dependent on the size distribution of the raindrops within the target volume. Since rainfall intensity and liquid water content are also dependent on the size distribution, one can readily ex-

* Z_e is not to be confused with Z which is generally known as the Rayleigh reflectivity factor and expressed as the summation of the sixth power of the diameters of the reflecting particles over a unit volume. Z_e represents the more accurate value, particularly when the diameters of the precipitation particles approach significant fractions of the wavelength of radiation (greater than about 3%).

pect some significant relationships between such parameters as attenuation, rain intensity, water content, and reflectivity. Such a relationship (not including attenuation) for Z (which is independent of wavelength) is graphically shown in Figure 1 [3] which applies to a rather wide range of rain drops in drizzle, warm rainfall, and temperate-latitude rainfall. The fixed parameters of the figure are: (1) $G(n) = 1.5$ and

$$(2) \frac{\bar{v}}{v_0} = 0.98.$$

$G(n)$, a size spectrum statistic, is represented by the expression:

$$G(n) = D_0^{-3} \frac{\sum (ND^6)}{\sum (ND^3)}$$

where D_0 is the median volume diameter, D the drop diameter, N the number of drops of diameter D per unit volume, and n is the spread factor of the size spectrum as defined by a family of spectra. This family of spectra is denoted by Atlas and Bartnoff [4] as:

$$f\left(\frac{D}{D_0}\right) = \left(\frac{3.34}{n}\right) \left(\frac{D}{D_0}\right)^{(18/n)-1} \left[2 - \left(\frac{D}{D_0}\right)^{2/n}\right]^8.$$

The fall velocity parameter is

$$\frac{\bar{v}}{v_0} = 0.98$$

where \bar{v} is the mass weighted average fall speed of the size spectrum and v_0 is the fall speed of the median volume drop. In terms of rain rate, \bar{v}/v_0 can be denoted in the following manner:

$$R(\text{mm hr}^{-1}) = 3.6 \times 10^{-2} v_0 (\bar{v}/v_0) M$$

[5], where M is the total liquid water content (gm m^{-3}) with \bar{v} and v_0 in cm sec^{-1} .

Of primary concern to the communication engineer is the prediction of path attenuation based on the precise radar-measured reflectivity or the equivalent reflectivity factor, Z_e . The basic relationship between Z_e and R or γ (attenuation coefficient) is usually expressed as a simple power law, i.e., $Z_e = aR^b$ and $\gamma = cR^d$ where the multiplicative parameter depends on the drop-size distribution for a fixed R and the exponent parameter depends on the variation of the drop size distribution with a variation in R . Furthermore, the attenuation coefficient can be ex-

○——MARSHALL-PALMER
 STRATIFORM, THEORETICAL.
 □-----BLANCHARD, WARM OROGRAPHIC.
 Δ-----D. M. A. JONES, HEAVY SHOWERS.
 X-----ATLAS-CHMELA, 16 APR 1954
 STRATIFORM WITH DRIZZLE.
 ●-----ATLAS-CHMELA, 27 APR 1954
 EVAPORATING STRATIFORM.

RAIN PARAMETER DIAGRAM
DERIVED ASSUMING
 $G(n) = 1.5, \frac{\bar{V}}{V_0} = 0.98$

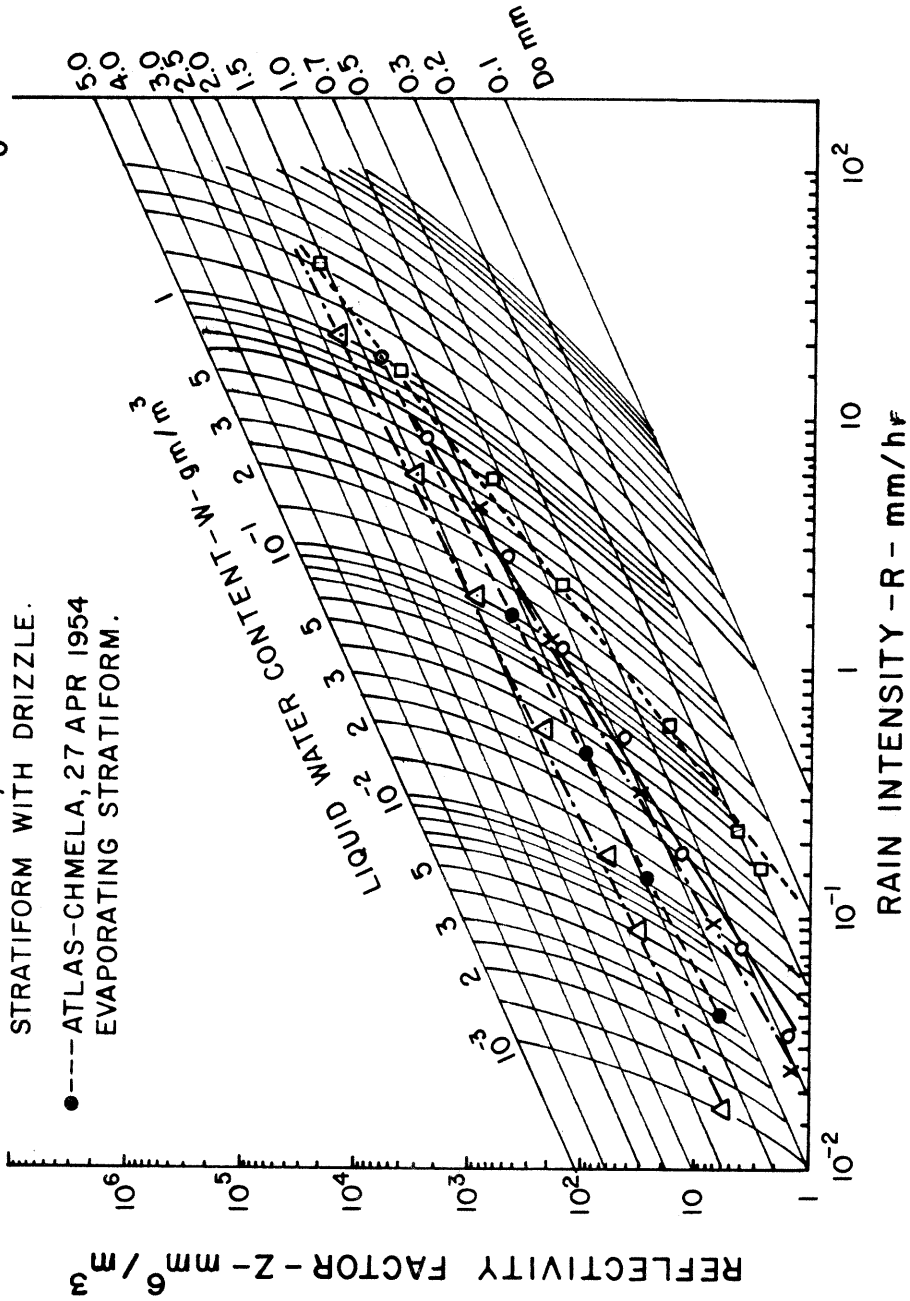


FIG. 1 RELATION BETWEEN REFLECTIVITY FACTOR (Z), LIQUID WATER CONTENT (W) AND MEDIAN DIAMETER (Do). [ATLAS AND CHMELA, [3]].

pressed explicitly as $\gamma = e Z e^f$ where e and f are regression coefficients. One procedure for estimating total path attenuation consists of calculating its magnitude from $A = \int_{\text{path}} \gamma_{\text{pred}} \cdot dS$, where A is the total path attenuation. It is assumed that $Z e$ is adequately evaluated over the entire path from radar measurements. To optimize the procedure, such predicted attenuations can subsequently be compared with the observed path attenuations, and the parameters e and f could then be adjusted to obtain the best fit between the predicted and the measured attenuation.

Figure 2 from Haroules and Brown [6], based on Gunn and East's work [7], shows the relationship between one-way attenuation and wavelength for several rain intensities. Mie's attenuation theory is applied here to the Laws and Parsons size distribution. The Laws and Parsons experimental results are actually expressed as a fraction of the total volume of water reaching the ground due to drops of radius "a" rather than as a constant size distribution. Table I shows such results as quoted by Ryde and Ryde [8]. Any extension of the Gunn and East attenuation-wavelength relationship to other cases thus requires adequate knowledge of their specific size distributions.

2. Rayleigh versus Mie Attenuation

The question frequently arises whether the Rayleigh formulation is adequate for determining reflectivity and attenuation. To answer this question, the following remarks need to be considered.

Figure 3 depicts the relationship between the Mie and Rayleigh attenuation for individual drops and indicates, for example, that for a water drop of radius less than about 0.6mm, the Rayleigh attenuation cross section is within about 20% of that of the Mie attenuation cross section in the wavelength region of 3cm. Moreover, in the 3cm region, for the Rayleigh attenuation cross section to agree within 50% of the Mie attenuation cross section, water drop diameter cannot exceed about 1mm. The spread between the Rayleigh and Mie cross-sectional values at a given size parameter becomes greater for greater wavelengths and less for the smaller wavelengths.

Figure 4 (Gunn and East [7]) gives an example of the Rayleigh-computed back-scattering cross sections per unit volume of a Laws and Parsons drop-size distribution and shows a close approximation to that of the Mie or exact computed back-scattering cross section per unit volume for wavelengths of about 3cm and greater. However, significant differences can occur for other size distributions as is shown in Section III where comparisons are made between the reflectivity factor and the equivalent reflectivity factor for drop-size distributions observed in New Jersey and North Carolina.

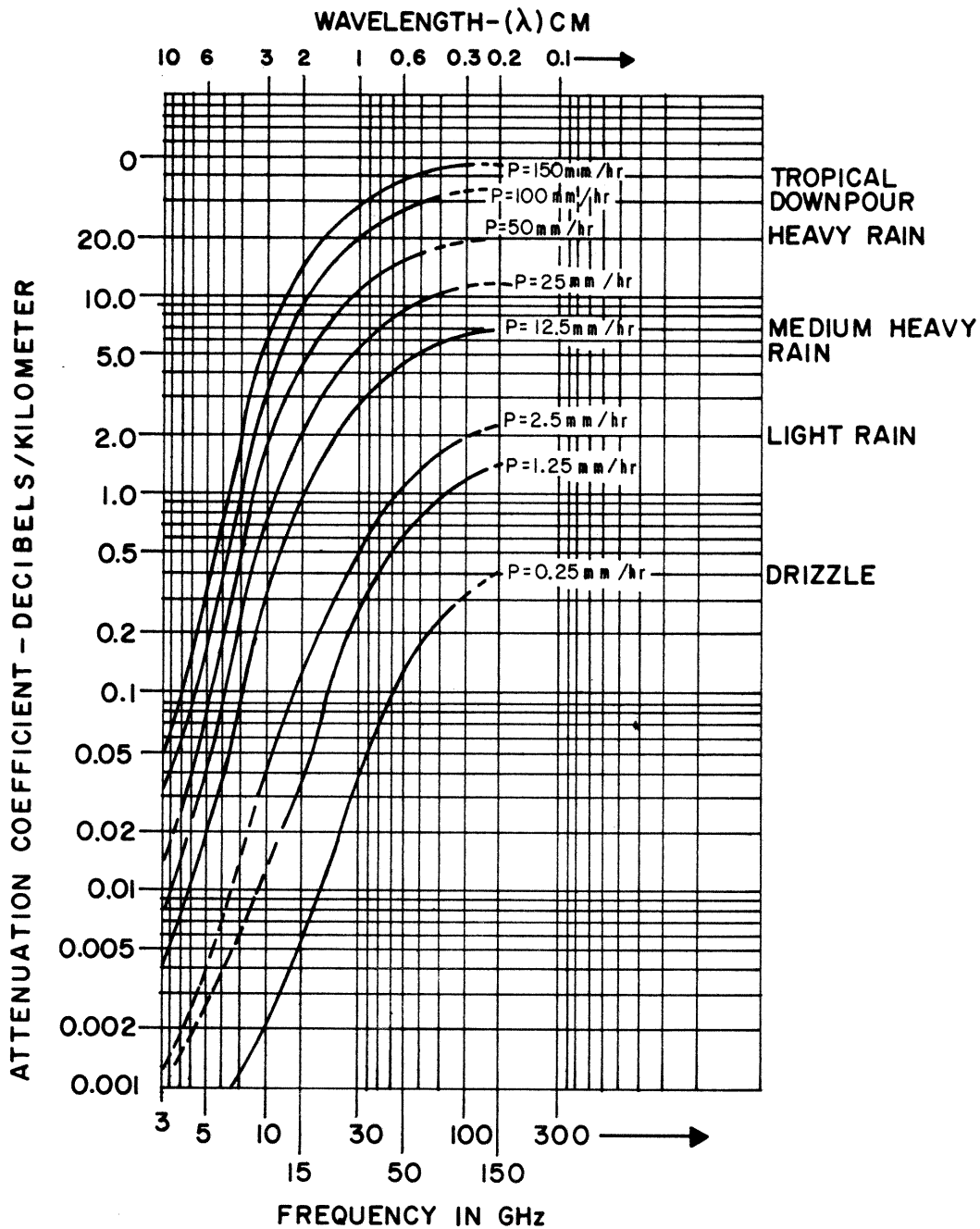


FIG. 2. RAINFALL ATTENUATION VERSUS FREQUENCY FOR VARIOUS PRECIPITATION RATES (HAROULES AND BROWN [6]) (FROM GUNN AND EAST [7])

TABLE I
 FRACTION OF TOTAL VOLUME REACHING GROUND CONTRIBUTED
 BY DROPS OF VARIOUS SIZES*
 (DROP RADIUS INTERVAL, $d_a = 0.025$ cm)

R (mm/hr)	0.25	1.25	2.5	12.5	25	50	100	150
a(cm)	% by Volume of Water Drops Reaching the Ground							
0.025	28	11	7	3	2	1	1	1
0.050	50	37	28	12	8	5	4	4
0.075	18	31	33	25	18	12	9	7
0.100	3	14	19	25	24	20	14	12
0.125	1	5	8	17	20	21	17	14
0.150		2	3	10	13	16	18	18
0.175		1	1	4	8	11	15	16
0.200			1	2	3	7	9	12
0.225				1	2	3	6	8
0.250				1	1	2	3	4
0.275					1	1	2	2
0.300						1	1	1
0.325							1	1

*After Laws and Parsons as quoted by Ryde and Ryde [8]

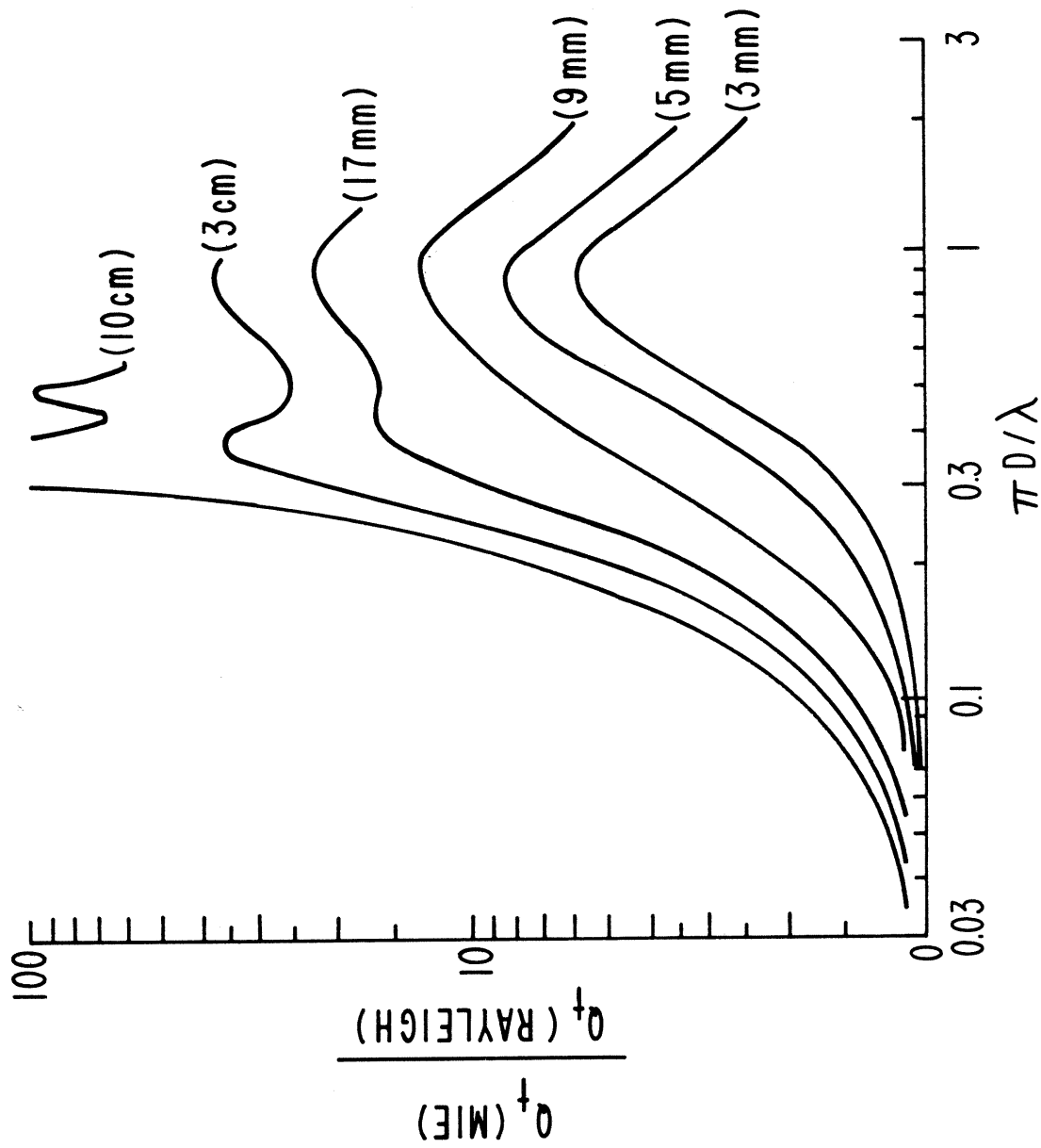


FIG. 3 - RATIO OF ACTUAL ATTENUATION TO THAT GIVEN BY THE RAYLEIGH APPROXIMATION FOR WATER AT 18°C. (HANDBOOK OF GEOPHYSICS [9])

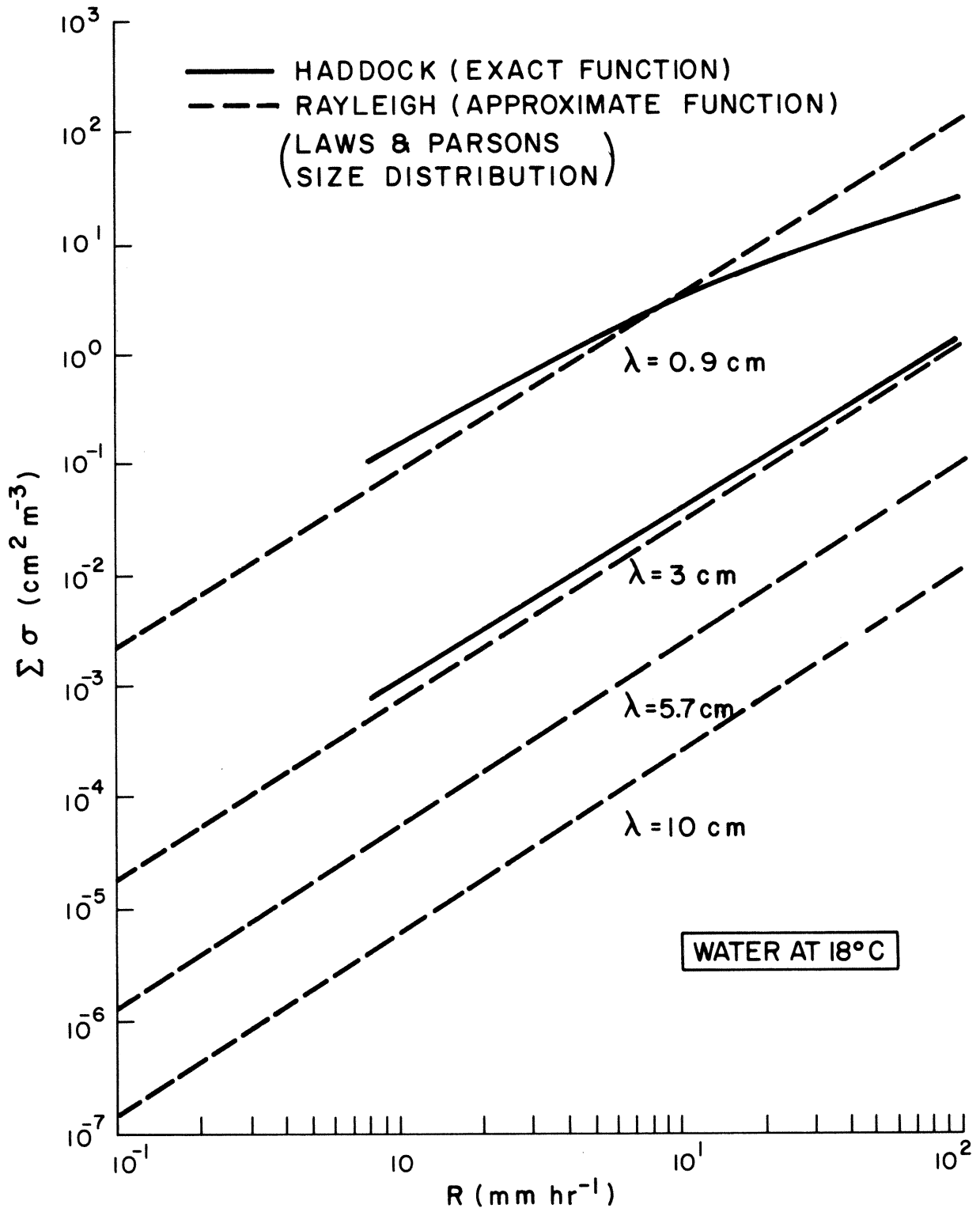


FIG. 4 EXACT (MIE) AND APPROXIMATE (RAYLEIGH) BACK-SCATTERING CROSS SECTIONS PER UNIT VOLUME OF RAIN-FILLED SPACE, PLOTTED AGAINST RAINFALL INTENSITY (GUNN & EAST [7])

B. Absorption vs Scattering, Temperature Effects, and Size Distribution

One question that must be answered concerning total attenuation is: what is the relative magnitude of scattering compared to absorption for the wavelengths of radiation which are of interest in this study? This is particularly important, for example, as will be pointed out later, in noise temperature and radiometer measurements. If the scattering component can be assumed insignificant relative to the absorption, then absorption can be assumed, with small error, approximately equal to the total attenuation. This substitution would be convenient since the total attenuation coefficient is the parameter which is inferred from the radar measurements, but the absorption coefficient is required for noise temperature calculations.

The complex index of refraction of the water droplet is the sole physical parameter which determines the absorption and scattering of an electromagnetic wave by a spherical particle of a given size parameter,

$$\frac{\pi D}{\lambda},$$

i.e., ratio of particle size to wavelength. The Mie cross sections can then be precisely calculated for known complex indices of refraction and size distributions.

Table II contains the real and imaginary components of refraction for water as a function of wavelength and temperature. The complex indices of refraction are given by $m = n - in'$, where n is the real component affecting the scattering properties, and $n' = \alpha\lambda/4\pi$ which affects the absorption properties and is proportional to $\text{Im}(-k)$, $\alpha =$ absorption coefficient, and

$$|K|^2 = \left| \frac{n^2 - 1}{n^2 + 2} \right|^2.$$

Some of the features that can be noted from the table are: (1) Temperature changes affect the scattering properties more than the absorption properties at the smaller wavelengths, i.e., 1.24 cm. At the higher wavelengths, i.e., 3.2cm - 10cm region, the absorption properties are more affected by temperature changes than are the scattering properties.

One can also note from this table that there are small changes of $|K|^2$ with temperature, indicating relatively small effects of temperature on Rayleigh scattering in the K, X, and C bands. Beyond the Rayleigh region, however, the scattering is a complex function of the refractive index, involving Bessel functions of order n where n varies from 1 to ∞ , but according to Ryde [10], the temperature effect on scattering is still

TABLE II

		Wavelength In Centimeters (cm)	10.0	3.21	1.24
20°C	$ K ^2$	$n = 8.88$	0.928	0.928	0.919
	$\text{Im}(-K)$	$n' = 0.63$	0.00474	0.0188	0.0471
10°C	$ K ^2$	$n = 9.02$	0.931	0.928	0.915
	$\text{Im}(-K)$	$n' = 0.90$	0.00688	0.0247	0.0615
0°C	$ K ^2$	$n = 8.99$	0.934	0.930	0.906
	$\text{Im}(-K)$	$n' = 1.47$	0.0110	0.0335	0.0807

not more than a few percent of that for the Rayleigh case. However, for the Rayleigh case the absorption parameter almost doubles for the 3.21cm wavelength as the temperature drops from 20°C to 0°C, i.e., temperature effects are very marked for small water drops where

$$\frac{\pi D}{\lambda} < 0.1.$$

The values of $\text{Im}(-K)$ vs temperature from Table II, moreover, indicate that the absorption diminishes for the Rayleigh solution with higher temperature at a given wavelength and at a given temperature with increasing wavelength. For drop-size distributions containing sufficient numbers of drops exceeding about 1 mm in diameter, i.e., rain rates of 2.5mm/hr and greater (for the Laws and Parsons distribution), however, the Mie solution yields the opposite temperature effect for 3.2 cm wavelength radiation in going from 0°C to about 20°C, i.e., attenuation increases as the temperature increases. This result is verified in section III for several drop-size distributions. Figure 5 illustrates the significant changes produced in the relationship between attenuation and temperature by varying the drop-size distribution with different rain rates for the Laws and Parsons distribution.

A plot of

$$\frac{Q_a}{Q_s}$$

vs D is shown in Figure 6 for wavelengths (λ) of 1.24, 3.21, and 10 cm at 20°C where Q_a is the absorption cross section and Q_s is the scattering cross section, and D is the rain drop diameter in millimeters. The theoretical relationship

$$\frac{Q_a}{Q_s} = \left(\frac{3 \lambda^3}{2 \pi^3 D^3} \right) \frac{\text{Im}(-K)}{|K|^2}$$

is employed for

$$\frac{\pi D}{\lambda} \leq 0.1.$$

The values of $\text{Im}(-K)$ and $|K|^2$ are obtained from Table II. The Laws and Parsons size distribution is assumed in the calculation of Q_a/Q_s . This figure verifies that absorption greatly exceeds the scattering for all wavelengths considered here, particularly at the greater wavelengths, for spherical droplets that are small compared to the wavelength, i.e., Rayleigh case. It also shows that as the drop size increases, the ratio of Q_a/Q_s sharply diminishes at all wavelengths.

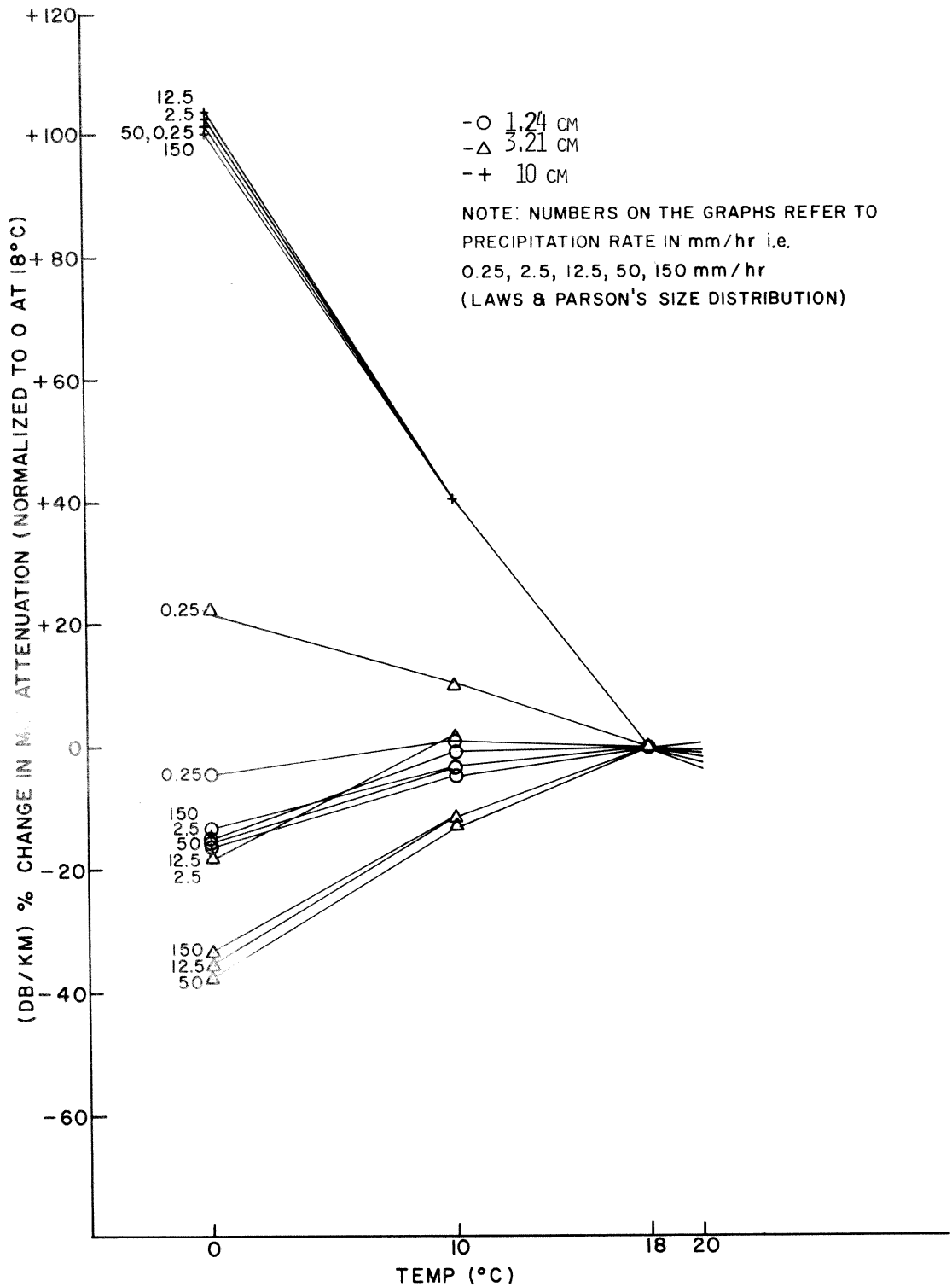
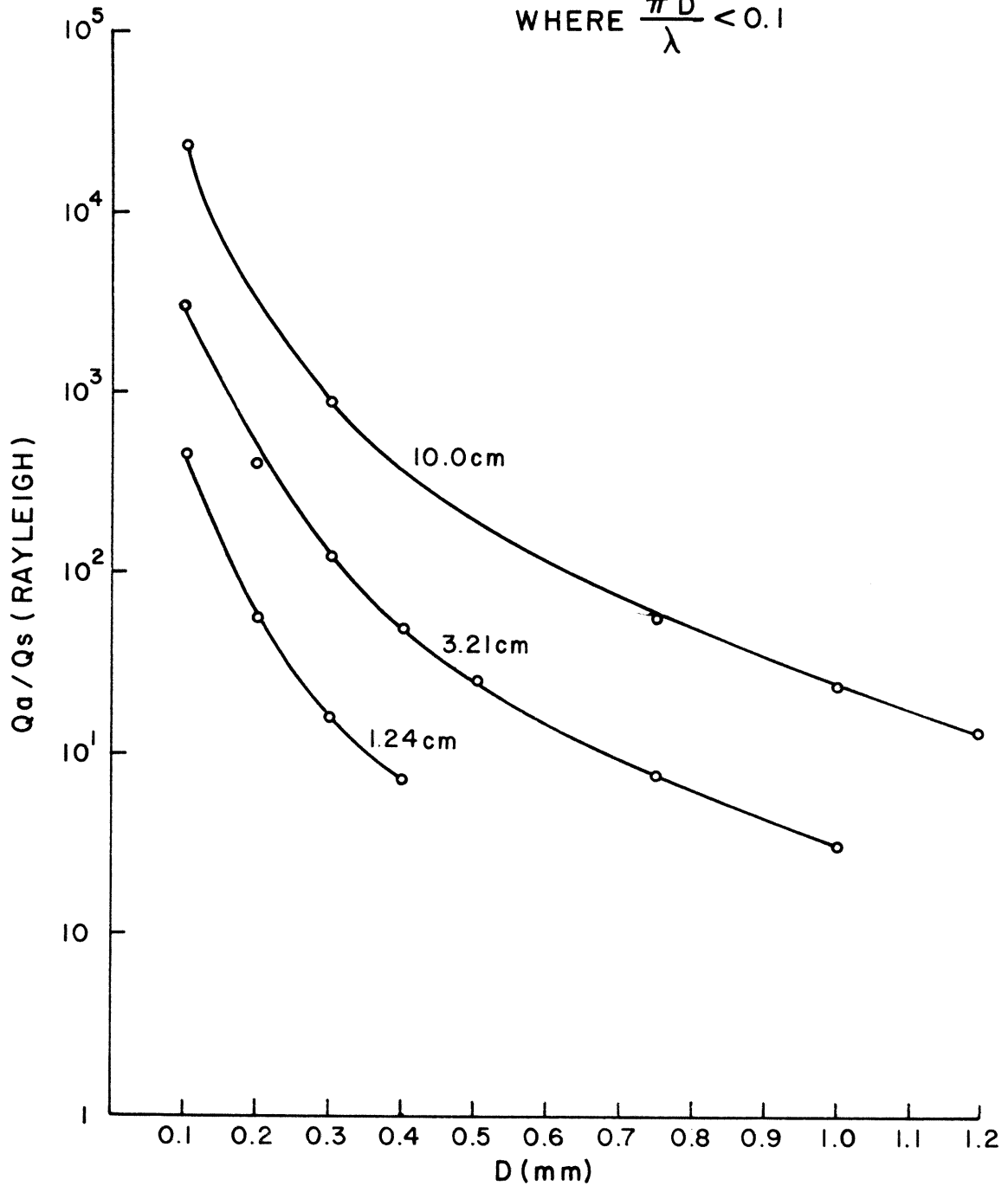


FIG.5 PERCENTAGE CHANGE IN MIE ATTENUATION VS TEMPERATURE (NORMALIZED AT 18°C) FOR DIFFERENT RAIN INTENSITIES FOR $\lambda = 1.24, 3.21, 10$ CM

LAWS & PARSONS
 SIZE DISTRIBUTION &
 WHERE $\frac{\pi D}{\lambda} < 0.1$



$\frac{Q_a}{Q_s}$ (ABSORPTION) RAYLEIGH VS RAINDROP DIAMETER (D) FOR
 $\frac{Q_s}{Q_s}$ (SCATTERING) RAYLEIGH $\lambda = 1.24, 3.21, 10.0$ cm AT 20° C.

FIG. 6

The temperature correction factors from Ryde and Ryde [8], as applied to the Mie attenuation as a function of temperature (normalized at 18°C), rain intensity, and wavelength, for the Laws and Parsons size distribution, are shown in graphical form in Figure 5. The general tendency is for the attenuation to increase with increasing temperature up to about 18°C for the 1.24 and 3.21cm wavelengths, as verified later in the empirical data analysis section. However, it is interesting to note that the reverse occurs for the 10cm wavelength and for drizzle-type rain (0.25mm/hr) in the case of the 3.21cm wavelength.

For the Mie case, Figure 7 (Setzer [11]) shows the ratio of the

$$\left(\frac{\text{absorption coefficient}}{\text{scattering coefficient}} \right)$$

vs rain and wavelength, on a log scale, for Laws and Parsons size distribution at 20°C. It can be noted that the scattering effects are very small as compared to the absorption effects except for the higher rain intensities in the K band when the ratio of the absorption to scattering diminishes to about a factor of two.

C. Parameter Variability

1. Variability in the Z-R Relationship: $Z = aR^b$

Table III (Borovikov and Kostraevev [12]) shows how widely the a and b parameters vary, not only according to the rain type and geographic conditions but also for a given rain type. This can be largely attributed to the wide variation of drop-size distributions plus the fact that many of the relationships involve the Rayleigh-type calculations where

$$Z = \sum_{i=1}^{i_2} n_i D_i^6$$

with n = number of drops of diameter D in a unit volume, with D varying in diameter from i_1 to i_2 .

Table III shows how the a and b parameters can vary for particular storm types, e.g., thunderstorms, showers, steady, and orographic rains. For example, for orographic rain, a and b vary from about 20 to 100 and 1.5 to 1.7, respectively, while for thunderstorms the coefficients vary from approximately 250 to 485 and from 1.4 to 2.4, respectively.

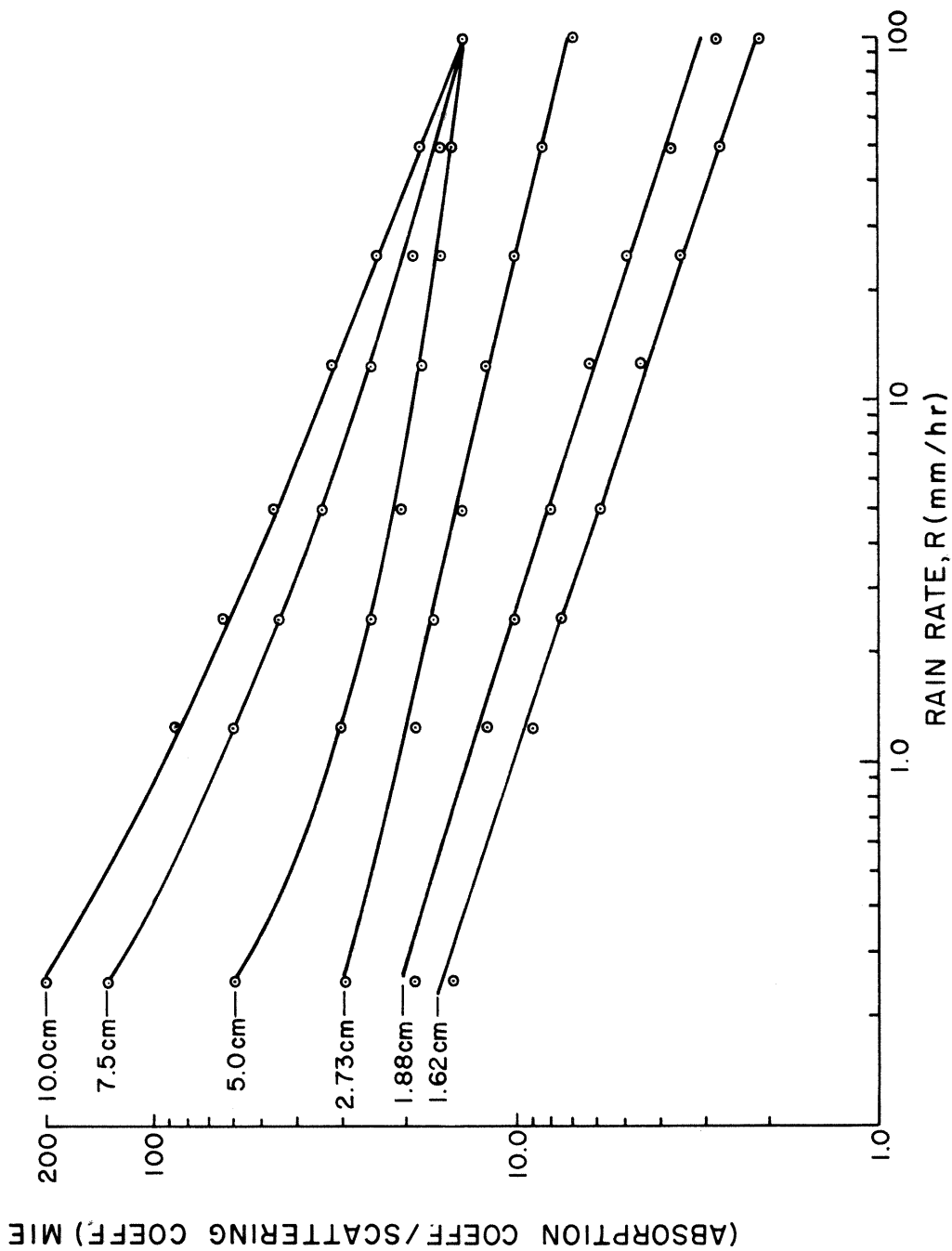


FIG. 7 RATIO OF THE MIE ABSORPTION COEFFICIENT TO THE SCATTERING COEFFICIENT vs RAIN RATE & WAVELENGTH. (SETZER [11])

TABLE III

Values of Parameters in $Z=aR^b$ relationships obtained by various authors from measurement data on raindrop-size distribution.

a	b	Author and Year	Location	Description
320	1.44	Wexler, 1947/104, from the data of Laws and Parsons, 1943/77/	Washington, USA	Showers
214	1.58	Wexler, 1947/104/ from the data of Laws and Parsons, 1943/77/	Washington, USA	Showers
224	1.54	Best, 1947/38/	Ainislas[sic], England	Rain showers
630	1.45	Best, 1947/38/	Shoeburyness, England	Rain showers
208	1.53	Anderson et al., 1947/37/	Hawaiian Islands	Various rains (probably nonorographic)
190	1.72	Marshall and Palmer, 1948/81/	Various loca- tions	Various types of rain
220	1.60	Marshall and Palmer, 1948/81/	Various loca- tions	Various types of rain
295	1.012	Hood, 1950/62/	Canada	Rain showers
180	1.55	Boucher, 1951/40/	Cambridge, Massachusetts, USA	Steady rains, showers and thunderstorms
31.0	1.71	Blanchard, 1953/39/	Hawaiian Islands	Orographic rain. Within cloud.
16.6	1.55	Blanchard, 1953/39/	Hawaiian Islands	Orographic rain. At Lower Cloud Boundary
290	1.41	Blanchard, 1953/39/	Hawaiian Islands	Thunderstorms
396	1.37	Jones, 1955/67/	Central Illinois USA	Various types of rain
486	2.37	Jones, 1955/67/	Central Illinois USA	Thunderstorms
380	1.24	Jones, 1955/67/	Central Illinois USA	Showers
313	1.25	Jones, 1955/67/	Central Illinois USA	Steady rains
160	1.54	Litvinov, 1956/12/	El'brus, USSR	Melting granular snow
257	1.55	Litvinov, 1956/12/	El'brus, USSR	Melting medium-granular snow
398	1.47	Litvinov, 1956/12/	El'brus, USSR	Melting nongranular snow
162	1.16	Atlas and Chmela, 1957/33/	Lexington, USA	Steady rains

TABLE III (cont)

a	b	Author and Year	Location	Description
215	1.34	Atlas and Chmela, 1957/33/	Lexington, USA	Steady rains
350	1.42	Atlas and Chmela, 1957/33/	Lexington, USA	Steady rains
310	1.34	Atlas and Chmela, 1957/33/	Lexington, USA	Steady rains
220	1.54	Saltman, 1957/21/from the data of Polyakova and Shifrin 1953/19/	Leningrad Region USSR	Showers and steady rains
303	1.7	Shupyatskii, 1957/25/	Moscow Region, USSR	Various types of rain, at rates of: up to 7 mm/hr between 7 and 60 mm/hr above 60 mm/hr
405	1.49			
289	1.59			
109	1.64	Ramana Murty & Gupta, 1959/88/	Kandla, India	Orographic monsoon rains
342	1.42	Ramana Murty & Gupta, 1959/88/	Delhi, India	Nonorographic monsoon rains
217	1.41	Jones & Mueller, 1960/69/	Miami, USA	Steady rains
292	1.42	Jones & Mueller, 1960/69/	Champagne, III USA	Steady rains
144	1.60	Jones & Mueller, 1960/69/	Miami, USA	Showers
251	1.56	Jones & Mueller, 1960/69/	Champagne, III USA	Showers
263	1.67	Jones & Mueller, 1960/69/	Miami, USA	Thunderstorms
256	1.67	Jones & Mueller, 1960/69/	Champagne, III USA	Thunderstorms
219	1.41	Sivaramakrishnan, 1961/93/	Poona, India	Thunderstorms
67.6	1.94	Sivaramakrishnan, 1961/93	Poona, India	Steady rains
66.5	1.92	Sivaramakrishnan, 1961/93/	Poona, India	Warm rains
204	1.70	Muchnik, 1961/16/	Kiev, USSR	Showers and steady rains

2. Attenuation Variability

Unexplained variability in attenuation measurements and estimates can occur as a result of the variation in the Z_e and attenuation relationship stemming from differing drop-size distributions. Also, nonrepresentative sampling due to large space and time variations can occur.

Large and real variations in attenuation can occur in space and time due to large gradients associated with convective shower cells and bands of showers or thunderstorms. Figure 8 shows the large intensity variations which occurred in a vertical cross section within a single thunderstorm during the early part of the mature stage in Ohio. Figure 9 shows the rain intensity variations (mm/hr) in two cells at Bedfordshire, England. The contours indicate the rapidity of significant changes which took place in only two minutes. Figure 10 illustrates significant changes taking place in a shower in Holmdel, New Jersey, within a time frame of only 10 seconds. It would be necessary, therefore, in making attenuation calculations for rain showers that short-period integrations be performed to obtain a better picture of the important changes occurring.

Figure 11 depicts wide variations of 1.97cm attenuation during a 4-hour rainstorm in Rosman, North Carolina on 1 October 1969. The attenuations are determined from direct satellite-to-earth-station measurements from the ATS-V experimental satellite. Starting with showers and ending as continuous rain and drizzle in this case (time percentage of occurrence also indicated in Figure 11 legend), the attenuation can vary by as much as a factor of ten. Table IV (Ippolito [13]) is presented to indicate weather category designations.

D. Path Diversity

Rain intensity and attenuation variations in three-dimensional space (or four dimensions, if one considers time) indicate the need to investigate the attenuations along more than one path. This would then lead to the determination of the outage time or the period during which the satellite-earth-terminal communication path becomes inoperative due to the signal fading or attenuation effects. Should the attenuation along one path exceed that along another, the communication system could be switched to the second path or vice versa. This alternating type of operation, which will increase communication reliability, is called switched-path diversity. Hogg [14] reports that this action can decrease the outage time by a factor of 10 or more, i.e., the attenuation drops below a critical time fading probability by a factor of ten. Figure 12 taken from Hogg [2] illustrates a case for Bedford, England, wherein a significant reduction in outage time was achieved by a space diversity of only 2km.

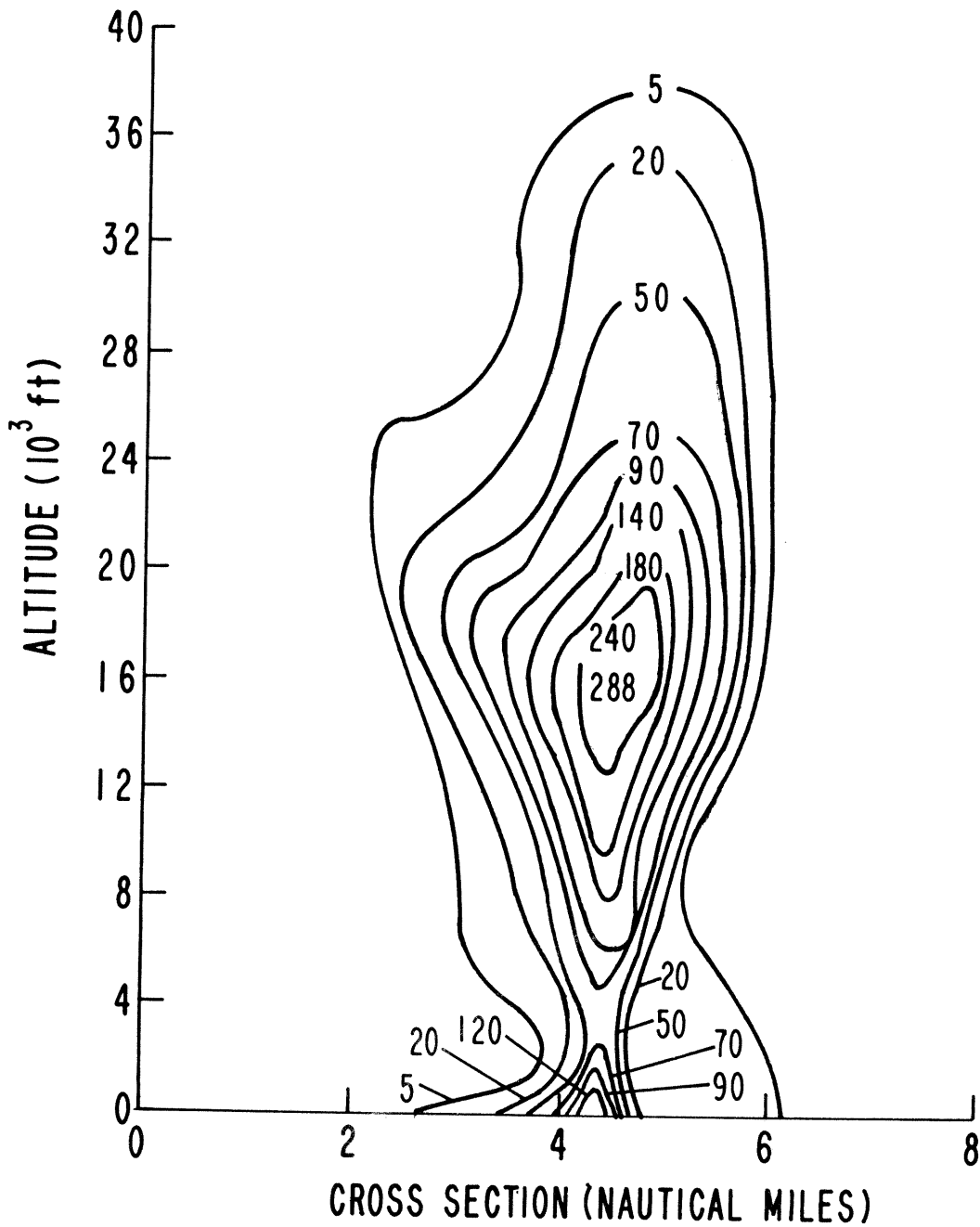


FIG. 8 WEST-EAST CROSS SECTION THROUGH AN OHIO THUNDERSTORM
 SHOWING THE DISTRIBUTION OF RAINFALL RATE IN mm h⁻¹.
 (HANDBOOK OF GEOPHYSICS [9])

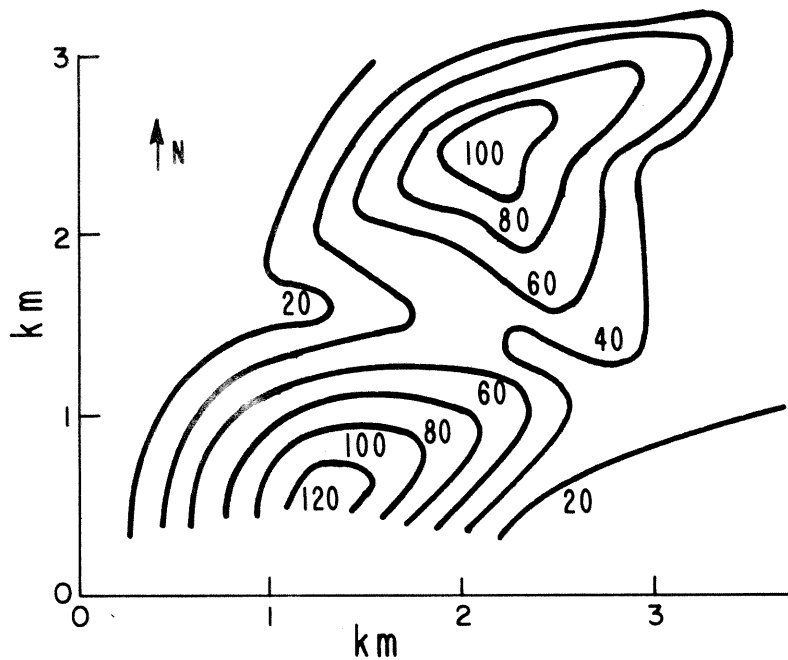
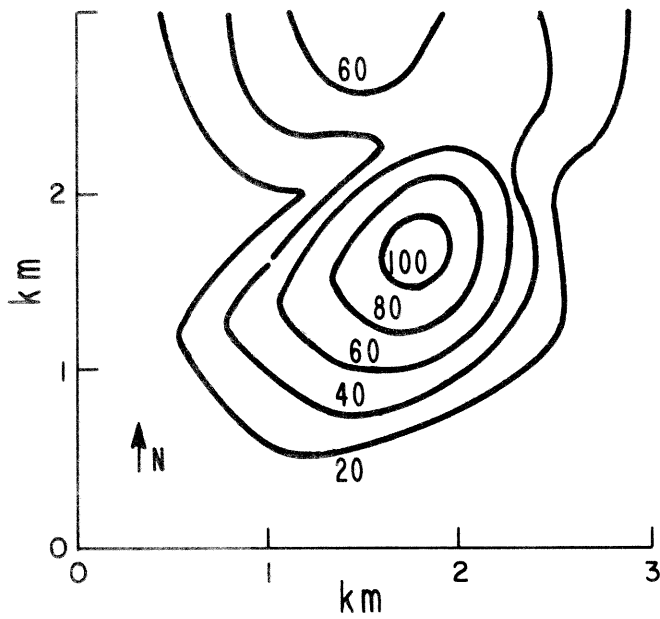


FIG. 9 (TOP) PLOT OF RAINFALL-RATE CONTOURS (IN MILLIMETERS PER HOUR), SHOWING TWO RAIN CELLS ON THE BEFORDSHIRE RAINGAUGE NETWORK; (BOTTOM) CONTOURS 2 MINUTES LATER (HOGG [2])

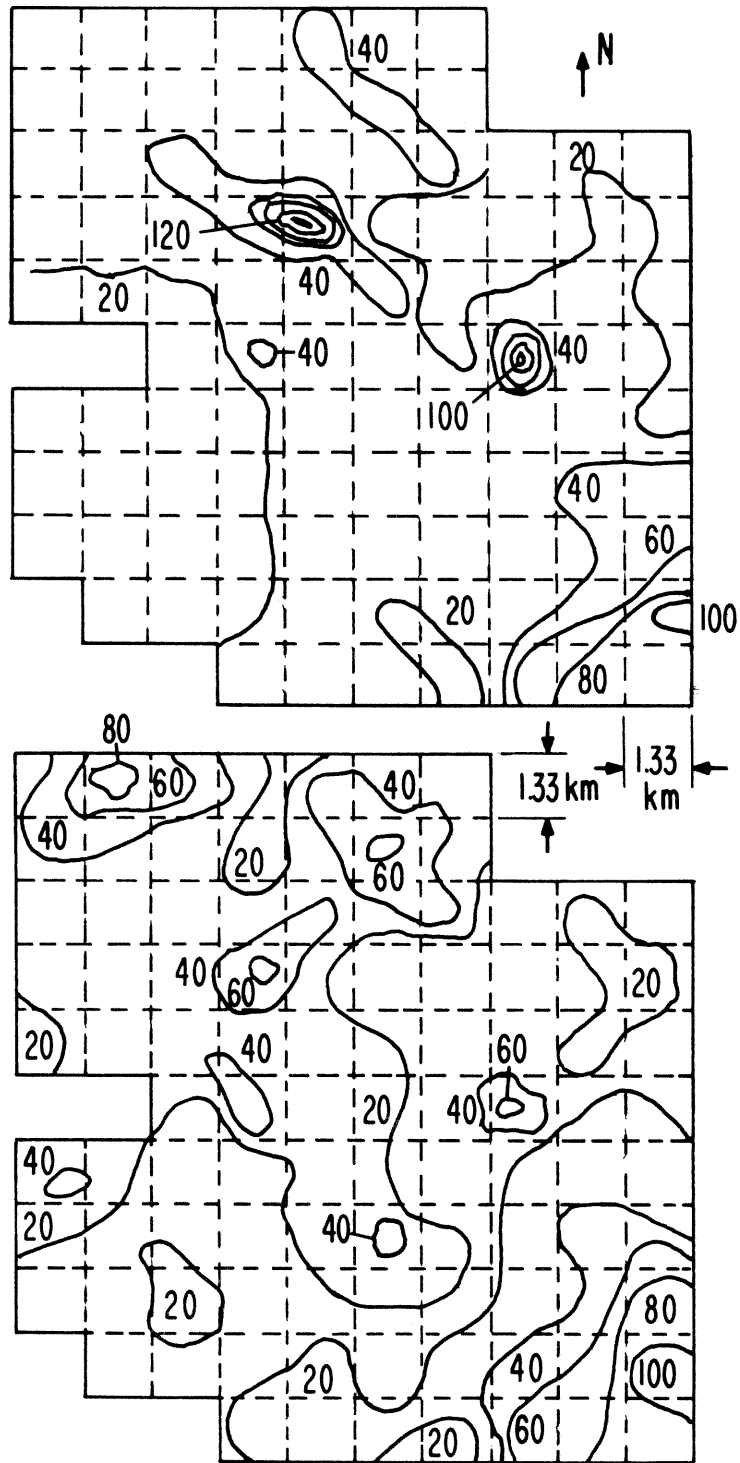


FIG. 10 (TOP) PLOT OF RAINFALL-RATE CONTOURS (IN MILLIMETERS PER HOUR) SHOWING SEVERAL RAIN CELLS ON THE HOLMDEL, NEW JERSEY RAIN-GAUGE NETWORK; (BOTTOM) TEN SECONDS LATER. (HOGG [2])

TABLE IV

WEATHER CATEGORY DESIGNATIONS
(in reference to Figure 11)

WEATHER CATEGORY	DEFINITION
• Fog drizzle	Localized dense cover, can include very light drizzle.
Δ Showers	Moderate to high intensity rainfall characterized by short durations and rapid fluctuations of intensity, as well as considerable variation in space. Rain of this type normally falls from clouds which extend to much higher altitudes than those causing drizzle.
0 Continuous rain	A uniform, light to moderate intensity rain which covers a relatively large geographical area, and which lasts for extended periods of time with a fairly constant rainfall rate. The drop sizes are larger than those associated with drizzle, and the associated cloud systems generally cover a larger geographical area than those associated with showers and thunderstorms.

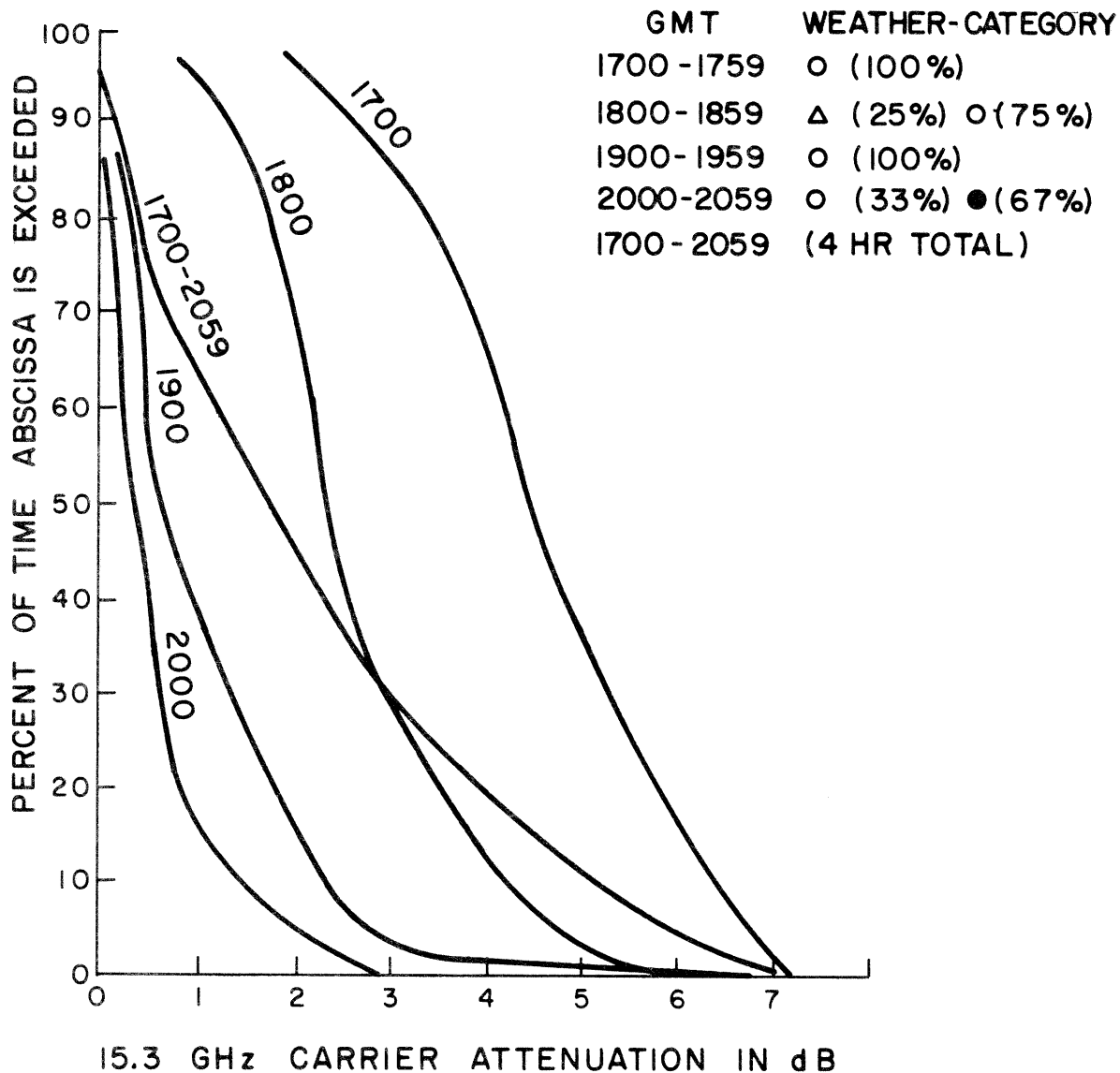


FIG. II % VARIATION OF 1.97 cm ATTENUATION VS TIME
 (AT ROSMAN, N.C., OCT. 1, 1969) (IPPOLITO [13])

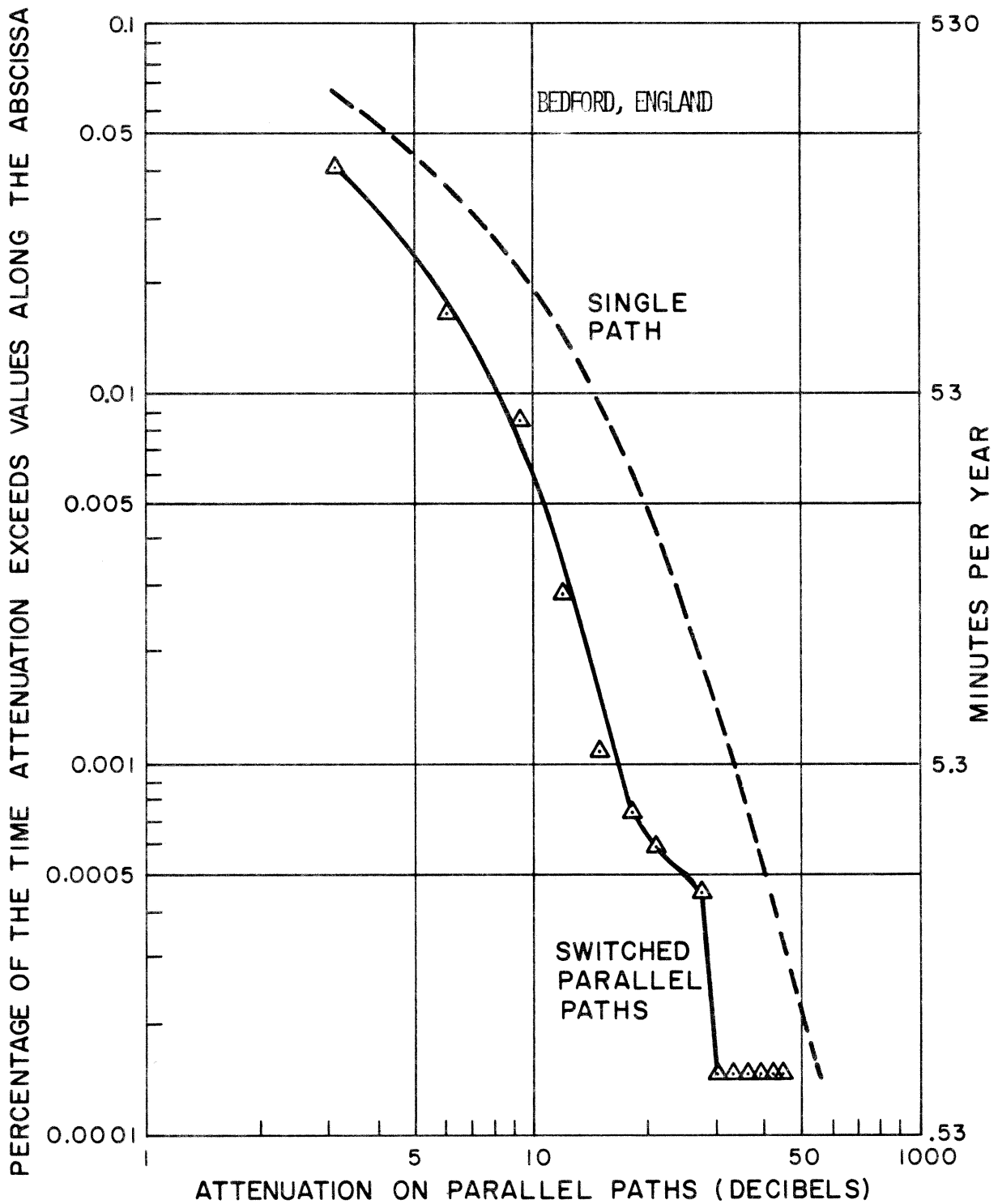


FIG. 12 DISTRIBUTION, IN PERCENTAGE OF TIME AND MINUTES PER YEAR, OF ATTENUATION AT FREQUENCY OF 30 GHz (HOGG [14])

Heavy, showery rains are generally quite localized at an instant in time which makes it possible to optimize terminal receiving station separations. However, the difficulty lies in identifying the areas, within and among storm cells at different altitudes, of sufficiently high intensities to pose an attenuation problem. Correlations of storm intensities and size distributions over the earth's surface should be established prior to the determination of optimum space diversity. Relationships of cell size to rain intensity require further study as does the correlation of point statistics at ground level with space statistics.

III. Data and Analysis

Although rainfall varies greatly from place to place, it is not feasible to measure rain attenuation parameters all over the world. It therefore becomes necessary to use whatever rainfall data are available to obtain correlations between the rain and attenuation vs probability of occurrence. This type of an approach is therefore largely adopted in the presentation and analysis of the following data from the Illinois State Water Survey Meteorological Laboratory (ISWSML). However, the communications engineer, in addition to the question of statistics on rainfall attenuation of the signal, is concerned with the variation of the precipitation intensity during short time intervals and over short distances so that he may design space or path diversity into his system, i.e., selecting significantly lower attenuation paths. Here is where rain gauges at optimum spacing plus drop-size distribution measurements at ground level would be particularly helpful.

To examine the complete scope of the attenuation prediction problem, answers to the following questions must be obtained through data collection and analysis:

1. How intense is the rainfall at ground level?
2. What is the spatial distribution of the rain at ground level?
3. What is the relationship between rainfall intensity and drop-size distribution at a point vs the average rainfall rate and drop-size distribution over an extended area?
4. How well do the ground measurements correlate with rain measurements within the cloud and between the cloud base and ground?
5. What percentage of time do rainfalls of different intensity and attenuation occur in different regions?
6. What is the true shape of the raindrop?
7. To what degree does absorption contribute to the total attenuation?

This section of the report, however, is devoted to providing some answers only to questions 1, 5, and 7.

The data reported in this section, based on raindrop-size distribution, is obtained through the original efforts of the Illinois State Water Survey Meteorological Laboratory (ISWSML). The ISWSML final report by E. A. Mueller and A. L. Sims [15] under contract DA-28-043-AMC-02071(E), with the Electronics Command, US Army, summarizes the results from drop-size distribution at different locations. Raindrop-size distributions at each of seven different geographic locations - Miami, Florida; Woody Island, Alaska; Corvallis, Oregon; Island Beach, New Jersey; Franklin, North Carolina; Bogor, Indonesia; and Majuro Atoll, Marshall Islands - were obtained by photographing drops with a special-built camera system similar to that described by Jones and Dean [16] and by Mueller [17]. This method involves a 70mm flash camera and optical system which samples 1/7 of a cubic meter of atmosphere near the ground seven times during a minute. This yields an atmospheric sample of one cubic meter. A drop-size distribution obtained from this one-minute sample is referred to as one sample of rain or one data point. The number of samples varied from 1703 in Corvallis, Oregon, to 4742 in Franklin, North Carolina, and represented approximately one year of data at each location. Drops of 0.4mm and greater diameter are measured by this method; however, the accuracy of the smaller size distribution is limited since the maximum overall accuracy expected is estimated to be + 0.2mm. Moreover, it is the equivalent spherical diameter of an elliptical drop that is recorded so that a rigorous analytical solution would require solutions from sources other than from the Mie scattering. The drop-size data collected by ISWSML have been converted to rainfall amounts, intensity, reflectivity, and attenuation by Mueller and Sims [15].

Table V shows the various geographic locations and the time periods involved for the ISWSML drop-size data. Table VI shows the γ (attenuation coefficient) vs R relationships for the different locations and for 0°C and 20°C water temperature based on computations dealing with mean class interval size distribution data and applying the method of least squares.

The following relationships are used for determining the appropriate precipitation parameters.

$$(1) R (\text{rainfall rate}) = k \int_{D_{\min}}^{D_{\max}} N(D) D^3 v(D) dD$$

where D is the drop diameter, N(D) is the number of drops of size D to D+dD, v(D) is the terminal fall velocity for a drop of size D and k is a unit adjusting constant. The v(D) values are those determined by Gunn and Kinzer [18]. This formulation assumes that the vertical velocity of the atmosphere is approximately zero.

TABLE V

LOCATION AND TIME PERIODS FOR THE ISWSML DROP-SIZE DATA

<u>LOCATION</u>	<u>PERIOD</u>
Miami, Florida	20 Aug 57.- 14 Aug 58
Corvallis, Oregon	19 Dec 57 - 28 June 58
Majuro Atoll, Marshall Islands	11 Mar 59 - 29 Apr 60
Woody Islands, Alaska	20 Aug 59 - 14 Aug 60
Bogor, Indonesia	31 Oct 59 - 10 Apr 61
Island Beach, New Jersey	30 Oct 60 - 24 May 62
Franklin, North Carolina	21 Dec 60 - 25 Mar 62

TABLE VI

TWO-WAY ATTENUATION COEFFICIENT (dB/km) VS RAINFALL RATE (mm/hr) FOR DIFFERENT GEOGRAPHIC LOCATIONS

20°C

Oregon	$\gamma(\text{dB/km}) = 1.82 \times 10^{-2} R(\text{mm/hr})$
Majuro	$\gamma = 2.37 \times 10^{-2} R$
Alaska	$\gamma = 2.07 \times 10^{-2} R$
New Jersey	$\gamma = 2.69 \times 10^{-2} R$
Indonesia	$\gamma = 2.92 \times 10^{-2} R$
North Carolina	$\gamma = 2.46 \times 10^{-2} R$

0°C

Oregon	$\gamma(\text{dB/km}) = 1.42 \times 10^{-2} R(\text{mm/hr})$
Alaska	$\gamma = 1.29 \times 10^{-2} R$
Florida	$\gamma = 2.25 \times 10^{-2} R$
Indonesia	$\gamma = 1.73 \times 10^{-2} R$
Illinois	$\gamma = 1.9 \times 10^{-2} R$
Majuro	$\gamma = 1.88 \times 10^{-2} R$
New Jersey	$\gamma = 1.85 \times 10^{-2} R$
North Carolina	$\gamma = 1.67 \times 10^{-2} R$

$$(2) \quad Z \text{ (computed reflectivity factor)} = \int_{D_{\min}}^{D_{\max}} N(D) D^6 dD$$

which appears in the expression for determining the radar back-scattering cross section for wavelengths $\geq 3\text{cm}$ when applying the Rayleigh theory.

(3) Z_e = the equivalent reflectivity factor which is computed using the Mie attenuation theory where $Z_e = 3.5 \times 10^3 \lambda^4 \sum \sigma_i$ and where σ_i = back-scattering cross section.

(4) The total attenuation (dB) and the attenuation coefficient computations (dB/unit distance) are based on the Mie attenuation theory.

The above-mentioned rainfall parameters, derived from the drop-size data taken at the various locations by the ISWSML, can then lead to the types of statistical attenuation models mentioned earlier.

The following graphs depict some of the results obtained from the data described above. Figures 13 and 14 show the variation of attenuation coefficient ratios for 1.87cm to 3.2cm and 3.2cm to 4.0cm wavelengths, respectively, with rain intensity for three different geographic areas. These curves are derived to provide a means for estimating $\gamma_{4.0\text{cm}}$ and $\gamma_{1.87\text{cm}}$ given the $\gamma_{3.2\text{cm}}$ vs R relationships that are developed.

Figure 15 shows the relationship between the scattering albedo and the reflectivity factor for a 3.2cm wavelength and water temperature of 18°C at Island Beach, New Jersey. The scattering albedo parameter can be defined as the ratio of the total scattering cross section to the total attenuation cross section. This parameter thus is a measure of the percentage of the total attenuation which is due to scattering and thereby also indicates the percentage that is due to absorption.

Note in Figure 15 that the albedo quickly increases with increasing reflectivity once the reflectivity approaches $10^4 \text{mm}^6/\text{m}^3$. This effect would thus correspond to a noticeably greater albedo following a sufficient increase in the rain intensity. Once the rain intensity increases beyond a certain point, an accompaniment of sufficient larger raindrops occurs which results in a significantly greater degree of scattering. Moreover, it is noteworthy that Figure 15 verifies the overall amount of scattering that occurs (< 10%) in comparison with the absorption for X-band radiation. It is interesting to compare the results presented in Figure 15 with those presented in Figure 7 (page 17), since Figure 7 was based on a Laws and Parsons drop-size distribution while Figure 15 was based on drop-size data collected by ISWSML at Island Beach, New Jersey. The figures compare favorably and confirm that scattering normally constitutes less than 10 percent of the total attenuation for X-band radia-

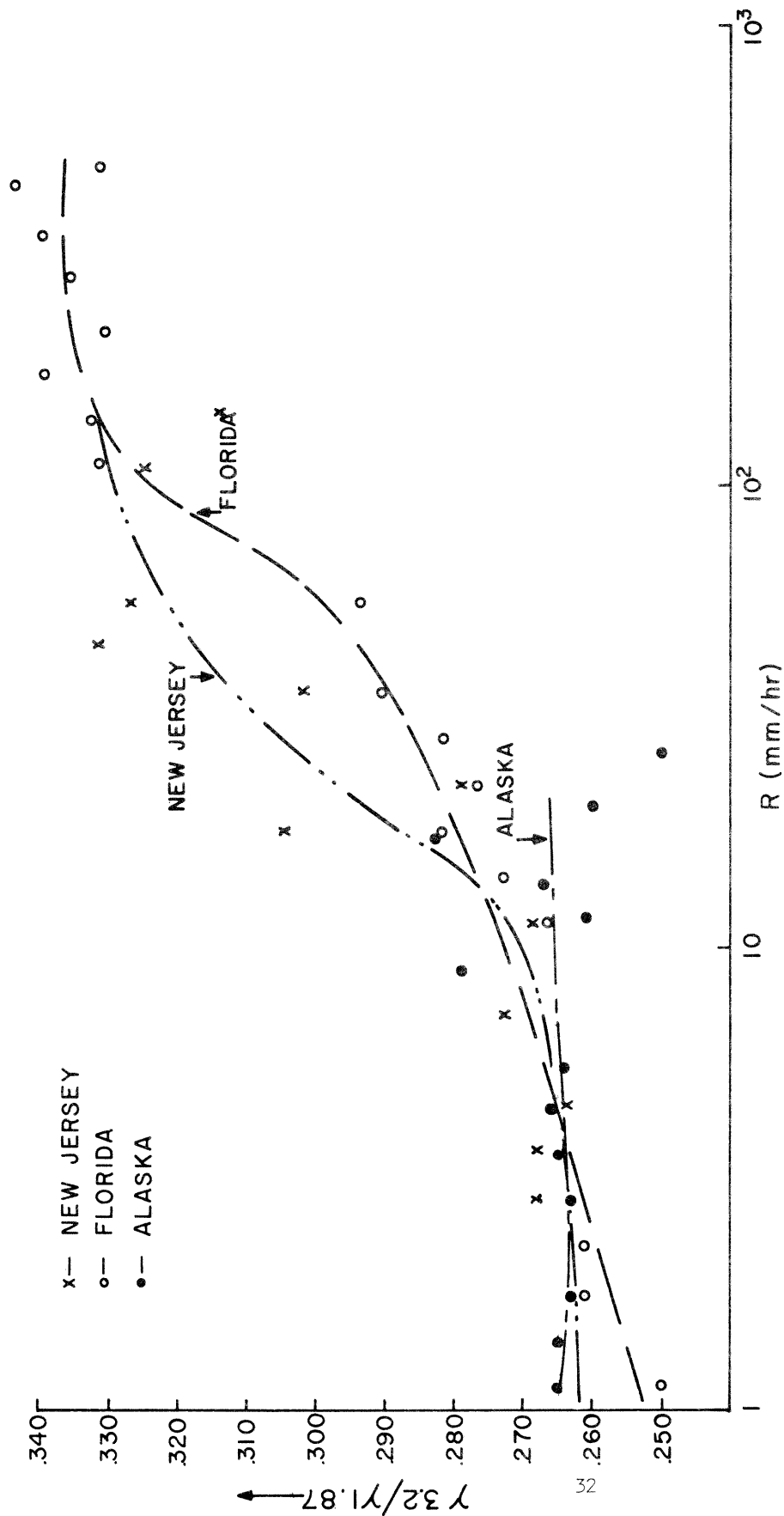


FIG. 13 RATIO OF 3.2 cm ATTEN. COEFF. TO 1.87 cm ATTEN. COEFF. vs RAINFALL RATE FOR DIFFERENT GEOGRAPHICAL LOCATIONS.

FLORIDA (○)
 NEW JERSEY (x)
 ALASKA (●)

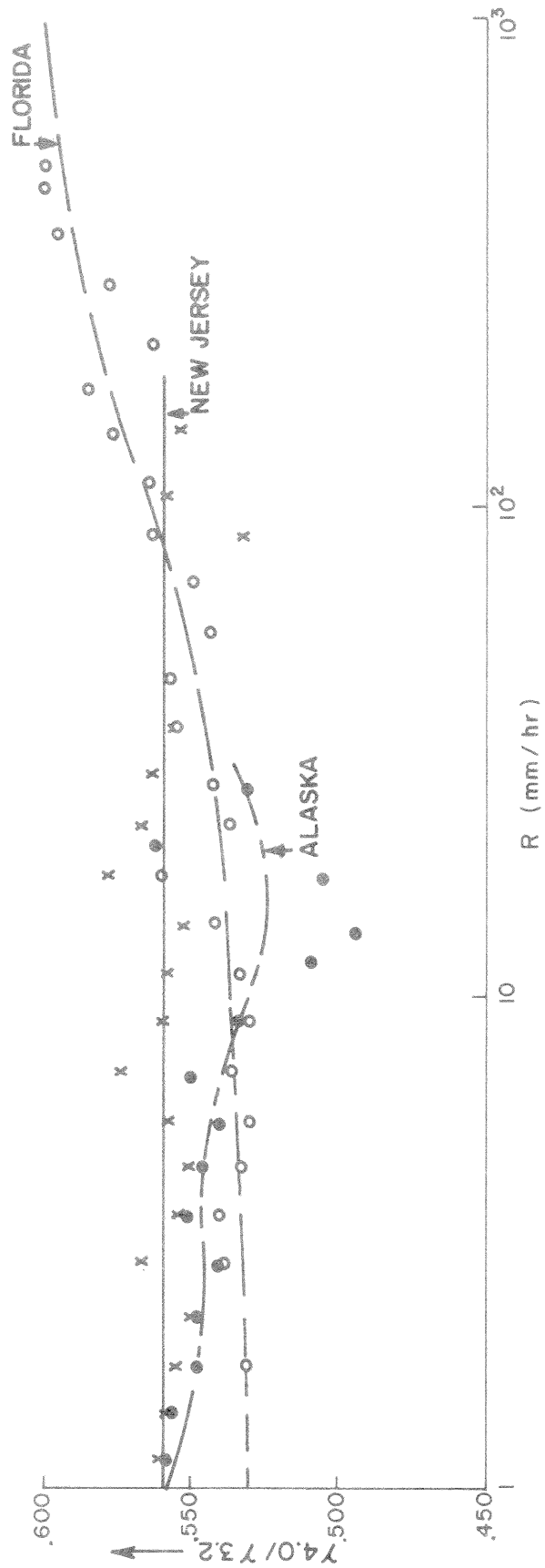


FIG. 14 RATIO OF 4cm ATTEN. COEFF. TO 3.2cm ATTEN. COEFF. vs RAINFALL RATE FOR DIFFERENT GEOGRAPHIC LOCATIONS

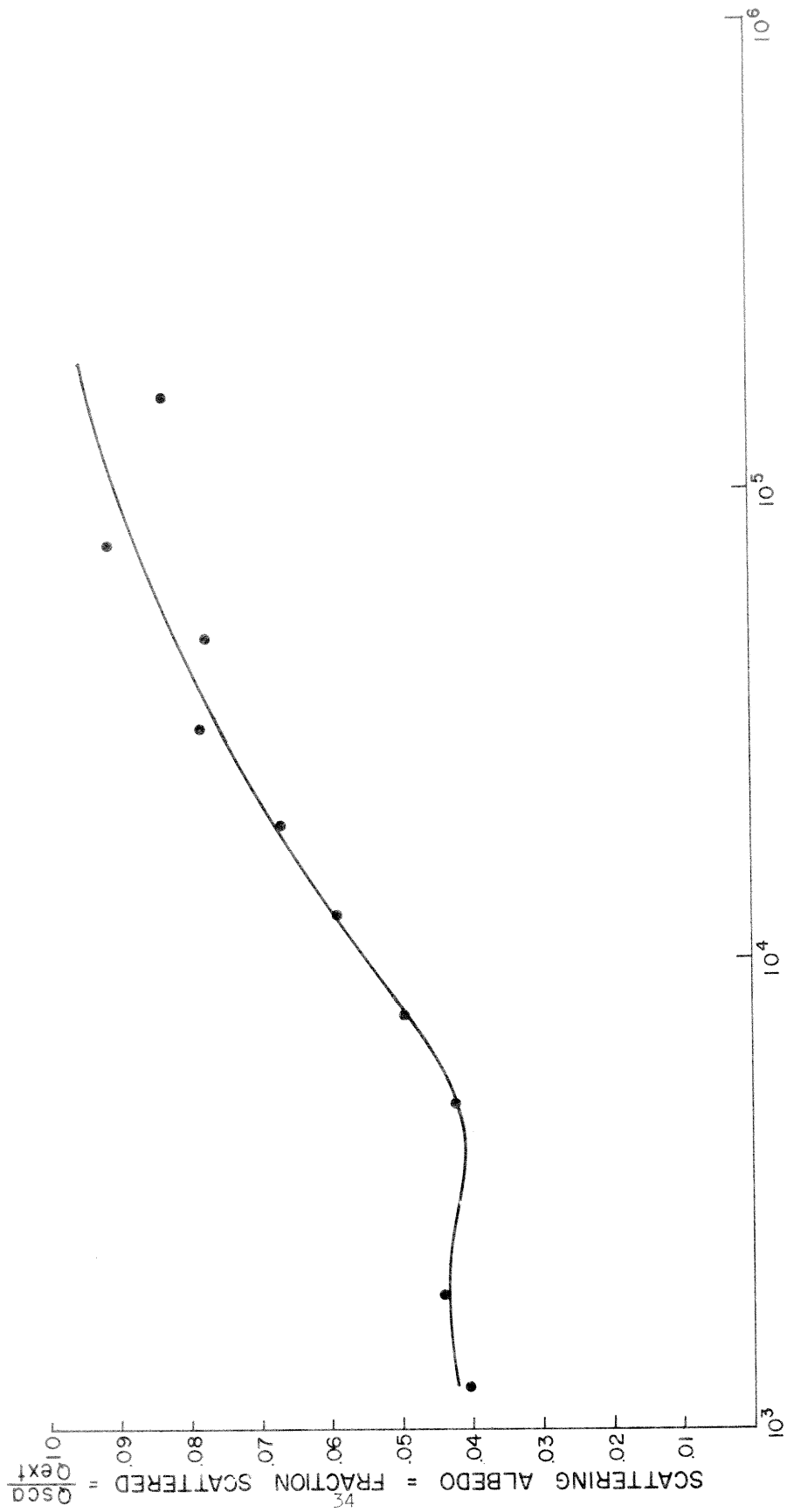


FIG.15 REFLECTIVITY FACTOR AT 3.2 cm, 18°C vs SCATTERING ALBEDO/ISLAND BEACH, N.J.

ation. With absorption, therefore, constituting > 90% of the total attenuation, it becomes possible to use the concept of effective noise temperature without encountering significant errors when the absorption coefficient is replaced by the attenuation coefficient.

Figure 16 relates the equivalent or Mie reflectivity factor to the Rayleigh reflectivity factor at 3.2cm, 18°C, for New Jersey and North Carolina locations. As the drops become proportionately larger with respect to wavelength, and as some of the drops become comparable in size to the wavelength, the difference between the Mie and Rayleigh back-scattering cross sections becomes significant. This is evident here in that the ratio of the Mie to Rayleigh reflectivity factor is increasing with an increase in the Rayleigh reflectivity factor due to a corresponding increase in the number of the larger drop sizes.

Figure 17 shows the relationship between the Mie calculated reflectivity factor, Z_e , at 3.2cm for 0°C and 20°C and the rainfall rate, R , in a New Jersey location. The Z_e values for the 0°C and the 20°C curves were derived from the relationship of Z_e to σ_{Mie} , i.e., $Z_e = 3.5 \times 10^3 \lambda^4 \Sigma \sigma_i$. The short-dashed curve was obtained from the long-dashed curve by applying the Mie-to-Rayleigh ratios given in Figure 15. In addition, Figure 17 provides a comparison between the Rayleigh and the Mie calculated reflectivity factors, wherein the Rayleigh results are obtained from Cataneo and Stout [19]. As one would anticipate, the difference between the Rayleigh reflectivity factor and the equivalent Mie reflectivity factor increases with increasing rain intensity.

With an increase of temperature from 0°C to 20°C, the equivalent reflectivity factor shows a marked increase, particularly for the greater intensities. It is also important to note that in the New Jersey area (Island Beach), where the raindrop sizes varied from about 0.5 to 4mm diameter [19], the Mie calculated Z_e vs R relationship is significantly different from the Rayleigh calculated Z vs R expression, particularly for the higher valued R , wherein the drop-size distribution shifts toward larger drop sizes.

Figures 18, 19, and 20 show some of the climatological aspects of rain intensity and attenuation probabilities for different geographic areas. Figure 18 is obtained by using the drop-size data collected at the various geographic locations by ISWSML and gives the probable number of minutes per year during which given rainfall rates are exceeded. Figure 19 is derived from Figure 18 and from the expressions relating γ_i to R in Table VI and is analogous to Figure 18 except that the abscissa is the attenuation coefficient. Figure 20, when compared with Figure 18, shows noticeable changes due to a temperature increase from 0° to 20°C, i.e., the curves shift toward higher attenuation coefficients with increasing temperature.

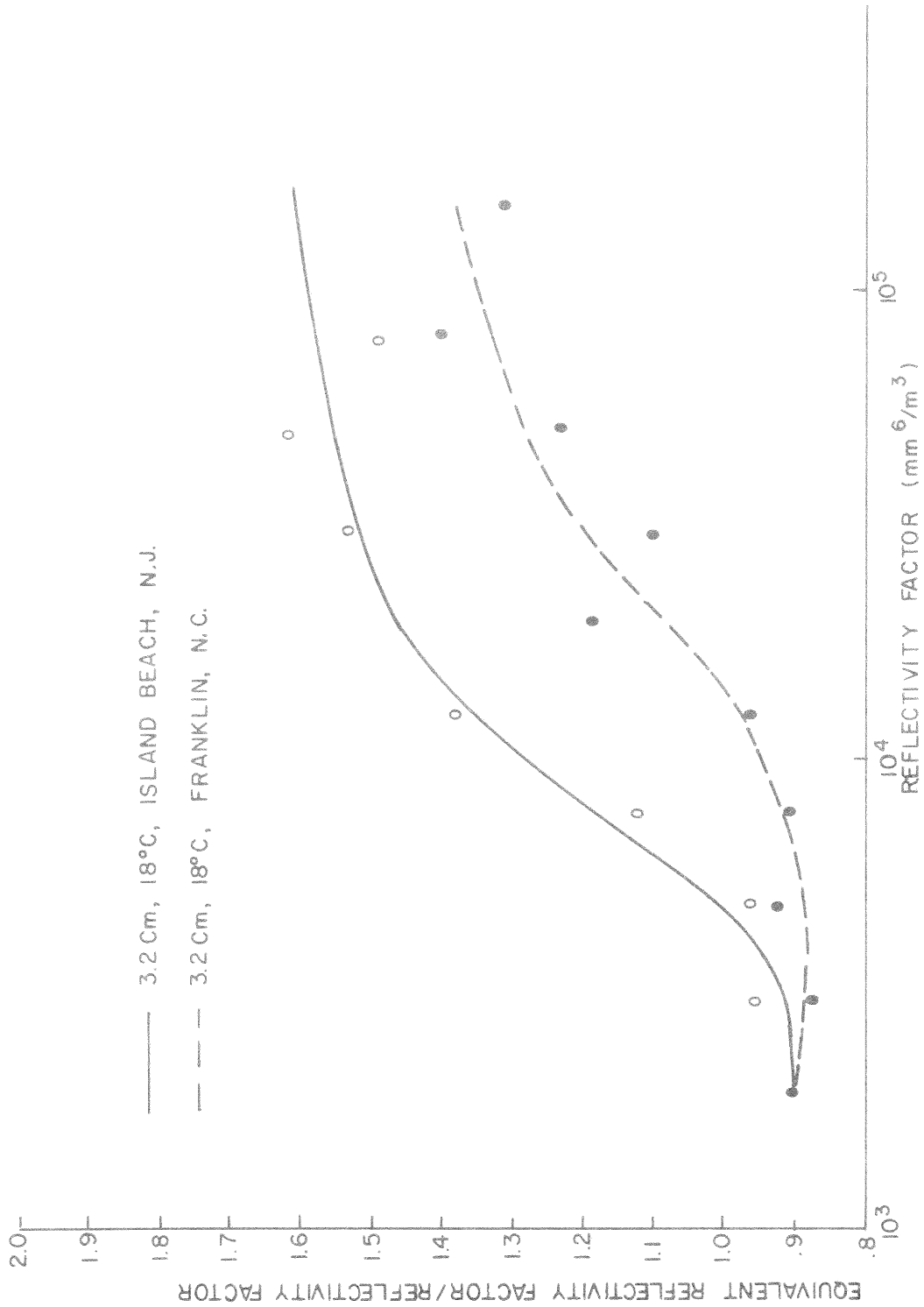


FIG. 16 EQUIVALENT (MIE) REFLECTIVITY FACTOR AT 3.2 Cm, 18°C vs REFLECTIVITY (RAYLEIGH) FACTOR AT 2 LOCATIONS

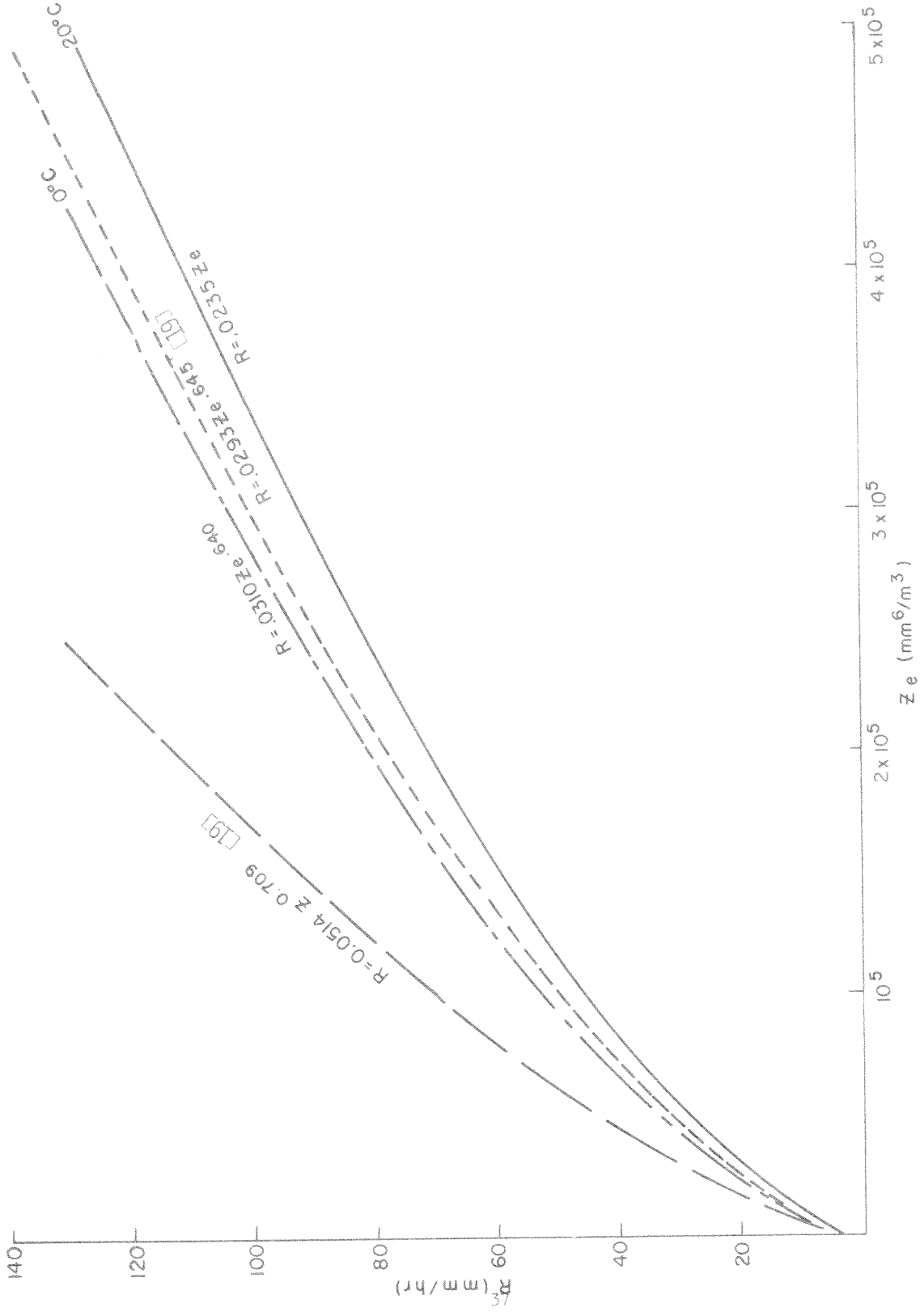


FIG. 17 RAINFALL INTENSITY vs REFLECTIVITY FACTOR & EQUIVALENT REFLECTIVITY FACTOR (MIE) AT 0°C AND 20°C IN THE NEW JERSEY AREA.

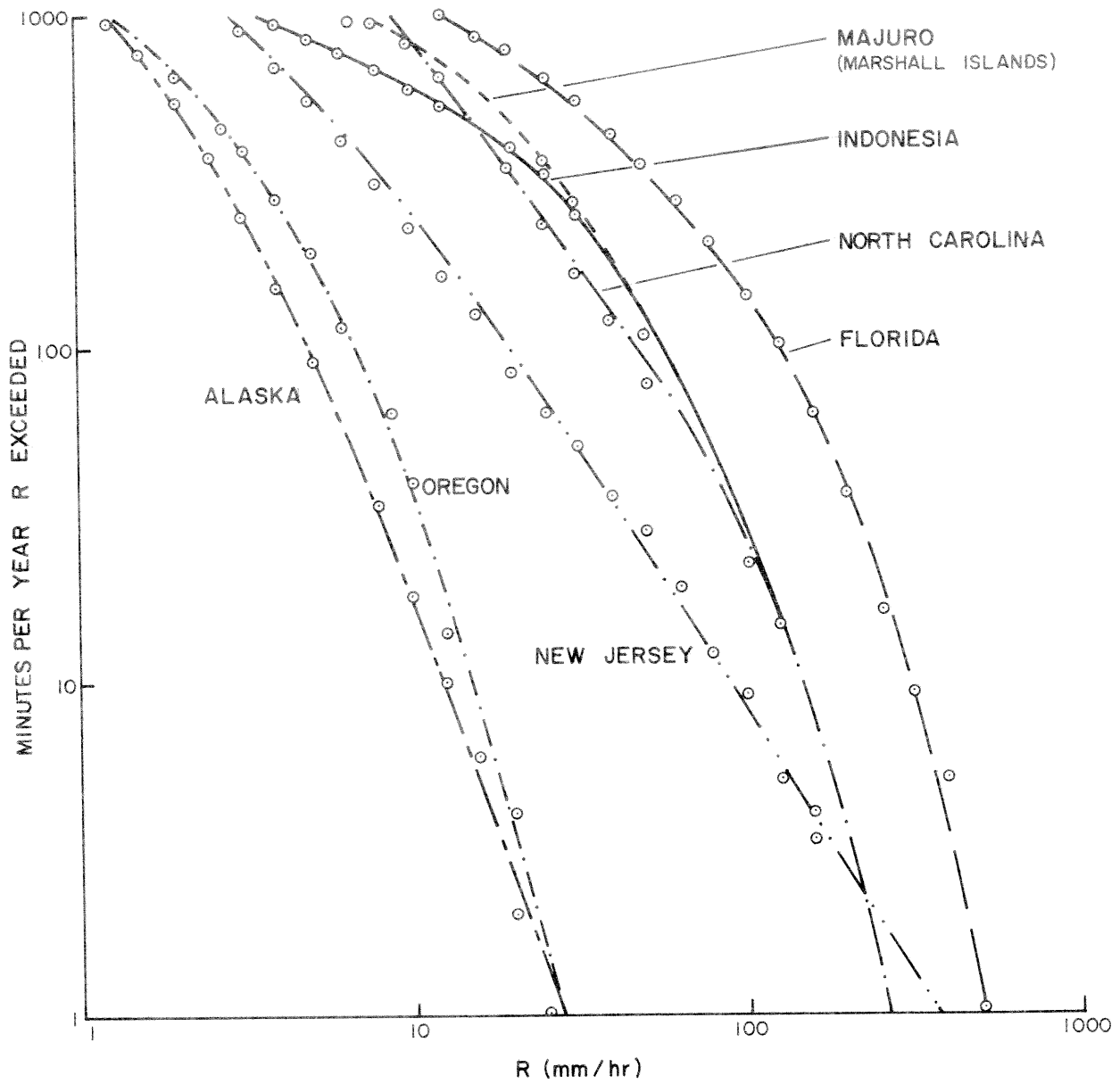


FIG. 18 RAINFALL INTENSITY OCCURRENCES FOR DIFFERENT GEOGRAPHIC LOCATIONS

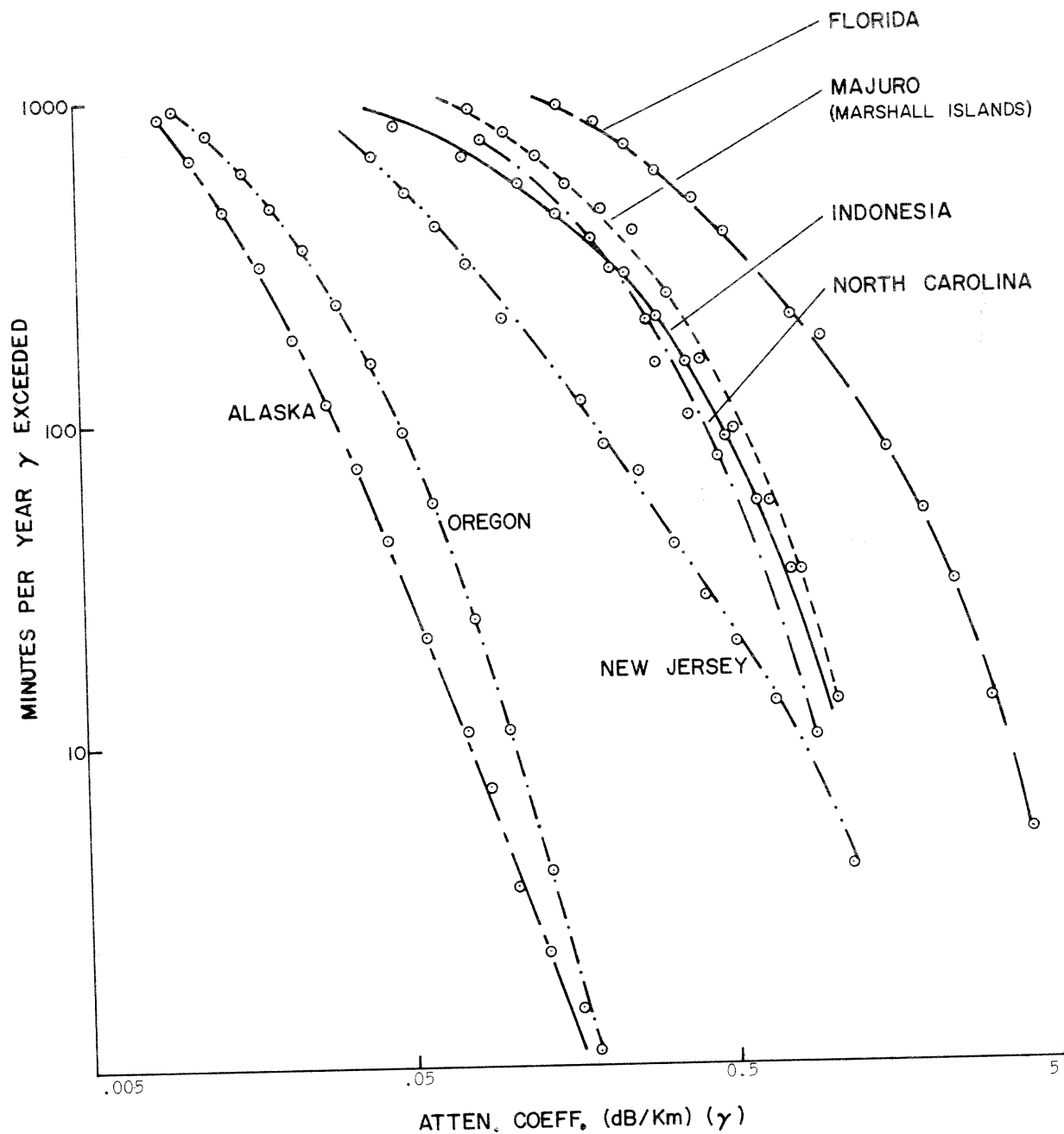


FIG. 19 ATTENUATION COEFFICIENT OCCURRENCES AT 3.2cm, 0°C FOR DIFFERENT GEOGRAPHIC LOCATIONS

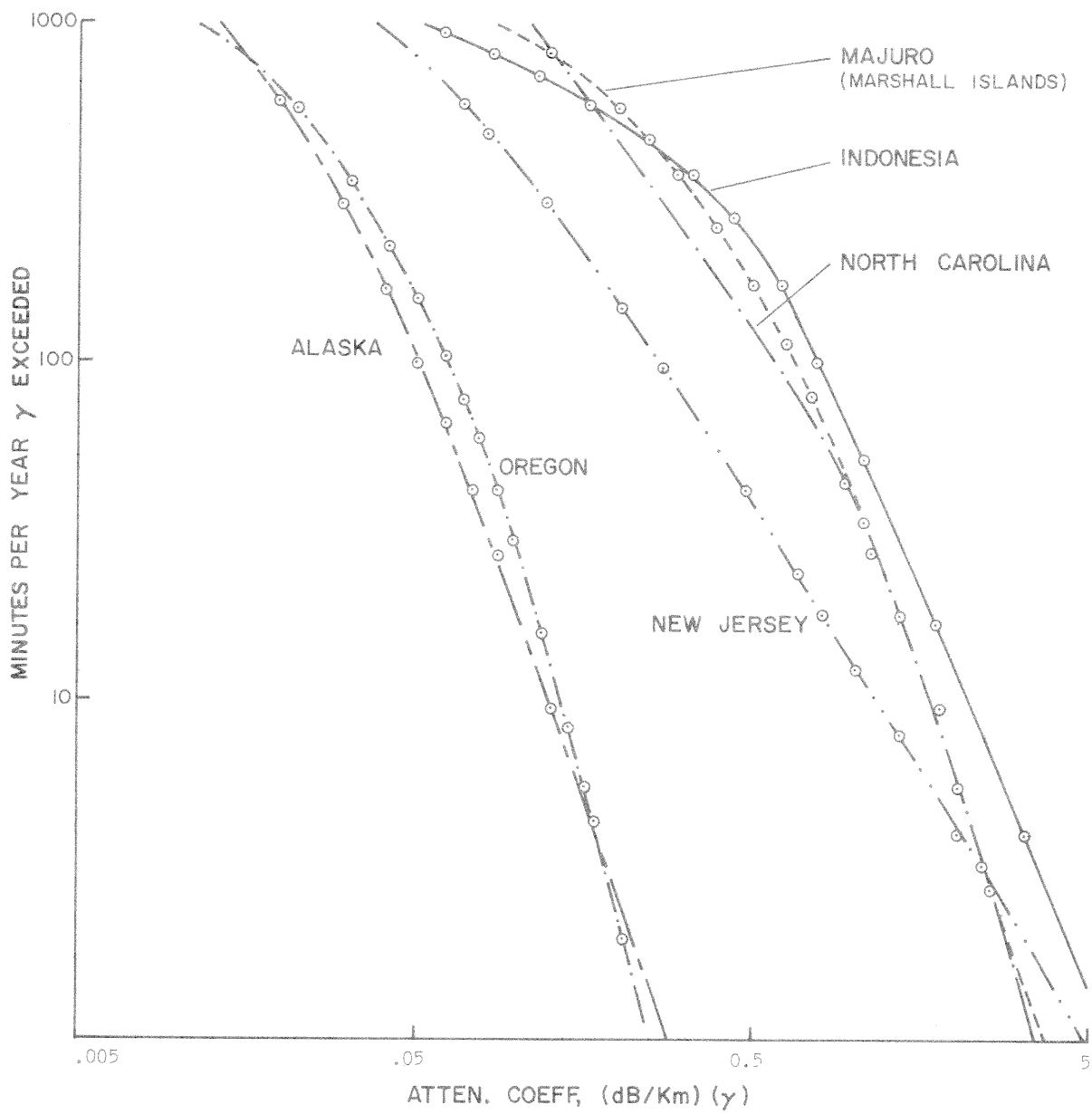


FIG. 20 ATTENUATION COEFFICIENT OCCURRENCES AT 3.2cm, 20°C FOR DIFFERENT GEOGRAPHIC LOCATIONS

The aforementioned information provides some of the statistics necessary to obtain adequate means for predicting the extent of long-term occurrences of any serious satellite signal degradations in any specific geographic location. Examination of Figures 18 and 19 reveals that there is a distinct geographic climatological variability, making it impossible to derive a universal relationship. These figures present strong evidence that the probability for greater attenuation is higher for the more southerly locations such as New Jersey, North Carolina, Marshall Islands, Indonesia, and particularly Florida as compared to the more northerly locations such as Alaska and Oregon. Moreover, it is of meteorological significance that the maximum attenuations occur in the Miami, Florida area, where convergence over the peninsula results in intense thunderstorm activity. It remains very questionable, however, as to what extent such statistics, as contained in Figures 18, 19, and 20, can be safely applied to other geographic regions. Moreover, adequate data are not presently available to enable one to apply, in general, the statistics of a given locality within a particular state or geographic region to those of another locality within the same state or geographic region. Before such attempts could be effectively carried out, it would be desirable to study the size distribution variations in the different localities for adequate periods of time.

The previous data and analysis, based on the ISWSML raindrop-size distributions, provide some answers to three of the seven questions raised earlier in this section concerning the intensity of rainfall, the percentage of time that rainfall of various intensity occurs in different regions, and the contribution of absorption to the total attenuation. The following further information concerning some of the remaining questions, however, are obtained from [14].

Bell Laboratories have conducted rainfall measurements with a network of 100 rain gauges distributed uniformly over a ground area of 10km^2 . The indicated rainfall for the complete rain-gauge network is sampled every 10 seconds, with a response time of one second. Contour maps of the rainfall derived from such a network indicate a cellular structure within the general rainfall. Their results indicated that rainfall intensities can change significantly within a 10-second interval and that while the probability of heavy rainfall may be high at a point, it may be low when averaged over an extended area or along a path. Further, the probability of an average rainfall rate of 150mm/hr along a 10km ground-to-ground path is two orders of magnitude less than the corresponding probability for a point along that path. They found that the average shape of raindrops is that of an oblate spheroid and that the drops are distributed in clumps rather than according to a well-defined size distribution. This latter finding tends to confirm the view that the Mie theory may not be strictly applicable to attenuation computations for raindrops.

A very important factor, mentioned earlier, is the outage time or period during which the satellite-earth-terminal communication path becomes inoperative due to signal fading. By making various assumptions (e.g., (1) the storm velocity and intensity over the propagation path between ground stations are constant and (2) the rainfall frequencies for the Mobile, Alabama area can be extended to other parts of the country in proportion to the distribution of annual point rates of one inch or more per hour), Hathaway and Evans [20] derived an approach to the problem of predicting outage time for ground stations at different separation distances due to rain for various geographic regions. Their results are shown in Figures 21 and 22. Figure 21 relates outage time to path lengths between ground stations for different parts of the USA. Figure 22 shows the geographic distribution in the USA of the outage time vs path length contours as represented in Figure 21.

IV Other Methods of Measuring Attenuation

Experimental data on the quantitative effects of rain on attenuation along earth-space communication paths are lacking. Theoretical treatment of the problem is hampered by the lack of detailed knowledge of rain characteristics such as the size distribution variations in the horizontal and vertical dimensions. Thus, the need for some other means for measuring the total atmospheric attenuation along the communication paths is apparent. Two possibilities are microwave radiometers and the dual-wavelength radar.

A. Effective Noise Temperature and the Microwave Radiometer

The rain is considered primarily as a medium whose emissivity equals its absorptivity and for which absorption constitutes the dominant term of attenuation indicated by the scattering curve presented in the preceding section. Absorbed radiation within the raindrops is emitted essentially as a black body, and this emitted radiation is recorded by the microwave radiometer, through its antenna, as the antenna temperature or the effective noise temperature. This effective noise temperature is affected by the temperature of the absorbing medium (rain in this case), the frequency or wavelength of the electromagnetic radiation, the angle of direction of the antenna, the absorption of the medium, and the temperature of any background source, such as the sun, cold sky, ocean, etc. The radiometer system has a very narrow field of view so that it measures the integrated absorption effects along a narrow cone containing the emitted radiation from all the absorbing matter in its path. This is made more feasible if the single and multiple scattering effects are negligible compared to the absorption, i.e., the single and total scattering albedos are negligibly small.

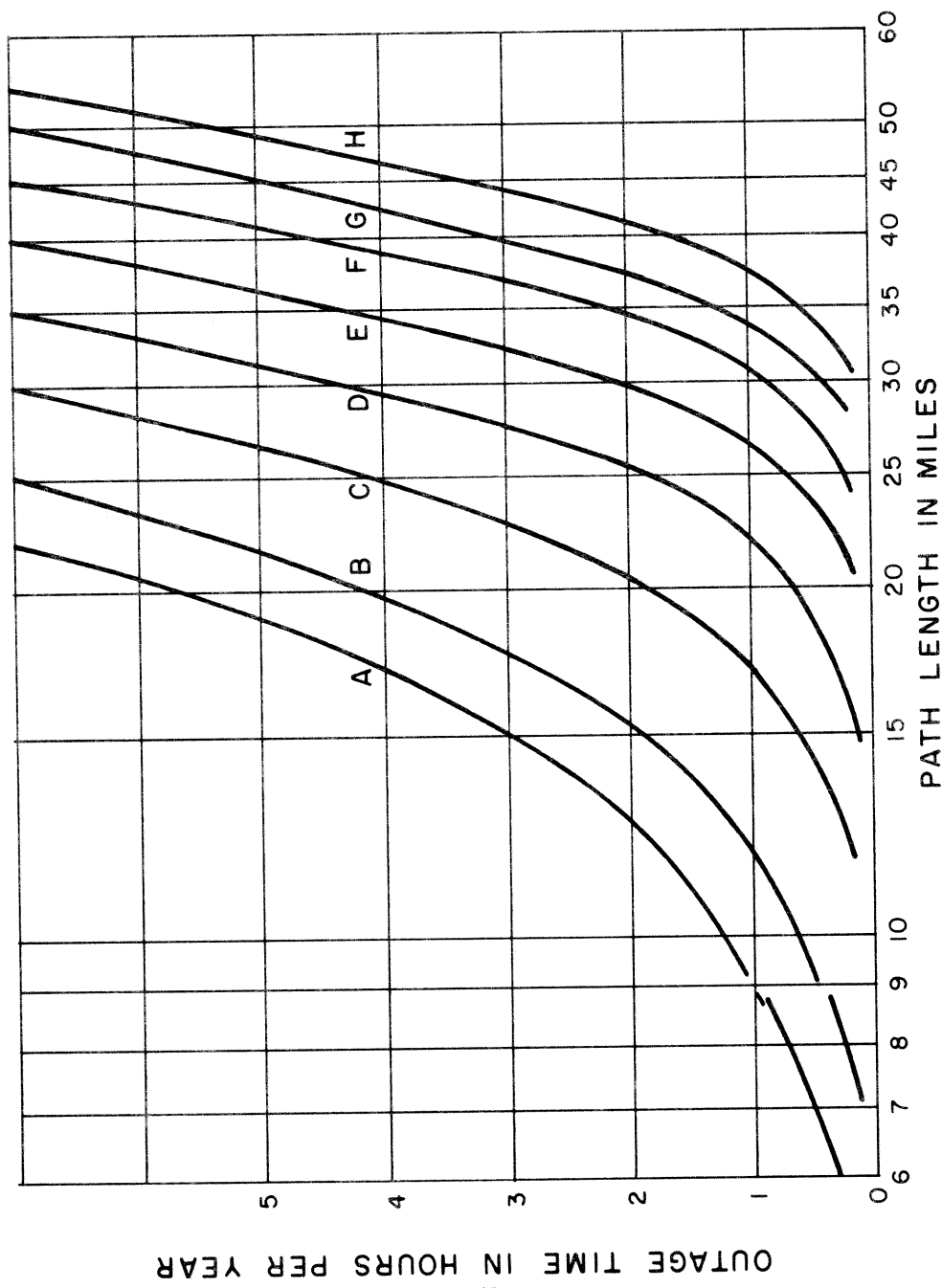


FIG. 21 EXPECTED OUTAGE TIME IN HOURS PER YEAR VS PATH LENGTH IN MILES FOR VARIOUS AREAS OF THE UNITED STATES (HATHAWAY & EVANS [20])

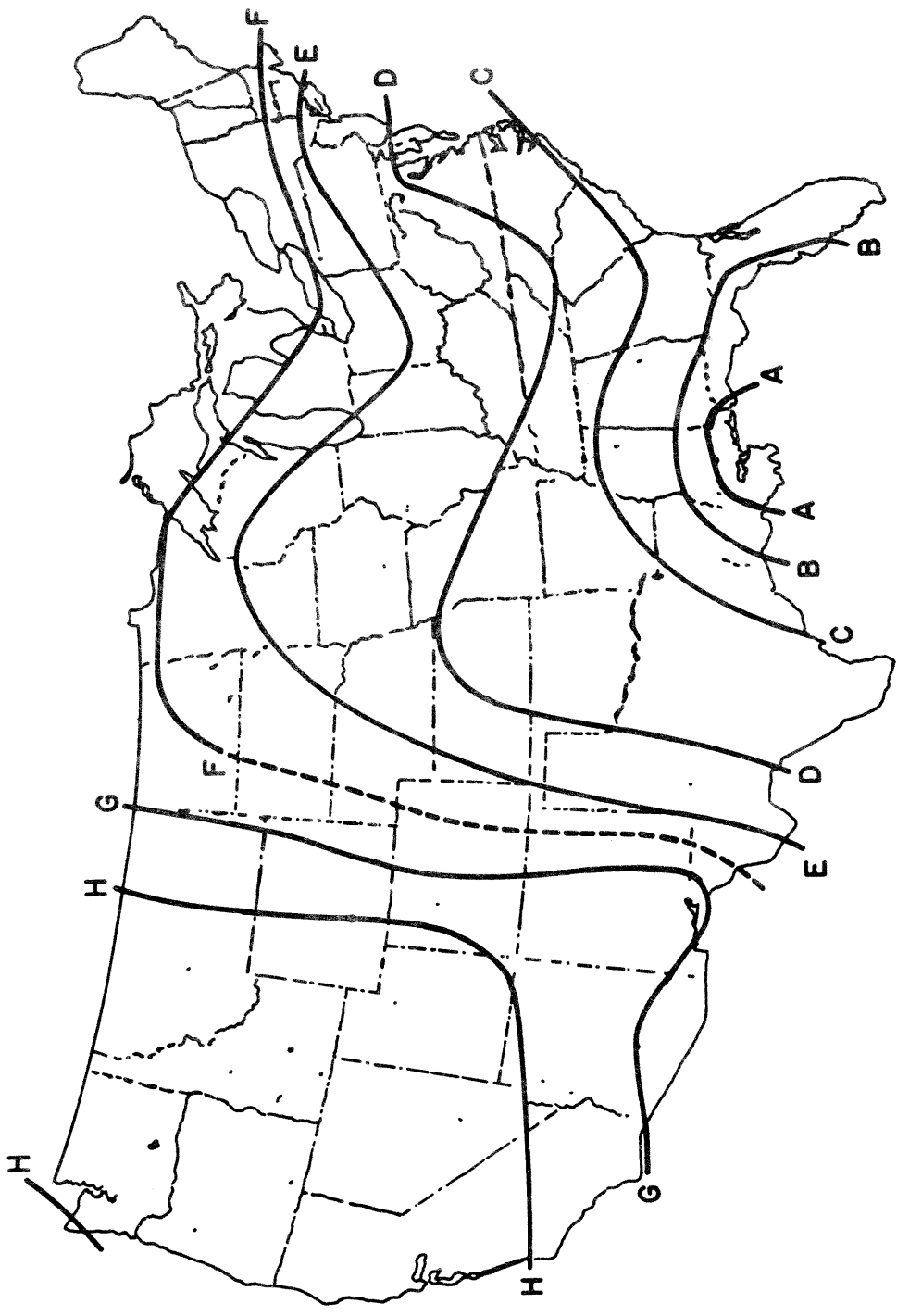


FIG. 22 CONTOURS OF CONSTANT PATH LENGTH FOR FIXED OUTAGE TIME. (HATHAWAY & EVANS [20])

A microwave antenna will transfer to its transmission line an amount of noise that is characteristic of the black-body radiation that it intercepts. The noise then becomes an additional limitation to the inherent main-equipment noise of the radar, resulting in a poorer value for the minimum detectable signal. The effective noise temperature, however, although a distinct disadvantage to the radar set, is the means by which the attenuation in an absorbing atmosphere is measured by the radiometer.

The concept of effective noise temperature arises from the equivalent black-body or thermal radiation emitted from a medium. It can be defined as that temperature that black bodies would have if they were radiating the same noise power. Kirchoff's, Planck's, and Rayleigh-Jeans' black-body radiation laws provide the theoretical foundation for the concept and quantitative evaluation of the effective noise temperature. Kirchoff's law establishes that any object in thermal radiation equilibrium with its surroundings, which absorbs energy, radiates the same amount of energy which it absorbs. This is also basically true of the atmosphere, and its constituents, which behave very much like a black body and emit thermal noise due to absorption properties and radiating temperature. The black-body radiating temperature is precisely defined by Planck's law for all frequencies, but for the case of the microwave frequency range dealt with here, the simplified version, known as the Rayleigh-Jeans' Law, is adequate.

The atmosphere's black-body emission temperature, measured by a radiometer, is related to the atmospheric attenuation by the radiation transfer theory. Under the assumption of a dynamic equilibrium in which the emission coefficient is related to the absorption coefficient and to Planck's and Rayleigh-Jeans' Laws by Kirchoff's black-body radiation law, the following expression is derived for a rain-filled, absorbing atmosphere, with no significant sources beyond

$$T_e = \int_0^{\infty} \frac{\alpha(s)}{4.34} T(s) \exp\left[-\int_0^s \frac{\alpha(s) ds}{4.34}\right] ds \quad (\text{Crane [21]})$$

where $\alpha(s)$ is the absorption coefficient in dB per unit length along the path s , which is approximately equal to the attenuation coefficient for the purposes of this study, $T(s)$ is the water drop temperature in degrees Kelvin ($^{\circ}\text{K}$), and T_e is the effective noise temperature in $^{\circ}\text{K}$ which the radiometer antenna "sees". Radiometer output, T_e , thus becomes a measure of the weighted integral of the attenuation in an absorbing medium along the path. Radar and radiometer measurements can then be compared after the appropriate range integral of the radar data has been computed. The measured value of T_e can then be used as an indirect method for evaluating the total absorption or attenuation in an absorbing medium by using an assumed or computed mean-absorption temperature for

the water droplets along the path. T_e would be measured at all elevation and azimuth angles to be encountered in operation with the satellite.

An example of a good correspondence between the measured attenuation of a received satellite signal at 15.3 GHz versus attenuation computed from the 16 GHz radiometer record at corresponding times during a rain storm is shown in Figure 23 (Penzias [22]). The dashed line corresponds to an attenuation ratio of 1:1 between 16 and 15.3 GHz, since the attenuation due to rain is taken to increase approximately with the square of the frequency in this wavelength region. The radiometer accuracy is ± 0.3 dB.

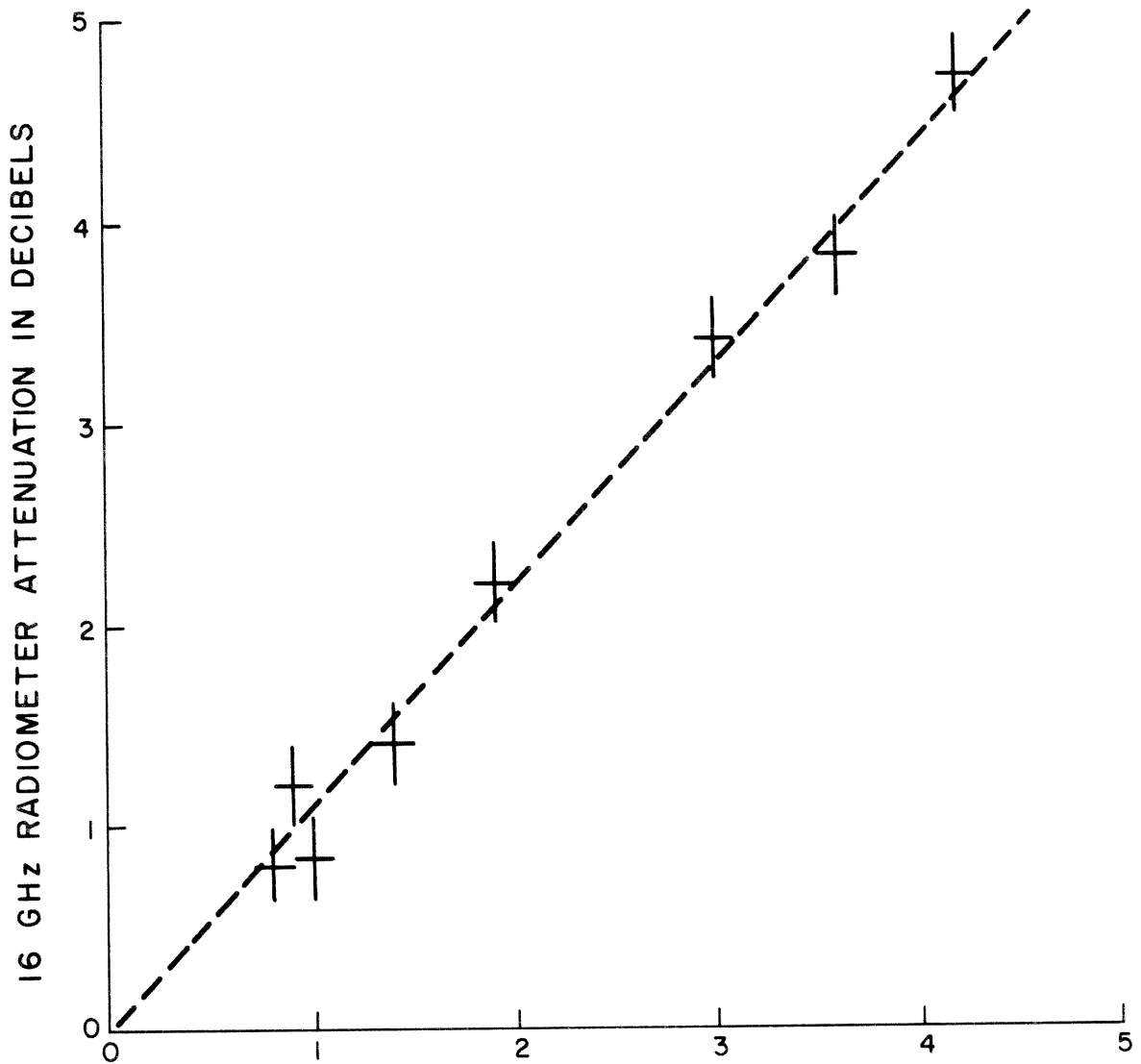
Figure 24 (Snider [23]) shows the sky brightness or effective noise temperature at 15 GHz as a function of elevation angle in the case of a clear sky (oxygen and water vapor effects) and light rain. For elevation angles less than about 20° the effective noise temperature increases sharply. The light rainfall curve of 5 mm/hr is determined on the assumption of a uniform rainfall. In general, however, computation of the rainfall effects requires summation of the losses due to the different rainfall intensities occurring along the communication path.

It must be emphasized that the radiometer measurements will give realistic values only in an absorbing atmosphere. Any degree of scattering, as indicated by the albedo factor, will introduce an error relative to the amount of scattering that occurs. For wavelengths under about 3.2cm, serious consideration must be given to the evaluation of errors due to the neglect of scattering effects for certain drop-size distributions.

B. Dual-Wavelength Radar

Radar methods previously employed for determining attenuation involve the determination of the reflectivity from the basic radar equation followed by a calculation of the attenuation from appropriate relationships such as Z_e vs R and γ vs R which lead to the γ vs Z_e relationship. Drop-size-distribution measurements then become necessary to obtain adequate relationships between Z_e vs R and γ vs R .

The technique that is briefly discussed here is essentially extracted from and described in further detail elsewhere (Eccles and Mueller [24]). This method employs two radar sets of different wavelengths located side by side and simultaneously ranging on identical volumes. The raindrops attenuate the average power received by each radar at different rates. The ratio of the average returned powers measured with the radars at the two wavelengths is a measure of the attenuation. It is desirable to choose one wavelength which is not attenuated by the rain, while the other wavelength is significantly attenuated. It is also preferable, but not necessary, for both wavelengths to be only slightly susceptible to attenua-



15.3 GHz SATELLITE SIGNAL ATTENUATION IN DECIBELS

FIG. 23 DATA RECORDED DURING STORM ON NOVEMBER 19 AND 20, 1969

(PENZIAs [22])

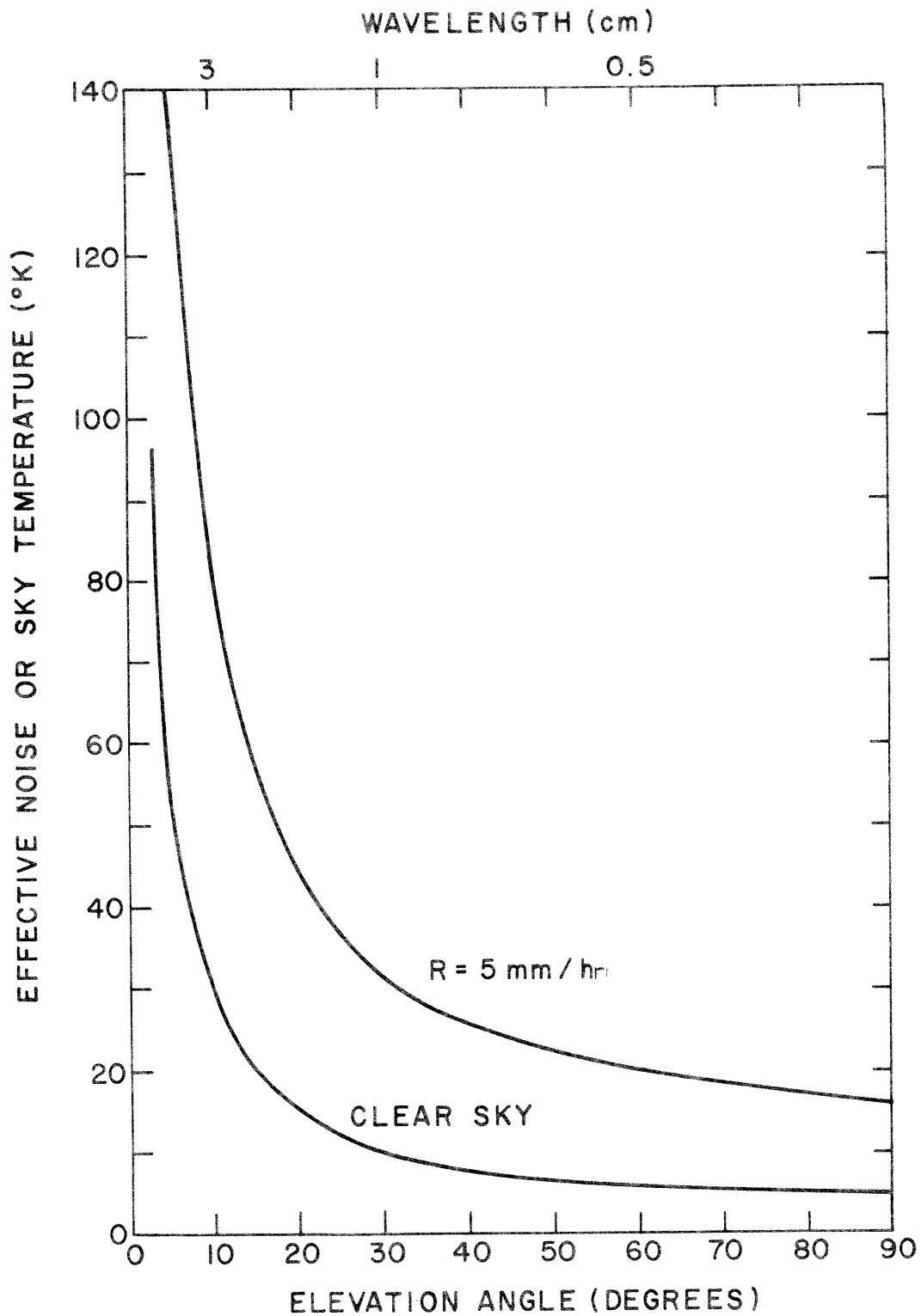


FIG. 24 EFFECTIVE NOISE OR SKY BRIGHTNESS TEMPERATURE AT 15 GHz FOR CLEAR SKY AND 5mm/hr RAINFALL RATE, (SNIDER [23])

tion due to the presence of oxygen and water vapor. The selection of one wavelength at 10cm and the other wavelength at 3 or 3.2cm may thus prove adequate. By referring to Figure 2 concerning the attenuation at different rain rates for different wavelengths or frequencies, one can note that the attenuation coefficient at 10cm is from 1 to 2% that at 3.2cm for the heavy and moderate rain and between 3 to 5% for the light rain. Therefore, for practical purposes, one may assume that the choice of these two wavelengths in a dual-wavelength system is a reasonably good one. One should also consider the appropriate hardware characteristics, i.e., the two radar beams should be (1) matched in beamwidth, (2) collimated, (3) reasonably narrow, and (4) should intersect the same rain volumes from identical ranges.

\bar{P}_{10} and \bar{P}_3 are the average echo powers returned at 10cm and 3cm wavelengths, respectively, from matched beams illuminating a volume at range r (km) and are given by

$$\bar{P}_3 = \frac{C_1 Z_e}{\kappa^2} 10^{-0.2 \int_{\kappa_0}^{\kappa_0+s} \gamma dr} \quad (1)$$

and

$$\bar{P}_{10} = \frac{C_2 Z_e}{\kappa^2} \quad (2)$$

where C_1 and C_2 are the radar constants, κ_0 is the range to the front of the storm, s is the distance from κ_0 to a point within the rain volume, and Z_e is the equivalent reflectivity factor due to rain. Taking the common log of the ratio of \bar{P}_{10} to \bar{P}_3 and multiplying through by 10 to change to dB, one obtains the relation:

$$\gamma = 10 \log \left[\frac{\bar{P}_{10}}{C_2} \div \frac{\bar{P}_3}{C_1} \right] \quad (3)$$

$$= 2 \int_{\kappa_0}^{\kappa_0+s} \gamma dr . \quad (4)$$

The ratio of

$$\frac{|Z_e|_{10}}{|Z_e|_3}$$

cancels out since it is approximately equal to unity for most rain-drop sizes. This can be shown as follows:

$$Ze = 3.5 \times 10^3 \lambda^4 \Sigma \sigma_i$$

where $\Sigma \sigma_i$ is the summation of the backscatter cross sections of the rain-drops contained in a unit volume (λ = wavelength). Since

$$\frac{|\Sigma \sigma_i|_{10}}{|\Sigma \sigma_i|_3} \approx 10^{-2}$$

for most rain drops (Godard [25]) and

$$\left(\frac{\lambda_{10}}{\lambda_3}\right)^4 \approx 10^2,$$

then

$$\frac{|Ze|_{10}}{|Ze|_3} \approx 1$$

for most practical purposes. As one continues further with Equation (4) by going to some other range $r_0 + s + s'$ inside the storm, average powers \bar{P}_3' and \bar{P}_{10}' are measured and the total relationship out to range $r_0 + s + s'$ is given by

$$2 \int_{r_0}^{r_0+s} \gamma dr + 2 \int_{r_0+s}^{r_0+s+s'} \gamma' dr = \log \left[\frac{\bar{P}_{10}'}{C_2} \div \frac{\bar{P}_3'}{C_1} \right]. \quad (5)$$

By subtracting (4) from (5), one gets

$$2 \int_{r_0+s}^{r_0+s+s'} \gamma' dr = 10 \log \left[\frac{\bar{P}_{10}' P_3}{\bar{P}_3' \bar{P}_{10}} \right] \quad (6)$$

and the effect of the attenuation up to the range $r_0 + s$ and the radar constants are eliminated. There is some average value of the attenuation coefficient, $\bar{\gamma}$ (dB/km), that applies over this increment in ranges such that

$$2 \bar{\gamma} s' = 2 \int_{r_0+s}^{r_0+s+s'} \gamma' dr. \quad (7)$$

Thus from (6) and (7):

$$\bar{\gamma}_s' = \frac{1}{2} \left[10 \log \left(\frac{\bar{P}_{10}' \bar{P}_3}{\bar{P}_3' \bar{P}_{10}} \right) \right] \text{ (in dB).}$$

Eccles and Mueller [24] further show that the method of averaging in range can improve the accuracy of the results from a dual-wavelength system, i.e., a minimum sensitivity of about 0.22dB/km with a standard deviation of about 0.1dB/km in the measurement of attenuation can be achieved if all the data in a rectangular plate-like volume of about 1km^2 area are properly averaged.

V. Conclusions and Recommendations

A. Conclusions

- (1) It is possible, at present, to make some long-term outage time predictions for certain geographic areas that are accurate to better than an order of magnitude.
- (2) It is possible to use radar and/or radiometer measurements to differentiate in real time between incidents of light, moderate, and heavy attenuation to within an average absolute accuracy of 10dB and possibly better.
- (3) Correlations of attenuation with backscatter can be quite poor as a result of the widely varying "a" and "b" parameters in time and three-dimensional space.
- (4) For a known drop-size distribution over a large enough ground area, the backscattering and attenuation distributions can be adequately determined with a single-wavelength radar set.
- (5) Estimates of path attenuation can be made with microwave radiometers or a dual-wavelength radar system without assuming a size distribution. These additional approaches can provide verifying data, perhaps leading subsequently to an improved method for estimating attenuation for satellite-to-earth-station communications.
- (6) For detecting noise-temperature fluctuations produced by clouds and rain, the radiometer is preferable to the radar because of its greater sensitivity.
- (7) It is possible to rely on short-term predictions based on ground-measured rainfall intensities for ascertaining the preferable communication

path of two or more paths separated by a distance greater than a rain-cell width. Using such an approach, when the cell blocks one path, the attenuation along the other path may be acceptable.

(8) It is possible to compute estimates of the attenuation along a particular path from the intensity of the radar returns of the AN/CPS-9 (or with the use of the US Army's most recent mobile weather radar, the AN/TPS-41/XE-2). The AN/CPS-9 weather radar operating at 9.4 GHz (3.2cm) and located about 7 miles south of Fort Monmouth was modified to include means for obtaining iso-echo contours. The AN/TPS-41 will be available in the near future and will be able to provide real-time, three-dimensional data on precipitation areas for slant ranges up to 240km. Iso-echo contouring devices will be included, capable of operating in three-level and ten-level modes.

(9) When major storm cells are observed they can be tracked and attempts made to predict their course. If the passage of a cell through the path to a satellite from a satellite ground terminal is anticipated, the attenuation and noise temperature increase can be computed, preferably with the additional aid of a radiometer, and the station involved notified at the earliest opportunity. During the storm's approach, refined and up-to-date estimates can be transmitted. To be more specific, for example, the first advisory notice can indicate (a) the probable time of onset of storm cells which possess the potential to produce moderate or high attenuations; (b) probable duration of such attenuation; (c) noise temperature increase; and (d) probability of the storm cell intercepting or crossing the transmission path. Updated predictions could subsequently be issued as available.

B. Recommendations

To acquire additional knowledge concerning the variability of the γ versus Z_e relationship in time and space and to investigate the relationship between surface drop-size distributions and those found at other altitudes in the storm, the following items are recommended for consideration:

(1) Measure the drop-size distribution at a sufficient number of points within the rain area at ground level on a continuous basis to determine changes in the γ vs Z_e relation in space and time.

(2) By appropriate use of the radar data, such as through an interpretation of the scope display of the radar data, it is possible to distinguish between the different values of Z_e . Computer techniques would be desirable for processing fields of Z_e and γ for large areas and for analyzing the fields to determine the optimum γ vs Z_e relationship.

(3) To improve the γ vs Z_e relationships in the air from ground-level measurements further, adequate correlations must be found between rain-

drop distributions in precipitating clouds and between the cloud base and ground level, and measurements made at the surface.

A method such as the following might be used: (a) Employ a radar scanning vertically as well as horizontally to obtain adequate three-dimensional spatial measurements of Z_e ; (b) correlate Z_e vs attenuation and size distribution in three-dimensional space and time with that at ground level; (c) include other meteorological data such as might be obtained from radiosondes, and (d) if significant correlations are found between the Z_e and γ relationships and the meteorological parameters, relationships for other geographic areas could be estimated.

(4) Explore the feasibility of using a dual-wavelength radar system and microwave radiometer measurements, such as indicated in this report.

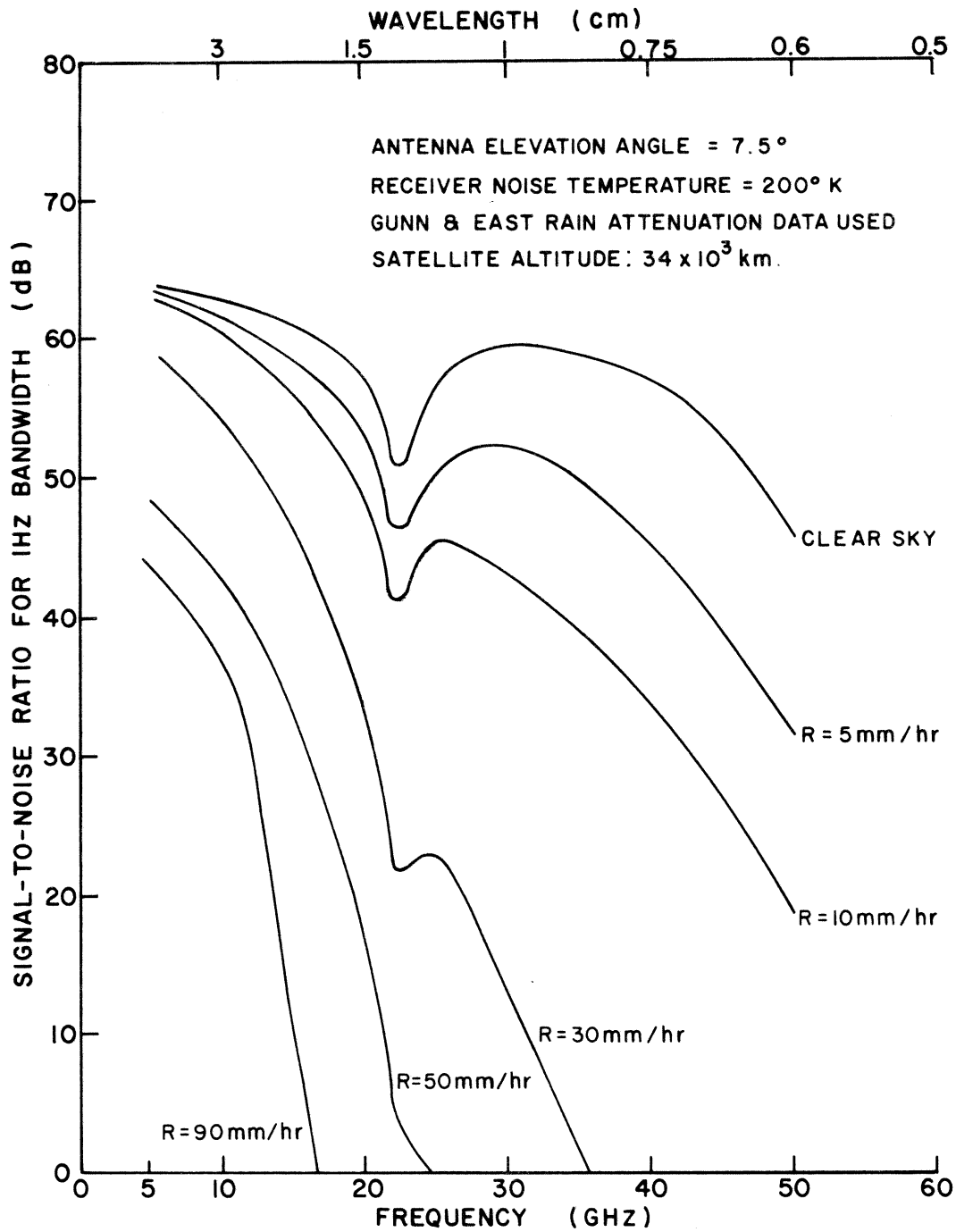


FIG. A† SIGNAL-TO- NOISE RATIO FOR MODEL SATELLITE SYSTEM FOR CLEAR SKY AND DIFFERENT RAINFALL RATES (SNIDER [23])

APPENDIX A

RADAR PERFORMANCE AND SENSITIVITY TO NOISE TEMPERATURE

(1) Performance Features

The Atmospheric Sciences Laboratory of the US Army Electronics Command at Fort Monmouth, New Jersey, employed an AN/CPS-9 weather radar at 9.4 GHz (3.2cm) in the Camp Evans Area about 7 miles south of Fort Monmouth on two rainy occasions recently. Unfortunately, the two storms analyzed were light in intensity. Insignificant amounts of attenuation were predicted and observed; however, these two cases do not adequately serve as a verification of the technique for proper identification and analysis of more intense storms. Generally, the confidence limits can be sizeable for estimates derived from radar. Preliminary results from an analysis of these two storms, however, show that the radar can serve as an effective tool for determining path attenuation and effective noise temperature for satellite communications. Supplementary means for aiding the radar to achieve meaningful results for the satellite communication problem are discussed in other portions of this report.

The US Army's most recent mobile weather-radar set is the AN/TPS-41. This set operates in the X-band with a tunable frequency range of 8500 to 9600 MHz and is designed to provide real-time, three-dimensional data on precipitation areas for slant ranges up to 240 km. The console consists of displays (required data indicators), plan-position-range-height (PP/RH) display, A/R display, and iso-echo contouring devices capable of operating in three-level and ten-level modes. An alarm is also provided to alert the operator of the occurrence of an echo that exceeds a variable predetermined limit.

Performance curves, such as shown in Figure A1 (Snider [23]) assuming uniform rain intensity of 1 km thickness at a uniform temperature of 15°C along the path, can be made available to the SATCOM engineer for determining outage times. This figure shows the S/N ratio for a 1 Hz bandwidth for different rainfall rates and clear sky. There is a sharp deterioration of the S/N ratio with decreasing wavelength, particularly at the greater rainfall rates. These curves can serve as a guide for estimating the maximum rainfall rate which may be penetrated for a given S/N ratio. The time interval during which the maximum rainfall rate is exceeded is equivalent to the outage time.

(2) Radar and Radiometer Sensitivity to Effective Noise Temperature

Skolnik [26] shows that S_{\min} , the minimum detectable signal, is equal to

$$kT_o B_n F_n \left(\frac{S_o}{N_o} \right)_{\min}$$

where k is Boltzmann's constant (1.38×10^{-23} Joules per $^{\circ}\text{K}$), T_o is the standard temperature taken as 290°K for electronic equipment according to the IEEE definition, B_n = receiver bandwidth (that of the IF amplifier in most receivers), F_n = receiver's noise figure, and

$$\left(\frac{S_o}{N_o}\right)_{\min}$$

is the minimum ratio of the output (IF) signal-to-noise ratio that is necessary for detection of the target. This assumes that the input receiver noise is kT_oB_n where the receiver is at a standard temperature of 290°K . However, when the receiver is connected to an antenna, the temperature "seen" by the receiver may be lower or higher than 290°K . With relatively "noisy" receivers, the effect of an antenna temperature different from 290°K would hardly be noticed unless the temperature were high enough. With low noise receivers, namely, masers and parametric amplifiers, the effect of antenna temperature is important except for very high signal returns such as from rainstorms.

It is possible, however, to calculate the radar antenna noise temperature in precipitation regions by measuring attenuation coefficients along the path (γ vs Z_e) and by including temperature data such as obtained from radiosonde measurements. The effective noise temperature relationship between $\alpha(s)$ [the absorption coefficient] and $T(s)$ [the water drop temperature] can then yield a value for the noise temperature, i.e.,

$$T_e = \int_0^{\infty} \frac{\alpha(s)}{4.34} T(s) \exp\left[-\int_0^s \frac{\alpha(s) ds}{4.34}\right] ds \quad [21] .$$

This approach for determining T_e can be adopted as a checking measure for the radiometer's direct evaluation of T_e .

APPENDIX B

COMMENTS ON ETAC REPORT NO. 4100

The following remarks are made in regard to ETAC Report No. 4100 (Thompson [1]).

Attenuation parameters are derived and determined for a wavelength of 3.8 cm and for different geographic regions indicating total dB loss vs time in hours per year during which given dB attenuation occurs. The total attenuation derivation is determined as a function of: (1) the average precipitation rate for a time T along the precipitation path between the satellite and ground terminal, (2) the translatory speed of the storm, and (3) the cosine of the elevation angle of the slant ray. A single expression relating the attenuation coefficient to the rainfall rate at 3.8 cm is assumed, i.e., $\gamma = 0.609R^{1.31}$ (γ in dB/mile, R the rain intensity in inches/hr).

No attention, however, is given to specific raindrop size distributions for different storm types and locations. This makes it very difficult to obtain an adequate correlation between attenuation and rain intensity. Moreover, the same rain intensity is assumed over the full path length which does not correspond with empirical evidence of significantly different intensities frequently occurring at different times and points in space during the progression of a storm.

The total attenuation subsequently derived in the ETAC Report is:

$$D(\text{dB}) = \frac{\text{constant} \cdot V(\bar{\kappa}) \cdot T}{\cos e} = \text{constant} \cdot VP(\bar{\kappa})^{0.31}$$

where $P = \bar{\kappa}t$ = total precipitation from the average rain intensity, $\bar{\kappa}$, during time T of the storm's presence along the communication path between the satellite and ground terminal, V = mean scalar speed of the storm in a given direction at the 10,000' altitude, and e = radar beam's elevation angle. There appears to be no restriction on the angle e, however, so that the total attenuation could unrealistically reach infinity as e approaches 90°. Furthermore, it is questionable whether the 10,000' mean wind speed adequately represents the storm's movement at all times and locations.

The approach taken by ETAC, nevertheless, is useful in initially deriving attenuation data for different geographic regions. It would be necessary, however, to take account of the aforementioned criticism, including different wavelengths, to obtain more effective results.

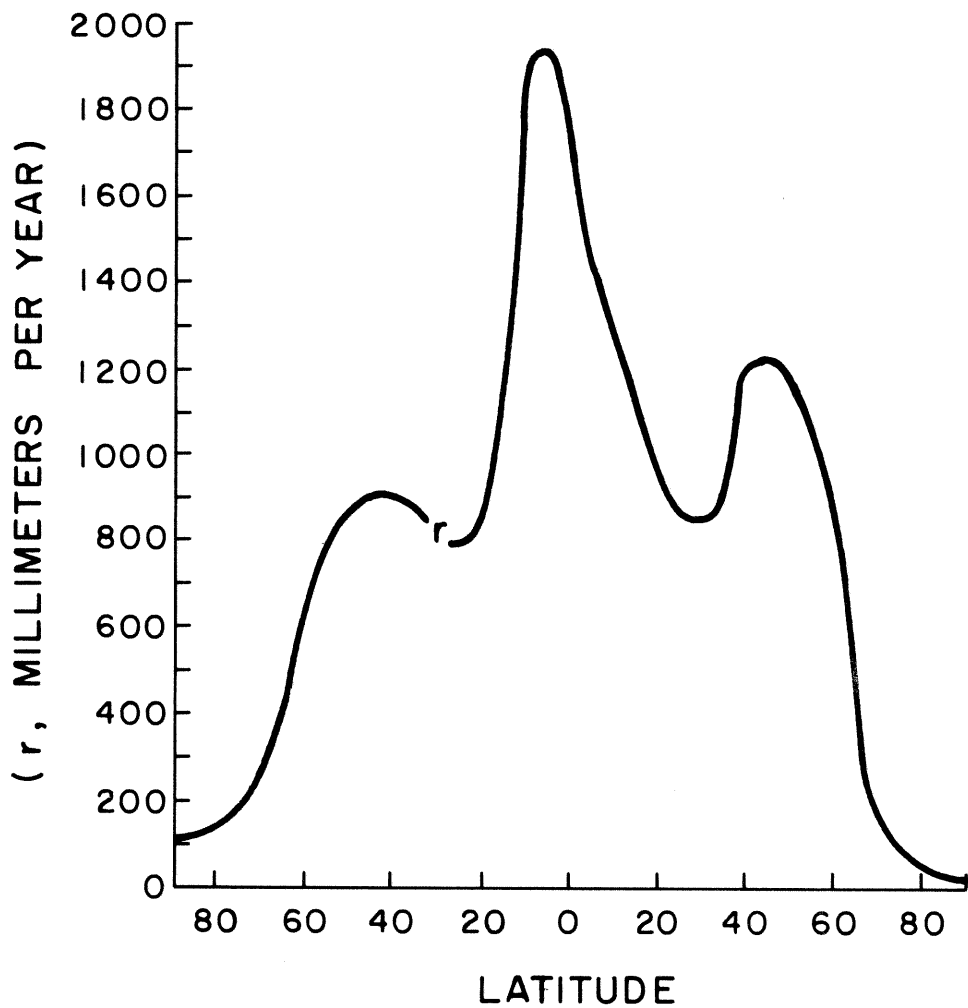


FIG. c1 THE AVERAGE ANNUAL LATITUDINAL DISTRIBUTION OF PRECIPITATION (r) (SELLERS [28])

APPENDIX C

METEOROLOGICAL AND CLIMATOLOGICAL ASPECTS OF PRECIPITATION

(1) Meteorological Aspects

The following type of information is helpful toward being aware of the basically different types of precipitation that may occur from atmospheric and terrain factors. Lack of data at present, however, precludes any determination of significant correlations between precipitation type and the precipitation intensity.

On the basis of causative storms, precipitation may be divided into three types (Foster [27]), namely, a) convective, b) orographic, and c) cyclonic. This classification is based on the meteorological phenomena which cause and accompany the precipitation.

Type a is due to the thermal convection of moisture-laden air. This requires both adequate heat and water vapor.

Type b is caused by the cooling of moisture-laden air masses which are lifted by contact with elevated land masses. This type is **most** pronounced on the windward side lying across the prevailing winds where those winds pass from the relatively warm ocean to the land.

Type c is frequently associated with low-pressure areas with accompanying frontal activity.

(2) Climatological Aspects

Figure C1 (Sellers [28]) shows the average latitude annual distribution of precipitation. The maximum total precipitation for the Northern and Southern Hemispheres occurs between about 20°N and 15°S latitudes due to the convective activity prevalent in tropical areas. A smaller maximum is present between the 40°-50°N and S latitudes where cyclonic storms frequently takes place. Although both hemispheres receive about the same average annual precipitation of about 1000 mm there is a somewhat greater amount in the Northern Hemisphere due to the average presence of the intertropical convergence zone slightly north of the equator. Between about the 20° to 70° latitudes, however, the Northern Hemisphere shows lower precipitation totals than the Southern Hemisphere.



AVERAGE FREQUENCY OF THUNDERSTORM DAYS FOR APRIL - SEPTEMBER (HAURWITZ AND AUSTIN [29])

FIG. D1

APPENDIX D

METEOROLOGICAL AND CLIMATOLOGICAL ASPECTS OF THUNDERSTORMS

a. Meteorological Aspects

Thunderstorm activity can be categorized with the following associations or occurrences as indicated by Foster [27]:

1. Heat or local convection (with a monthly frequency maximum mostly in the summer and a minimum during winter months)
2. Warm frontal
3. Cold frontal
4. Occluded frontal
5. Cold air mass (with cold air initially in an unstable position above a warm air mass)
6. Horizontally converging air currents
7. Orographic effects

The classification and recognition of the above preconditions can serve as an aid in predicting the occurrence of thunderstorms.

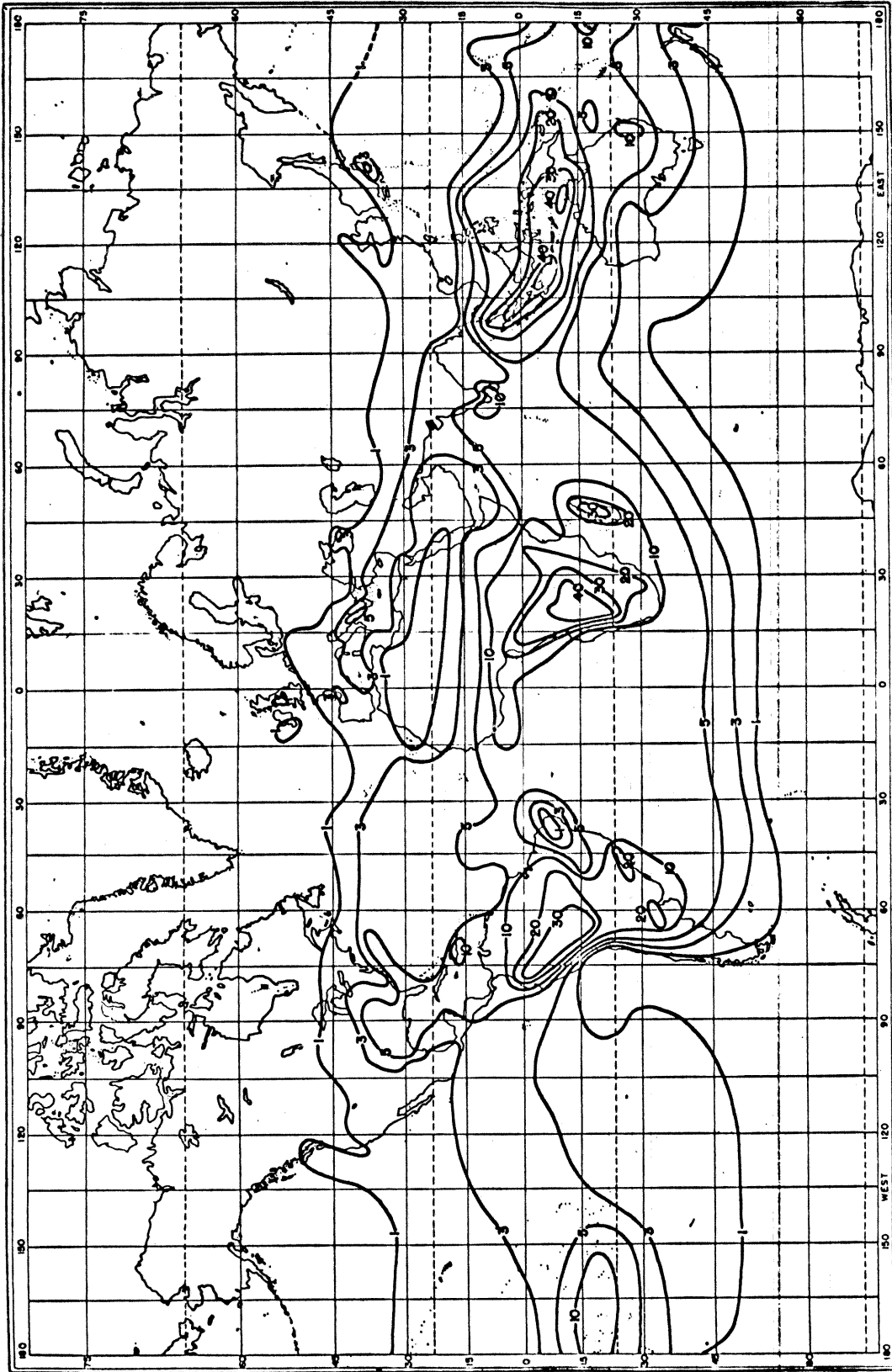
b. Climatological Aspects

Since thunderstorms are frequently associated with maximum attenuation throughout the world, some climatological features, such as those obtained from Haurwitz and Austin [29], are important. It is also noteworthy that Cataneo [30] applies the annual thunderstorm activity as one of the two basic parameters for an estimation of the a and b parameters for the relationship in different locations throughout the world.

The following general remarks can be made in regard to Figures D1 and D2:

The April - September period (Figure D1) shows regions of maximum thunderstorm frequency over the Gulf of Mexico and Caribbean regions, southeastern Gulf states, New Mexico, central Africa, and parts of southeast Asia including the East Indies. Beyond about 65°N latitude and 45°S latitude, thunderstorm activity seldom occurs.

The October-March period (Figure D2) shows the maximum frequency almost entirely occurring in the Southern Hemisphere land masses between the equator and 30°S latitude. In addition, the waters between India, the East Indies, and northern Australia show maximum frequencies.



AVERAGE FREQUENCY OF THUNDERSTORM DAYS FOR OCTOBER - MARCH (HAURWITZ AND AUSTIN [29])

FIG. D2

Knowledge of such climatological features can at least provide an indication of those regions of the world where maximum or high attenuations are most likely to occur. One must bear in mind, however, that by definition a thunderstorm is not always accompanied by rain even though usually there is heavy or intense rain.

LITERATURE CITED

1. Thompson, W. I., III, 1962, "Precipitation Attenuation of 8 Kmc - Final Estimates," Environmental Technical Applications Center Report No. 4100, ESSA.
2. Hogg, D. C., 1968, "Millimeter-Wave Communication through the Atmosphere," Science, 59, No. 3810, 39.
3. Atlas, D., and A. C. Chmela, 1957, "Physical-Synoptic Variations of Drop-Size Parameters," Proc. 6th Weather Radar Conference, Amer. Met. Soc., 4, 21-29.
4. Atlas, D., and S. Bartnoff, 1953, "Cloud Visibility, Radar Reflectivity, and Drop-Size Distribution," J. Meteorology, 10, 21, 143.
5. Atlas, D., 1955, "The Radar Measurement of Precipitation Growth," Dept. of Meteorology, MIT.
6. Haroules, G. G., and W. E. Brown, III, 1969, "The Simultaneous Investigation of Attenuation and Absorption of the Earth's Atmosphere at Wavelengths from 4 Centimeters to 8 Millimeters," J. Geophys. Res., 74, no. 18, 4453.
7. Gunn, K. L., and T. W. R. East, 1954, "The Microwave Properties of Precipitation Particles," Quart. J. Roy. Met. Soc., LXXX, 522.
8. Ryde, J. W., and D. Ryde, 1945, "Attenuation of Centimeter and Millimeter Waves by Rain, Hail, Fogs and Clouds," General Electric Co. Res. Labs. Ltd., Wembley, England, Report No. 8670.
9. Handbook of Geophysics, 1960, Air Force Cambridge Research Laboratory, Macmillan Co., p. 13-161.
10. Ryde, J. W., 1946, "The Attenuation and Radar Echoes Produced at Centimeter Wavelength by Various Meteorological Phenomena," Meteorological Factors in Radio Wave Propagation, p 169-188, The Physical Society, London, England.
11. Setzer, D. E., 1970, "Computed Transmission Through Rain at Microwave and Visible Frequencies," The Bell System Tech. J., 48, 1873.
12. Borovikov, A. M., and V. V. Kostrav (Editors), 1969, "Radar Measurement of Precipitation Rate, Leningrad, Translated 1970, Israel Program for Scientific Translations (Clearinghouse for Federal Scientific and Technical Information).

13. Ippolito, L. J., 1970, "Mm Wave Propagation Measurements from ATS-V," IEEE Transactions on Antennas and Propagation, 18, No. 4, 535.
14. Hogg, D. C., 1969, "Effects of Atmospheric Water on Electromagnetic Wave Propagation," from report entitled "Satellite Communications and Atmospheric Water-- Present and Future," Proceedings of the NATO Advanced Study Institute, 26 August-6 September, edited by D. R. Hay, Univ. of Western Ontario, London, Canada.
15. Mueller, E. A., and A. L. Sims, 1969, "Relationships between Reflectivity, Attenuation, and Rainfall Rate Derived from Drop Size Spectra," Final Report, US Army Contract DA-28-043 AMC-02071(E), Illinois State Water Survey Meteorological Laboratory (ISWSML), Urbana, Illinois.
16. Jones, D. M. A., and L. A. Dean, 1953, "A Raindrop Camera Research Report No. 10," US Army Contract NO. DA 36-039 sc-42446, Illinois State Water Survey Meteorological Laboratory (ISWSML), Urbana, Illinois.
17. Mueller, E. A., 1960, "Study on Intensity of Surface Precipitation using Radar Instrumentation," Quarterly Technical Report No. 10, US Army Contract No. DA 36-039 sc-75055, Illinois State Water Survey Meteorological Laboratory (ISWSML), Urbana, Illinois.
18. Gunn, R., and G. O. Kinzer, 1948, "The Terminal Velocity of Fall for Water Droplets in Stagnant Air," J. Meteor., 6, 243.
19. Cataneo, R., and G. E. Stout, 1968, "Raindrop Size Distribution in Humid Continental Climates and Associated Rainfall Radar Reflectivity Relationships," J. Appl. Meteor., 7, no. 5, 901.
20. Hathaway, S. D., and H. W. Evans, 1959, "Radio Attenuation at 10 Kmc and Some Implications Affecting Relay System Engineering," The Bell System Tech. J., 38, 1.
21. Crane, R. K., 1968, "Simultaneous Radar and Radiometer Measurements of Rain Shower Structure, Lincoln Labs., MIT.
22. Penzias, A. A., 1970, "First Results from 15.36MHz Earth-Space Propagation Study," The Bell System Tech. J., 49, 1242.
23. Snider, J. B., 1968, "A Proposed Program for the Study of Atmospheric Attenuation of Satellite Signals, Environmental Science Services Administration.
24. Eccles, P. J., and E. A. Mueller, 1970, "The Capability of a Dual Wavelength Radar System for Estimating Attenuation and Liquid Water Content," 14th Radar Meteorology Conference, 17-20 November, Tucson, Arizona.

25. Godard, S. L., 1970, "Propagation of Centimeter and Millimeter Wavelengths Through Precipitation," IEEE Transactions on Antennas and Propagation, 18, No. 4, 530.
26. Skolnik, M. I., 1962, Introduction to Radar Systems, McGraw Hill, New York.
27. Foster, E. E., 1949, Rainfall and Runoff, p. 23, Macmillan Co., New York.
28. Sellers, W. D., 1965, Physical Climatology, p. 84, University of Chicago Press.
29. Haurwitz, B., and J. M. Austin, 1944, Climatology, p. 64, McGraw Hill, New York.
30. Cataneo, R., 1968, "A Method for Estimating Rainfall Rate - Radar Reflectivity Relationships," 13th Radar Meteorology Conference Proceedings, 20-23 August, Edited by J. S. Marshall, McGill University, Montreal, Canada.

ATMOSPHERIC SCIENCES RESEARCH PAPERS

1. Miers, B. T., and J. E. Morris, Mesospheric Winds Over Ascension Island in January, July 1970, ECOM-5312, AD 711851.
2. Webb, W. L., Electrical Structure of the D- and E-Region, July 1970, ECOM-5313, AD 714365.
3. Campbell, G. S., F. V. Hansen and R. A. Dise, Turbulence Data Derived from Measurements on the 32-Meter Tower Facility, White Sands Missile Range, New Mexico, July 1970, ECOM-5314, AD 711852.
4. Pries, T. H., Strong Surface Wind Gusts at Holloman AFB (March-May), July 1970, ECOM-5315, AD 711853.
5. D'Arcy, E. M., and B. F. Engebos, Wind Effects on Unguided Rockets Fired Near Maximum Range, July 1970, ECOM-5317, AD 711854.
6. Matonis, K., Evaluation of Tower Antenna Pedestal for Weather Radar Set AN/TPS-41, July 1970, ECOM-3317, AD 711520.
7. Monahan, H. H., and M. Armendariz, Gust Factor Variations with Height and Atmospheric Stability, August 1970, ECOM-5320, AD 711855.
8. Stenmark, E. B., and L. D. Drury, Micrometeorological Field Data from Davis, California; 1966-67 Runs Under Non-Advection Conditions, August 1970, ECOM-6051, AD 726390.
9. Stenmark, E. B., and L. D. Drury, Micrometeorological Field Data from Davis, California; 1966-67 Runs Under Advection Conditions, August 1970, ECOM-6052, AD 724612.
10. Stenmark, E. B., and L. D. Drury, Micrometeorological Field Data from Davis, California; 1967 Cooperative Field Experiment Runs, August 1970, ECOM-6053, AD 724613.
11. Rider, L. J., and M. Armendariz, Nocturnal Maximum Winds in the Planetary Boundary Layer at WSMR, August 1970, ECOM-5321, AD 712325.
12. Hansen, F. V., A Technique for Determining Vertical Gradients of Wind and Temperature for the Surface Boundary Layer, August 1970, ECOM-5324, AD 714366.
13. Hansen, F. V., An Examination of the Exponential Power Law in the Surface Boundary Layer, September 1970, ECOM-5326, AD 715349.
14. Miller, W. B., A. J. Blanco and L. E. Traylor, Impact Deflection Estimators from Single Wind Measurements, September 1970, ECOM-5328, AD 716993.
15. Duncan, L. D., and R. K. Walters, Editing Radiosonde Angular Data, September 1970, ECOM-5330, AD 715351.
16. Duncan, L. D., and W. J. Vechione, Vacuum Tube Launchers and Boosters, September 1970, ECOM-5331, AD 715350.
17. Stenmark, E. B., A Computer Method for Retrieving Information on Articles, Reports and Presentations, September 1970, ECOM-6050, AD 724611.
18. Hudlow, M., Weather Radar Investigation on the BOMEX, September 1970, ECOM-3329, AD 714191.
19. Combs, A., Analysis of Low-Level Winds Over Vietnam, September 1970, ECOM-3346, AD 876935.
20. Rinehart, G. S., Humidity Generating Apparatus and Microscope Chamber for Use with Flowing Gas Atmospheres, October 1970, ECOM-5332, AD 716994.
21. Miers, B. T., R. O. Olsen, and E. P. Avara, Short Time Period Atmospheric Density Variations and a Determination of Density Errors from Selected Rocket-sonde Sensors, October 1970, ECOM-5335.
22. Rinehart, G. S., Sulfates and Other Water Solubles Larger than 0.15μ Radius in a Continental Nonurban Atmosphere, October 1970, ECOM-5336, AD 716999.
23. Lindberg, J. D., The Uncertainty Principle: A Limitation on Meteor Trail Radar Wind Measurements, October 1970, ECOM-5337, AD 716996.
24. Randhawa, J. S., Technical Data Package for Rocket-Borne Ozone-Temperature Sensor, October 1970, ECOM-5338, AD 716997.

25. Devine, J. C., The Fort Huachuca Climate Calendar, October 1970, ECOM-6054.
26. Allen, J. T., Meteorological Support to US Army RDT&E Activities, Fiscal Year 1970 Annual Report, November 1970, ECOM-6055.
27. Shinn, J. H., An Introduction to the Hyperbolic Diffusion Equation, November 1970, ECOM-5341, AD 718616.
28. Avara, E. P., and M. Kays., Some Aspects of the Harmonic Analysis of Irregularly Spaced Data, November 1970, ECOM-5344, AD 720198.
29. Fabrici, J., Inv. of Isotopic Emitter for Nuclear Barometer, November 1970, ECOM-3349, AD 876461.
30. Levine, J. R., Summer Mesoscale Wind Study in the Republic of Vietnam, December 1970, ECOM-3375, AD 721585.
31. Petriw, A., Directional Ion Anemometer, December 1970, ECOM-3379, AD 720573.
32. Randhawa, J. S., B. H. Williams, and M. D. Kays, Meteorological Influence of a Solar Eclipse on the Stratosphere, December 1970, ECOM-5345, AD 720199.
33. Nordquist, Walter S., Jr., and N. L. Johnson, One-Dimensional Quasi-Time-Dependent Numerical Model of Cumulus Cloud Activity, December 1970, ECOM-5350, AD 722216.
34. Avara, E. P., The Analysis of Variance of Time Series Data Part I: One-Way Layout, January 1971, ECOM-5352, AD 721594.
35. Avara, E. P., The Analysis of Variance of Time Series Data Part II: Two-Way Layout, January 1971, ECOM-5353.
36. Avara, E. P., and M. Kays., The Effect of Interpolation of Data Upon the Harmonic Coefficients, January 1971, ECOM-5354, AD 721593.
37. Randhawa, J. S., Stratopause Diurnal Ozone Variation, January 1971, ECOM-5355, AD 721309.
38. Low, R. D. H., A Comprehensive Report on Nineteen Condensation Nuclei (Part II), January 1971, ECOM-5358.
39. Armendariz, M., L. J. Rider, G. Campbell, D. Favier and J. Serna, Turbulence Measurements from a T-Array of Sensors, February 1971, ECOM-5362, AD 726390.
40. Maynard, H., A Radix-2 Fourier Transform Program, February 1971, ECOM-5363, AD 726389.
41. Devine, J. C., Snowfalls at Fort Huachuca, Arizona, February 1971, ECOM-6056.
42. Devine, J. C., The Fort Huachuca, Arizona 15 Year Base Climate Calendar (1956-1970), February 1971, ECOM-6057.
43. Levine, J. R., Reduced Ceilings and Visibilities in Korea and Southeast Asia, March 1971, ECOM-3403, AD 722735.
44. Gerber, H., et al., Some Size Distribution Measurements of AgI Nuclei with an Aerosol Spectrometer, March 1971, ECOM-3414, AD 729331.
45. Engebos, B. F., and L. J. Rider, Vertical Wind Effects on the 2.75-inch Rocket, March 1971, ECOM-5365, AD 726321.
46. Rinehart, G. S., Evidence for Sulfate as a Major Condensation Nucleus Constituent in Nonurban Fog, March 1971, ECOM-5366.
47. Kennedy, B. W., E. P. Avara, and B. T. Miers, Data Reduction Program for Rocketsonde Temperatures, March 1971, ECOM-5367.
48. Hatch, W. H., A Study of Cloud Dynamics Utilizing Stereoscopic Photogrammetry, March 1971, ECOM-5368.
49. Williamson, L. E., Project Gun Probe Captive Impact Test Range, March 1971, ECOM-5369.
50. Henley, D. C., and G. B. Hoidale, Attenuation and Dispersion of Acoustic Energy by Atmospheric Dust, March 1971, ECOM-5370, AD 728103.
51. Cionco, R. M., Application of the Ideal Canopy Flow Concept to Natural and Artificial Roughness Elements, April 1971, ECOM-5372, AD 730638.
52. Randhawa, J. S., The Vertical Distribution of Ozone Near the Equator, April 1971, ECOM-5373.
53. Ethridge, G. A., A Method for Evaluating Model Parameters by Numerical Inversion, April 1971, ECOM-5374.

54. Collett, E., Stokes Parameters for Quantum Systems, April 1971, ECOM-3415, AD 729347.
55. Shinn, J. H., Steady-State Two-Dimensional Air Flow in Forests and the Disturbance of Surface Layer Flow by a Forest Wall, May 1971, ECOM-5383, AD 730681.
56. Miller, W. B., On Approximation of Mean and Variance-Covariance Matrices of Transformations of Joint Random Variables, May 1971, ECOM-5384, AD 730302.
57. Duncan, L. D., A Statistical Model for Estimation of Variability Variances from Noisy Data, May 1971, ECOM-5385.
58. Pries, T. H., and G. S. Campbell, Spectral Analyses of High-Frequency Atmospheric Temperature Fluctuations, May 1971, ECOM-5387.
59. Miller, W. B., A. J. Blanco, and L. E. Traylor, A Least-Squares Weighted-Layer Technique for Prediction of Upper Wind Effects on Unguided Rockets, June 1971, ECOM-5388, AD 729792.
60. Rubio, R., J. Smith and D. Maxwell, A Capacitance Electron Density Probe, June 1971, ECOM-5390.
61. Duncan, L. D., Redundant Measurements in Atmospheric Variability Experiments, June 1971, ECOM-5391.
62. Engebos, B. F., Comparisons of Coordinate Systems and Transformations for Trajectory Simulations, July 1971, ECOM-5397.
63. Hudlow, M. D., Weather Radar Investigations on an Artillery Test Conducted in the Panama Canal Zone, July 1971, ECOM-5411.
64. White, K. O., E. H. Holt, S. A. Schleusener, and R. F. Calfee, Erbium Laser Propagation in Simulated Atmospheres II. High Resolution Measurement Method, August 1971, ECOM-5398.
65. Waite, R., Field Comparison Between Sling Psychrometer and Meteorological Measuring Set AN/TMQ-22, August 1971, ECOM-5399.
66. Duncan, L. D., Time Series Editing By Generalized Differences, August 1971, ECOM-5400.
67. Reynolds, R. D., Ozone: A Synopsis of its Measurements and Use as an Atmospheric Tracer, August 1971, ECOM-5401.
68. Avara, E. P., and B. T. Miers, Noise Characteristics of Selected Wind and Temperature Data from 30-65 km, August 1971, ECOM-5402.
69. Avara, E. P., and B. T. Miers, Comparison of Linear Trends in Time Series Data Using Regression Analysis, August 1971, ECOM-5403.
70. Miller, W. B., Contributions of Mathematical Structure to the Error Behavior of Rawinsonde Measurements, August 1971, ECOM-5404.
71. Collett, E., Mueller Stokes Matrix Formulation of Fresnel's Equations, August 1971, ECOM-3480.
72. Armendariz, M., and L. J. Rider, Time and Space Correlation and Coherence in the Surface Boundary Layer, September 1971, ECOM-5407.
73. Avara, E. P., Some Effects of Randomization in Hypothesis Testing with Correlated Data, October 1971, ECOM-5408.
74. Randhawa, J. S., Ozone and Temperature Change in the Winter Stratosphere, November 1971, ECOM-5414.
75. Miller, W. B., On Approximation of Mean and Variance-Covariance Matrices of Transformations of Multivariate Random Variables, November 1971, ECOM-5413.
76. Horn, J. D., G. S. Campbell, A. L. Wallis (Capt., USAF), and R. G. McIntyre, Wind Tunnel Simulation and Prototype Studies of Barrier Flow Phenomena, December 1971, ECOM-5416.
77. Dickson, David H., and James R. Oden, Fog Dissipation Techniques for Emergency Use, January 1972, ECOM-5420.
78. Ballard, H. N., N. J. Beyers, B. T. Miers, M. Izquierdo, and J. Whitacre, Atmospheric Tidal Measurements at 50 km from a Constant-Altitude Balloon, December 1971, ECOM-5417.
79. Miller, Walter B., On Calculation of Dynamic Error Parameters for the Rawinsonde and Related Systems, January 1972, ECOM-5422.

80. Richter, Thomas J., Rawin Radar Targets, February 1972, ECOM-5424.
81. Pena, Ricardo, L. J. Rider, and Manuel Armendariz, Turbulence Characteristics at Heights of 1.5, 4.0, and 16.0 Meters at White Sands Missile Range, New Mexico, January 1972, ECOM-5421.
82. Blanco, Abel J., and L. E. Traylor, Statistical Prediction of Impact Displacement due to the Wind Effect on an Unguided Artillery Rocket During Powered Flight, March 1972, ECOM-5427.
83. Williams, B. H., R. O. Olsen, and M. D. Kays, Stratospheric-Ionospheric Interaction During the Movement of a Planetary Wave in January 1967, March 1972, ECOM-5428.
84. Schleusener, Stuart A., and Kenneth O. White, Applications of Dual Parameter Analyzers in Solid-State Laser Tests, April 1972, ECOM-5432.
85. Pries, Thomas H., Jack Smith, and Marvin Hamiter, Some Observations of Meteorological Effects on Optical Wave Propagation, April 1972, ECOM-5434.
86. Dickson, D. H., Fogwash I An Experiment Using Helicopter Downwash, April 1972, ECOM-5431.
87. Mason, J. B., and J. D. Lindberg, Laser Beam Behavior on a Long High Path, April 1972, ECOM-5430.
88. Smith, Jack, Thomas H. Pries, Kenneth J. Skipka, and Marvin Hamiter, Optical Filter Function for a Folded Laser Path, April 1972, ECOM-5433.
89. Lee, Robert P., Artillery Sound Ranging Computer Simulations, May 1972, ECOM-5441.
90. Lowenthal, Marvin J., The Accuracy of Ballistic Density Departure Tables 1934-1972, April 1972, ECOM-5436.
91. Cantor, Israel, Survey of Studies of Atmospheric Transmission from a 4π Light Source to a 2π Receiver, April 1972, ECOM-5435.
92. Barr, William C., Accuracy Requirements for the Measurement of Meteorological Parameters Which Affect Artillery Fire, April 1972, ECOM-5437.
93. Duchon, C. E., F. V. Brock, M. Armendariz, and J. D. Horn, UVW Anemometer Dynamic Performance Study, May 1972, ECOM-5440.
94. Gomez, R. B., Atmospheric Effects for Ground Target Signature Modeling I. Atmospheric Transmission at 1.06 Micrometers, June 1972, ECOM-5445.
95. Bonner, R. S., A Technical Manual on the Characteristics and Operation of a Cloud Condensation Nuclei Collection/Detection/Recording Instrument, June 1972, ECOM-5447.
96. Horn, J. D., R. D. Reynolds, and T. H. Vonder Haar, Survey of Techniques Used in Display of Sequential Images Received from Geostationary Satellites, June 1972, ECOM-5450.
97. Bonner, R. S., and H. M. White, Microphysical Observations of Fog in Redwood Valley near Arcata-Eureka, California, July 1972, ECOM-5455.
98. Waite, R. W., Reliability Test of Electronics Module of Meteorological Measuring Set AN/TMQ-22(XE-4), June 1972, ECOM-5448.
99. Doswell, C. A., III, An Iterative Method for Saturation Adjustment, June 1972, ECOM-5444.
100. Doswell, C. A., III, A Two-Dimensional Short-Range Fog Forecast Model, May 1972, ECOM-5443.
101. Seagraves, Mary Ann B., A General-Purpose Meteorological Rocket Data Reduction Program, August 1972, ECOM-5463.
102. Loveland. Loveland, R. B., J. L. Johnson, and B. D. Hinds, Differential Magnetic Measurements Near Cumulus Clouds, August 1972, ECOM-5463.
103. Cantor, Israel, and Michael Hudlow, Rainfall Effects on Satellite Communications in the K, X, and C Bands, July 1972, ECOM-5459.

DISTRIBUTION LIST

Commanding Officer
Picatinny Arsenal
ATTN: SMUPA-VA6, Bldg 59
Dover, NJ 07801
2

Chief, Analytical Sci Off
Biological Def Rsch Lab
ATTN: AMXBL-AS
Dugway, Utah 84022

Commanding Officer
Fort Detrick
ATTN: Tech Library
SMUFD-AE-T
Frederick, MD 21701

Commanding Officer
Edgewood Arsenal
ATTN: SMUEA-TSTI-TL
Edgewood Arsenal, MD 21010

Commanding Officer
US Army Nuclear Def Lab
ATTN: Library
Edgewood Arsenal, MD 21010
2

Commanding Officer
Aberdeen Proving Ground
ATTN: Tech Lib, Bldg 313
Aberdeen Proving Ground, MD 21005
2

Commanding Officer
US Army Ballistics Rsch Lab
ATTN: Tech Info Div
Aberdeen Proving Ground, MD 21005

Dir of Meteorological Sys
Office of Applications (FM)
Natl Aero & Space Admin
Washington, D. C. 20546

Director
US Weather Bureau
ATTN: Librarian
Washington, D. C. 20235

Dr. A. D. Belmont
Research Div
Control Data Corp
Minneapolis, Minn 55440

Chief, Aerospace Environ Div
CODE S&E-AERO-Y
NASA
Marshall Space Flight Center, Alabama 35802

Commandant
US Army Field Artillery School
ATTN: ATSF-A-G-RA-RK
Ft. Sill, OK 73503

Technical Library
WSMR, New Mexico 88002
3

Natl Aeronautics & Space Admin
George C Marshall Space Flight Center
Aero-Astrodynamic Laboratory
ATTN: S&E-AERO-YS/Mr. D. Camp
Marshall Space Flight Center, Alabama 35812

Dr. F. de Percin
Chief, Atmospheric Sci Branch
Environmental Sciences Division
US Army Research Office
3045 Columbia Pike
Arlington, VA 22204

Geophysics Officer
Code 3250
Pacific Missile Range
Point Mugu, CA 93042

US Army Liaison Office
MIT, Bldg 25, Rm 131
77 Massachusetts Avenue
Cambridge, Mass 02139

The Library of Congress
ATTN: Exchange & Gift Div
Washington, D. C. 20540
2

Head, Atmospheric Sci Section
National Science Foundation
1800 G Street, N.W.
Washington, D. C. 20550

Director, Systems R&D Service
Federal Aviation Admin
800 Independence Avenue S.W.
Washington, D. C. 20590

Technical Processes Br - D823
Room 806, Libraries Div - NOAA
8060 13th Street
Silver Spring, MD 20910

William A. Main
USDA Forest Service
215 Natural Resources Building
Michigan State University
East Lansing, Mich 48823

NASA Headquarters
Meteorology & Sounding Branch
(CODE SAM)
Space Applications Programs
Washington, D. C. 20546

Chief, Fallout Studies Branch
Division of Biology & Medicine
Atomic Energy Commission
Washington, D. C. 20545

Director
Atmospheric Physics & Chem Lab
Room 31
NOAA Dept of Commerce
Boulder, Colorado 80302

Natl Center for Atmos Research
NCAR Library, Acquisitions-Rept
Boulder, Colorado 80302

E&R Center, Bureau of Reclamation
ATTN: D-751, Bldg 67
Denver, Colorado 80225

Natl Oceanographic Data Center - D722
Natl Oceanic & Atmos Admin
US Dept of Commerce
Rockville, MD 20852

Institute of Sci & Technology
The University of Michigan
Box 618, (IRIA Library)
Ann Arbor, Mich 48107

NASA Scientific & Tech Info Fac
ATTN: Acquisitions Br (S-AK/DL)
P. O. Box 33
College Park, MD 20740
2

Battelle Memorial Institute
Strategic Technology Office
Information Analysis Center
505 King Avenue
Columbus, Ohio 43201

Infrared Info & Analysis Center
University of Michigan
Institute of Science & Technology
Box 618
Ann Arbor, Mich 48107

VELA Seismic Info Center
University of Michigan
Box 618
Ann Arbor, Mich 48107

Commanding General
US Army Elect Command
ATTN: AMSEL-RD-LNF
Ft Monmouth, NJ 07703

Commanding Officer
US Army Engineer Topographic Labs
Ft Belvoir, VA 22060

CO, USA Foreign Sci & Tech Center
ATTN: AMXST-ISI
220 7th Street, NE
Charlottesville, VA 22901

Commanding General
US Army Elect Command
ATTN: AMSEL-BL
Ft Monmouth, NJ 07703
3

Commanding General
US Army Elect Command
ATTN: AMSEL-BL-AP
Ft Monmouth, NJ 07703

Commanding General
US Army Elect Command
ATTN: AMSEL-BL-TE
Ft Monmouth, NJ 07703

Commanding General
US Army Elect Command
ATTN: AMSEL-BL-FM-A
Ft Monmouth, NJ 07703

Environmental Protection Agency
Division of Meteorology
Research Triangle Park, North Carolina 27711

Commandant
US Army Field Artillery School
ATTN: Dept of Target Acquisition
Ft Sill, OK 73503

Commandant
US Army Field Artillery School
ATTN: Met. Division
Ft Sill, OK 73503

Armament Dev & Test Center
ADTC(DLOSL)
Eglin AFB, FL 32542

Gary D. Atkinson, LtC USAF
Chief, Technical Services Div
DCS/Aerospace Sciences
ATTN: AWS/DNTI
Scott AFB, IL 62225

Director
National Security Agcy
ATTN: TDL
Ft George G Meade, MD 20755

Commander, Naval Ship Sys Command
Tech Library, RM 3 S-08
Washington, D. C. 20360

Commander
Naval Weather Ser Command
Washington Navy Yard (Bldg 200)
Washington, D. C. 20390

Commanding Officer
Harry Diamond Laboratory
ATTN: Library
Washington, D. C. 20438

Rome Air Devel Center
ATTN: Documents Library (TDL)
Griffiss AFB, NY 13440

Air Force Cambridge Rsch Labs
ATTN: LC(1124)
L. G. Hanscom Field
Bedford, Massachusetts 01730

Air Force Avionics Laboratory
ATTN: AFAL/DOT, STINFO
Wright-Patterson AFB, Ohio 45433
2

HQ, AFCS(EICRW)
Richards-Gebaur AFB, MO 64030

Ofc of Asst Ch of Staff for Intelligence
Dept of the Army
ATTN: ACSI-DD
Washington, D. C. 20310
2

Commanding General
US Army Materiel Command
ATTN: AMCRD-H
Washington, D. C. 20315

Commanding General
US Army Missile Command
ATTN: AMSMI-RR, Dr. J. P. Hallowes
Redstone Arsenal, Alabama 35809

CG, US Army Missile Cmd
Redstone Scientific Info Center
ATTN: Chief, Document Section
Redstone Arsenal, Alabama 35809
2

Commanding General
US Army Test & Eval Cmd
ATTN: NBC Directorate
Aberdeen Proving Ground, MD 21005

Commanding Officer
USACDC FAA
Ft Sill, OK 73503

Commanding Officer
Frankford Arsenal
ATTN: Library, H1300, Bl. 51-2
Philadelphia, PA 19137

Commanding Officer
Frankford Arsenal
ATTN: W1000-65-1 (Mr. Helfrich)
Philadelphia, PA 19137

Commanding Officer
USASA Test & Eval Cen
Ft Huachuca, Arizona 85613

Commanding Officer & Dir
US Navy Ele Lab
ATTN: Library
San Diego, CA 92152

Commander
US Naval Ordnance Lab
ATTN: Tech Library
White Oak, Silver Spring, MD 20910

Commander
Naval Elect Sys Cmd HQ
ATTN: CODE 05611
Washington, D. C. 20360

Commandant, Marine Corps
HQ, US Marine Corps
ATTN: CODE A04C
Washington, D. C. 20380

Marine Corps Dev & Educ Cmd
Development Center
ATTN: C-E Div
Quantico, VA 22134

Commander
US Naval Weapons Lab
ATTN: KEB-2F(FENN)
Dahlgren, VA 22448

Commander, Naval Air Sys Command
Meteorological Div (AIR-540)
Washington, D. C. 20360

Air Force Cambridge Rsch Labs
ATTN: LKI
L. G. Hanscom Field
Bedford, Mass. 01730
2

AFCRL (LYV)
L. G. Hanscom Field
Bedford, Mass. 01730

HQ, Elect Sys Div (TRI)
L. G. Hanscom Field
Bedford, Mass. 01730

Recon Central/RSA
AF Avionics Lab
Wright-Patterson AFB, Ohio 45433

HQ, Air Weather Service
ATTN: AWWAS/TF (R. G. Stone)
Scott AFB, IL 62225

US Air Force Security Ser
ATTN: TSG
San Antonio, TX 78241

HQ, Air Force Sys Command
ATTN: DLTE
Andrews AFB, MD 20331

Air Force Weapons Lab
ATTN: WLIL
Kirtland AFB, NM 87117

Ofc of Asst Ch of Staff for DS-SSS
Dept of the Army
Rm 3C466, The Pentagon
Washington, D. C. 20315

Ofc Asst Sec of the Army (R&D)
ATTN: Asst for Research
Rm 3-E-379, The Pentagon
Washington, D. C. 20310

Chief of Rsch & Development
ATTN: CRDES
Washington, D. C. 20315
2

Commanding General
US Army Materiel Command
ATTN: AMCMA-EE
Washington, D. C. 20315

Commanding General
US Army Materiel Command
ATTN: AMCRD-TV
Washington, D. C. 20315
2

Commanding General
US Army Missile Command
ATTN: AMSMI-RRA, Bldg 7770
Redstone Arsenal, AL 35809

CG, US Army Missile Command
Redstone Scientific Info Cen
ATTN: Chief, Document Section
Redstone Arsenal, AL 35809
3

Commanding General
US Army Combat Devel Command
Intelligence & Control Sys Gr.
ATTN: INCSCSD-C
Ft Belvoir, VA 22060
2

Commanding Officer
US Army Limited War. Lab
ATTN: CRDLWL-7C
Aberdeen Proving Ground, MD 21005

Director
US Army Ballistic Lab
ATTN: AMXRD-BSP (Dr. Reuyl)
Aberdeen Proving Ground, MD 21005

Commanding General
US Army Test & Eval Command
ATTN: AMSTE-EL
Aberdeen Proving Ground, MD 21005

Commanding General
US Army Test & Eval Command
ATTN: AMSTE-FA
Aberdeen Proving Ground, MD 21005

Commanding General
US Army Test & Eval Command
ATTN: AMSTE-NBC
Aberdeen Proving Ground, MD 21005

Commanding General
US Army Munitions Cmd
ATTN: AMSMU-RE-R
Dover, NJ 07801

Director
US Army Munitions Command
Operations Research Group
Aberdeen Proving Ground, MD 21010

Commanding General
US Army Munitions Command
ATTN: AMSMU-RE-P
Dover, NJ 07801

Commanding Officer
Picatinny Arsenal
ATTN: SMUPA-TVI
Dover, NJ 07801

Commanding Officer
USA Garrison
ATTN: Tech Ref. Div.
Fort Huachuca, Arizona 85613

Chief, A.M. & EW Division
ATTN: USAEPG-STEEP-TD
Fort Huachuca, Arizona 85613

US Army Rsch. Off. - Durham
Box CM, DUKE Station
ATTN: CRDARD-IP
Durham, N. Carolina 27706

USA Security Agcy Combat Dev Actv
ATTN: IACDA-P(T) & IACDA-P(L)
Arlington Hall Station, Bldg 420
Arlington, Virginia 22212
2

Technical Support Directorate
ATTN: Technical Library
Bldg 3330
Edgewood Arsenal, MD 26010

Commandant
US Army Chemical Cen & School
Micromet. Section (Chem. Br.)
Ft McClellan, Ala 36201

Director
USA Engr Waterways Exper Sta
ATTN: Rsch Center Library
Vicksburg, Mississippi 39180
2

CG, Deseret Test Center
ATTN: STEPDP-TT-ME(S) MET DIV
Bldg 103, Soldiers Circle
Fort Douglas, Utah 84113

Commanding General
USA CDC Combat Arms Group
Ft. Leavenworth, Kansas 66027

Commanding Officer
Eustis Directorate
US Army Air Mobility R&D Lab
ATTN: Technical Library
Fort Eustis, VA 23604

Director, US Army Advanced Matl Concepts
Agcy
ATTN: AMXAM
Washington, D. C. 20315

Commanding Officer
USACDC CBR Agcy
Ft. McClellan, Ala 36201

Commanding General
US Army Materiel Command
ATTN: AMCRD R (H. Cohen)
Washington, D. C. 20315

Commanding Officer
US Army Combat Dev Cmd
Communications-Elect Agcy
Ft Monmouth, NJ 07703

US Army Liaison Office
MIT-Lincoln Lab, Rm A-210
P. O. Box 73
Lexington, Mass. 02173

HQ, US Army Combat Dev Cmd
ATTN: CDCLN-EL
Ft Belvoir, VA 22060

Commanding General
US Army Tank-Automotive Cmd
ATTN: AMSTA-Z, Mr. R. McGregor
Warren, Michigan 48090

Commanding General
US Army Elect Command
ATTN: AMSEL-GG-TD
Ft Monmouth, NJ 07703
2

Commanding General
US Army Elect Command
ATTN: AMSEL-EW
Ft Monmouth, NJ 07703

Commanding General
US Army Elect Command
ATTN: AMSEL-ME-NMP-PS
Ft Monmouth, NJ 07703

Commanding General
US Army Elect Command
ATTN: AMSEL-MS-TI
Ft Monmouth, NJ 07703

Commanding General
US Army Elect Command
ATTN: AMSEL-XL-D
Ft Monmouth, NJ 07703

Commanding General
US Army Elect Command
ATTN: AMSEL-WL-D
Ft Monmouth, NJ 07703

Commanding General
US Army Elect Command
ATTN: AMSEL-NL-D
Ft Monmouth, NJ 07703

Commanding General
US Army Elect Command
ATTN: AMSEL-KL-D
Ft Monmouth, NJ 07703

Commanding General
US Army Elect Command
ATTN: AMSEL-VL-D
Ft Monmouth, NJ 07703

Commanding General
US Army Elect Command
ATTN: AMSEL-CT-D
Ft Monmouth, NJ 07703
3

Commanding General
US Army Elect Command
ATTN: AMSEL-SC
Ft Monmouth, NJ 07703

Commanding General
US Army Elect Command
ATTN: AMSEL-RD-D
Ft Monmouth, NJ 07703

Commanding General
US Army Combat Dev Cmd
ATTN: CDCMR-E
Ft Belvoir, VA 22060

President
US Army Artillery Board
Ft Sill, OK 73503

Dir of Defense Rsch & Engin
ATTN: Tech Library
RM 3E-1039, The Pentagon
Washington, D. C. 20301

Defense Intelligence Agcy
ATTN: DIAAP-10A2
Washington, D. C. 20301

Director, Defense Nuclear Agency
ATTN: Tech Library
Washington, D. C. 20305

Naval Ships Systems Command
ATTN: CODE 20526 (Tech Lib)
Main Navy Bldg, Rm 1528
Washington, D. C. 20325

Director
US Naval Rsch Laboratory
ATTN: CODE 2627
Washington, D. C. 20390
2

CO, Edgewood Arsenal
Defense Devel & Engineering Lab
ATTN: SMUEA-DDW-2, Mr. H. Tannenbaum
Edgewood Arsenal, MD 21010

Commanding Officer
Aberdeen Proving Ground
ATTN: STEAP-TL
Aberdeen Proving Ground, MD 21002

Director, Ballistic Rsch Labs
US Army Aberdeen Rsch & Dev Cen
ATTN: AMXRD-BTL, Mr. F. J. Allen
Aberdeen Proving Ground, MD 21005

Commanding Officer
US Army Ballistic Rsch Labs
ATTN: AMXBR-B & AMXBR-1A
Aberdeen Proving Ground, MD 21005
2

Commanding Officer
US Army Land Warfare Lab
ATTN: CRDLWL-4A
Aberdeen Proving Ground, MD 21005

Commanding Officer
US Army Elect Proving Ground
ATTN: STEEP-MT-EA
Ft Huachuca, Arizona 85613

Commanding Officer
US Army Dugway Proving Ground Library
ATTN: STEDP-TL, Tech Library
Dugway, Utah 84022

Commanding Officer
US Army Cold Regions R&E Lab
ATTN: CRREL-RP (Dr. Yin Chao Yen)
Hanover, New Hampshire 03755

Commanding Officer
Yuma Proving Ground
ATTN: STEYP-AD(TECH LIBRARY)
Yuma, Arizona 85364

Commanding Officer
US Army Arctic Test Center
APO Seattle 98733
2

CO, US Army Tropic Test Center
ATTN: STETC-AD-TL
APO New York 09827
2

Commanding Officer
USACDC Inst of Nuclear Studies
Ft Bliss, TX 79916

Commanding Officer
USADDC Inst of Systems Analysis
ATTN: CDISA-SSCI & CDISA-STANO
Ft Belvoir, VA 22060

Commanding General
US Army Missile Command
ATTN: AMSMI-RFG, Mr. N. Bell
Redstone Arsenal, AL 35809

Commanding Officer
Frankford Arsenal
ATTN: SMUFA-N-5300, Mr. M. Schoenfield
Bldg 201
Philadelphia, PA 19137

Commanding Officer
US Army Satellite Comm Agcy
ATTN: AMCPM-SC-3
Ft Monmouth, NJ 07703

Director
Night Vision Lab (USAECOM)
ATTN: ASMEL-NV-OR, Mr. S. Segal
Ft Belvoir, VA 22060

Sylvania Elect Sys-Western Div
ATTN: Technical Reports Lib
P. O. Box 205
Mountain View, CA 94040

NASA HEADQUARTERS
Prg. Ch, MET & Soundings (SRM)
Earth Observations Programs
Washington, D. C. 20546

Library-R51-Tech Reports
Environmental Research Labs
NOAA
Boulder, Colorado, 80302

Commandant
US Army Air Defense School
ATTN: C&S Dept, MSL SCI DIV
Ft Bliss, TX 79916

Defense Documentation Center
ATTN: DDC-TCA
Cameron Station (Bldg 5)
Alexandria, VA 22314
12

Director, USN Research Lab.
ATTN: Code 6530, H. Shenker
Washington, D. C. 20390

Mr. E. F. Corwin
Head, Met Research Branch
Meteorological Division
Naval Air Sys Cmd (AIR-5401)
Washington, D. C. 20360

Commanding Officer
US Army Combat Dev Cmd
Intelligency Agency
ATTN: CDCINT-P, Cpt Thoresen
Ft. Huachuca, Arizona

Director
US Army Advanced Materiel Concepts Agency
2461 Eisenhower Avenue
Alexandria, VA 22314

University of Oklahoma
Research Institute
Field Artillery Research Off
P. O. Box 3124
Ft. Sill, OK 73503

Dir US Naval Research Lab
ATTN: CODE 6530, H. Shenker
Washington, D. C. 20390

UNCLASSIFIED

Security Classification

DOCUMENT CONTROL DATA - R & D

(Security classification of title, body of abstract and indexing annotation must be entered when the overall report is classified)

1. ORIGINATING ACTIVITY (Corporate author) Atmospheric Sciences Laboratory White Sands Missile Range, New Mexico		2a. REPORT SECURITY CLASSIFICATION Unclassified	
		2b. GROUP	
3. REPORT TITLE RAINFALL EFFECTS ON SATELLITE COMMUNICATIONS IN THE K, X, AND C BANDS			
4. DESCRIPTIVE NOTES (Type of report and inclusive dates)			
5. AUTHOR(S) (First name, middle initial, last name) Israel Cantor and Michael Hudlow			
6. REPORT DATE July 1972		7a. TOTAL NO. OF PAGES 66	7b. NO. OF REFS 30
8a. CONTRACT OR GRANT NO.		8a. ORIGINATOR'S REPORT NUMBER(S) ECOM-5459	
b. PROJECT NO.		9b. OTHER REPORT NO(S) (Any other numbers that may be assigned this report)	
c. DA Task No. IT06211A12605-54			
d.			
10. DISTRIBUTION STATEMENT Approved for public release; distribution unlimited.			
11. SUPPLEMENTARY NOTES		12. SPONSORING MILITARY ACTIVITY U. S. Army Electronics Command Fort Monmouth, New Jersey	
13. ABSTRACT <p>A survey-type investigation is made into the feasibility of short- and long-term predictions of attenuation and noise temperature fluctuations for satellite communications. The feasibility of using a weather radar, such as the AN/CPS-9, at 9.4 GHz (3.2 cm) for real-time predictions of the above parameters is explored. The suitability of weather radar for such applications is evaluated. Raindrop size data and Mie attenuation theory are used for the derivation of statistical curves that provide attenuation coefficients for various geographic areas and temperatures. Related results of other investigators are included. Some concepts are also presented of Mie vs Rayleigh scattering, absorption vs scattering, parameter and rain structure variability, path diversity, noise temperature, microwave radiometry, and dual-wavelength radar feasibility. Furthermore, information is added in regard to some of the general meteorological as well as the climatological aspects of precipitation, particularly thunderstorms.</p>			

DD FORM 1473
1 NOV 66REPLACES DD FORM 1473, 1 JAN 64, WHICH IS
OBSOLETE FOR ARMY USE.

UNCLASSIFIED

Security Classification

UNCLASSIFIED

Security Classification

14. KEY WORDS	LINK A		LINK B		LINK C	
	ROLE	WT	ROLE	WT	ROLE	WT
1. Satellites 2. Communications 3. Precipitation 4. Drop-size distributions 5. Signal degradations						

UNCLASSIFIED

Security Classification

